NANOSTRUCTURED TITANIUM DIOXIDE: SYNTHESIS, CHARACTERIZATION AND PHOTOACTIVE APPLICATION

BY

FREDERICK PAAKWAH BUABENG (10278265)

DEPARTMENT OF MATERIALS SCEINCE AND ENGINEERING,

UNIVERSITY OF GHANA, LEGON

This Thesis is submitted to the University of Ghana, Legon in partial fulfillment of requirement for the award of MPHIL Materials Science & Engineering degree

2016

NANOSTRUCTURED TITANIUMDIOXIDE: SYNTHESIS, CHARACTERIZATION AND PHOTOACTIVE APPLICATION

FREDERICK PAAKWAH BUABENG (10278265)

DEPARTMENT OF MATERIALS SCIENCE AND ENGINEERING,

UNIVERSITY OF GHANA, LEGON

This Thesis is submitted to the University of Ghana, Legon in partial fulfillment of requirement for the award of MPHIL Materials Science & Engineering degree

JULY 2016

DECLARATIONS

Candidate's Declaration

I hereby declare that this thesis which is the result of my own original research under strict supervision was prepared in accordance with the University of Ghana's academic regulations and that no part of it has been presented for another degree in this University or elsewhere.

Candidate's name: **Frederick Paakwah Buabeng** (10278265)

Signature..... Date…… **18th July, 2016** ……...

Supervisors' declaration

I hereby declare that the preparation and presentation of the thesis were supervised in accordance with the guidelines on supervision of thesis laid down by the University of Ghana.

Supervisor's name: **Dr. David Dodoo-Arhin**, (University of Ghana, Ghana)

Signature..... Date…… **18th July, 2016** ……...

Co-Supervisor's name: Prof. Julius M. Mwabora, (University of Nairobi, Kenya)

Signature..... Date…… **18th July, 2016** ……...

Head of Department's declaration

I hereby declare that this thesis has been prepared, supervised and accepted in accordance with the guidelines on the thesis laid down by the University of Ghana.

Head of Department's name: **Dr. David Dodoo-Arhin**

Signature..... Date..... **18th July, 2016**.....

ABSTRACT

Dye pollutants contaminate water bodies when they are improperly disposed into the ecosystem. Effects caused by the disposal of these dye pollutants include aesthetic pollution, eutrophication and perturbations in aquatic life. This work aims to mitigate these water contamination problems by studying possible degradation of these pollutant compounds. Semiconductor photocatalytic process using nanocrystalline TiO_2 as the semiconductor catalyst was adopted in this work to photodegrade Rhodamine B dye and Sudan III dye solutions by exposing it to UV light. In this work, we explored the synthesis of porous TiO_2 nanostructured powders via chemical means such as the Sol gel and Hydrothermal techniques. The as-produced nanoparticles were then characterized via X-Ray Diffraction (XRD), Scanning Electron Microscopy (SEM), Brunauer–Emmett–Teller (*BET*) surface area analysis, Fourier Transform Infra-Red, and Raman Spectroscopy for their microstructure, morphology, optical, porosity and adsorption properties. The photocatalytic degradation of Rhodamine B and Sudan III dyes were studied at various exposure times to the UV light up to 150 minutes with 30 minutes interval. The XRD and Raman spectra of the samples showed that, the anatase phase of TiO_2 was produced when the Sol gel method was used in the nanoparticles synthesis. The Hydrothermal method also resulted in the synthesis of anatase phase of TiO_2 except the sample calcined at 600 °C which showed about 15% rutile phase. Fourier Transform Infra-Red spectrum on the TiO_2 prepared by Sol gel method showed bands at 3228cm^{-1} and 1635 cm^{-1}, which is attributed to O-H stretching and stretching of titanium carboxylate, respectively and these peaks were seen disappearing after calcining at different temperatures. Only the strong absorption between 800 and 410 cm^{-1} remained, which were attributed to the obtained TiO_2 nanoparticles. The highest BET surface area was reported to be 207.7 m^2/g which was assigned to the as-prepared TiO_2 nanoparticles synthesized by the

Hydrothermal technique. The adsorption and desorption isotherms of this sample exhibited typical type IV pattern with hysteresis loop characteristic of mesoporous material according to the classification of IUPAC. 94% degradation of Rhodamine B dye was observed after 150 minutes irradiation of UV light when TiO_2 catalyst synthesized by Sol gel technique and calcined at 300 °C was used in photodegrading Rhodamine B dye solution and a 100% degradation was seen after 150 minutes UV light irradiation in Sudan III dye when Hydrothermal prepared catalyst calcined at 300 °C was used. The SEM micrographs obtained also showed that nearly spherical TiO_2 nanoparticles were produced. The present results obtained showed that a mesoporous spherical anatase TiO_2 nanoparticles with high photocatalytic activity and high surface area were synthesized. They were highly crystalline with grain size ranging from 2 nm to 30 nm. These synthesized TiO_2 nanoparticles can be applied in the degradation of wide range of dye pollutants.

ACKNOWLEDGEMENTS

My sincere appreciation goes to the **AMSEN** and **Carnegie** for funding my work. I thank **Dr David Dodoo-Arhin** for supervising my thesis as well as **Prof Julius M. Mwabora** who was my co-supervisor. This thesis would not have been made possible without them. My gratitude also goes to **Dr. Benjamin Agyei-Tuffour** and **Dr. Emmanuel Nyankson** for their contributions.

I owe a lot to **Biotechnology** and **Physics** lab technicians at University of Ghana for allowing me to use their laboratory. I also thank **Dr Prince Amaniampong** of Nangyang Technical University for assisting me with the characterization of my samples.

DEDICATION

I dedicate this thesis to my parents, Mr. Stephen Buabeng and Mrs. Juliana Nyarkoh for their care, guidance and support throughout my education. I also dedicate this work to my supervisor and Head of Department, Dr David Dodoo-Arhin and also to all my loved ones especially Doreen Nolda Jehu Appiah as well as all who played positive role in my life.

CONTENTS

LIST OF FIGURES

LIST OF TABLES

LIST OF ACRONYMS AND ABBREVIATIONS

HT_As	TiO_2 as-prepared nanoparticles by hydrothermal technique
HT_200	TiO_2 prepared by hydrothermal technique and calcined at 200°C
HT_300	TiO_2 prepared by hydrothermal technique and calcined at 300°C
HT_400	TiO_2 prepared by hydrothermal technique and calcined at 400°C
HT_500	TiO_2 prepared by hydrothermal technique and calcined at 500°C
HT_600	TiO_2 prepared by hydrothermal technique and calcined at 600°C
SG_As	TiO_2 as-prepared nanoparticles by sol gel technique
SG_200	TiO_2 prepared by sol gel technique and calcined at 200°C
SG_300	TiO_2 prepared by sol gel technique and calcined at 300°C
SG_400	TiO_2 prepared by sol gel technique and calcined at 400°C
SG_500	TiO_2 prepared by sol gel technique and calcined at 500°C

SG_600	TiO_2 prepared by sol gel technique and calcined at 600°C
BET	Brunauer–Emmett–Teller
FTIR	Fourier Transform Infra-Red
SEM	Scanning Electron Microscopy
XRD	X-Ray Diffraction
ETAD	Ecological and Toxicological Association of the Dyestuffs Manufacturing Industry
ASAP	Accelerated Surface Area and Porosimetry System
IUPAC	International Union of Pure and Applied Chemistry
TTIP	Titanium Isopropoxide
FDA	Food and Drugs Authority
IPA	Isopropyl Alcohol
ICSD	Inorganic Crystal Structure Database
NIST	National Institute of Standards and Technology
SRM	Standard Reference Materials
WPPM	Whole Powder Pattern Modelling
SSA	Specific Surface Area
IP	Intracrystalline Pressure

CHAPTER ONE

1.0. Introduction

Due to rapid industrialization growth in recent decades, a considerable amount of toxic waste is being discharged on daily basis. With increasing concern of public health, waste treatment and management has become significant in modern times. These ongoing processes compromise the quality of water for use in daily activities since the need for clean water by the society is of great importance [1, 2, 3]. Dye pollutants from the textile industry, dye industry, food industry, leather and paper industries as well as among others. contaminate the environment when they are improperly disposed [4–8]. These synthetic polymeric dyes have a wide spectrum of applications and hence making their use inevitable. The only way forward is to develop safe disposal mechanisms and methodologies so that they can coexist with the ecosystem to provide a green environment.

It has been reported that 1-20% of the total world production of dyes is lost during synthesis and dyeing process. Therefore, discharging these dyes into the ecosystem can cause aesthetic pollution, eutrophication and perturbations in aquatic life [6, 9–12]. Industries in Ghana including textile industry, paper industry, and others make use of these dyes for a wide range of designs and applications. It is therefore important to render these dyes non-toxic before it is discharged to the environment, to inhibit their harmful effects on the ecosystem.

Two industries that make the most use of dyes are the textile and paper industries. As such, these industries have shown a significant increase in the use of synthetic complex organic dyes as the colouring elements. The annual world production of textile industries is approximated to be about 30 million tons which requires 700,000 tons of different types of dyes, and this causes

considerable environmental pollution problems [13]. Various colour designs in textiles in recent times have led to the expansion of worldwide textiles industry and hence, making use of these synthetic dyes increase in demand. Therefore, it has become necessary to degrade these dyes effectively and at the same time ensuring that no harmful by-products are produced, which may pose a threat to the ecosystem. In fact, agencies such as the Ecological and Toxicological Association of the Dyestuffs Manufacturing Industry (ETAD) have been established to control and devise strategies and methodologies to combat the effects of these dye pollutants. (ETAD) was inducted in 1974 with the aim of minimizing environmental damage, protecting users and consumers and cooperating with government and public concerns in relation to the toxicological impact of these dye products [14].

In an attempt to mitigate these problems, physical, chemical and biological wastewater treatment methods have been adopted to reduce their impact on the environment. Waste can be degraded by the application of heat, light, chemical reagents and by means of ultrasound [15]. However, some of these techniques have significant drawbacks since they are nondestructive so they end up transforming the organic compounds from one phase to the other [16]. Most dyes are non-degradable and toxic and they are also characterized by very long half-life periods in the environment [15]. It is known that dyes such as Sudan III are mostly non-biodegradable in aerobic environments due to the strong electron withdrawing character of the azo group, while in anaerobic environments, they can be reduced to more hazardous intermediates such as aromatic amines [14].. For instance, a process normally adopted commercially, such as coagulation and adsorption, do not result in the complete destruction of the dye effluent but transfer components of the dye from one phase to another, thus causing secondary loading environment [14].

Azo synthetic dyes such us Sudan dyes have been identified as contaminants in different food stuffs and their presence is regularly reported [17]. They are also used extensively in cosmetics, waxes, solvents and textiles. However, it has been reported that Sudan dyes are metabolized to possible carcinogenic colourless amines that can form DNA adducts entailing mutations [17]. Hence they have been declared suspected carcinogens and classified group 3 compounds by the International Agency for Research on Cancer [17].

It was also reported by Ghanaian Daily Graphic on 10th October, 2015 that Sudan IV dye was detected in Ghanaian palm oil and this raised an alarm and brought panic among the public. As a precaution, the Food and Drugs Authority (FDA) raised alerts concerning food items very high [18]. These and many other issues call for the concern to render such dyes harmless before they are released into the environment because, the mismanagement of these dyes can cause global problems that might be expensive to control. It has therefore become so important to adopt strategies to break down the chemical makeup of these dyes by a photodegradation process before they can be discharged into the environment.

Methodologies normally used in purifying dye contaminated water include; adsorption on organic or inorganic materials, photocatalytic degradation, oxidation processes, microbiological, or enzymatic decomposition [3]. Of these, semiconductor photocatalytic degradation with UV-radiated TiO_2 nanoparticles has been identified to be most effective process for the degradation of various organic compounds and dyes [4, 9, 19, 20]. This technique has also been demonstrated to be very effective in degrading phenol, organic dyes and other emerging contaminants [21]. This process is carried out using a semiconductor catalyst with a wide band gap such as TiO_2. Hydroxyl radicals are generated in the process upon radiation and the presence of an oxidation

agent, facilitated by electron-hole pairs [16, 21–23]. These hydroxyl radicals are very reactive in nature and results in the organic substance being degraded [21].

Although diverse photocatalysts such as TiO_2, ZnO, CdS and In_2S_3. have been used recently in photocatalytic activities, it has been reported that, TiO_2 is the most effective candidate [1]. This process has gained a lot of interest for environmental remediation. The destructive power of nanocrystalline TiO_2 is superb; making series of compounds such as families of dyes, pesticides, herbicides, pharmaceuticals, cosmetics, phenolic compounds and toxins. susceptible to degradation by nanocrystalline TiO_2 photocatalysis [1]. This is due to the high photocatalytic activity, high chemical stability and antibacterial properties of nanostructured TiO_2, which is used as the photocatalyst in this reaction [24–27]. Moreover, TiO_2 has strong oxidizing power and long-term photostability. It is also inexpensive, easily synthesized and nontoxic which makes it a suitable catalyst of choice [21**,** 28]. These unique properties exhibited by TiO_2 are largely due to its nanostructure, morphology, crystalline phase and dimensionality [29].

However, TiO_2 used as a catalyst for the degradation of most dyes fall short in certain areas. It has a low surface area and also, the quantum yield is relatively low as a result of the rapid recombination of the electron-hole pair generated in the photo-degradation process. To combat these problems, TiO_2 doped with transition metals or metal complex dye sensitized TiO_2 have been developed recently [15].

In this thesis, the photocatalytic degradation of rhodamine B and Sudan III dyes with TiO_2 nanoparticles as catalyst were studied at various exposure times to the UV light source. The photocatalytic activity of the synthesized TiO_2 was evaluated by determining the percentage degradation of the respective dye solutions over time when TiO_2 was used as the catalyst.

1.1. Aims and Objectives

Concerns about harmful effects of some dyes and other related issues have motivated this study to be done.. The main objective of this study is to mitigate the devastating effect of industrial dyes on the environment by developing effective strategies and techniques to degrade these dyes.

The specific objectives are to:

a. Synthesize TiO_2 nanoparticles using the sol-gel and hydrothermal methods.
b. Characterize the TiO_2 catalysts prepared
c. Incorporate the synthesized TiO_2 nanoparticles into the photodegradaion of Rhodamine B and Sudan III dyes.

CHAPTER TWO

2.0. Literature Review

2.1. Properties and Structure of TiO_2

Titanium dioxide was first produced at large scale in 1923 and it was obtained from a variety of ores [30]. It is a versatile n-type semiconductor transition-metal oxide and is a very useful material which has found its usefulness in various forms of application related to catalysis, electronics, photonics, sensing, medicine, and controlled drug release [31]. TiO_2 comprises of eleven phases of which some only exist in high pressure states, and the others belonging to four crystal systems (orthorhombic, monoclinic, tetragonal and cubic). However, the common phases of TiO_2 are anatase, brookite and rutile belonging to tetragonal, orthorhombic and tetragonal crystal systems respectively. Most of these phases occur naturally in mineral ores and are therefore extracted from its ores. Known sources of TiO_2 include ilmenite ($FeTiO_3$), leucoxene ores and rutile beach sand [32], [33].

The TiO_2 particle sizes have a significant contribution in the determination of its characteristics as well as its potential application. Working with TiO_2 on a smaller particle size scale increases its potential applications. In these modern times that nanotechnology is popular, a lot of interest in how TiO_2 can play a role in this field is being pursued by many scientist and researchers. [32].

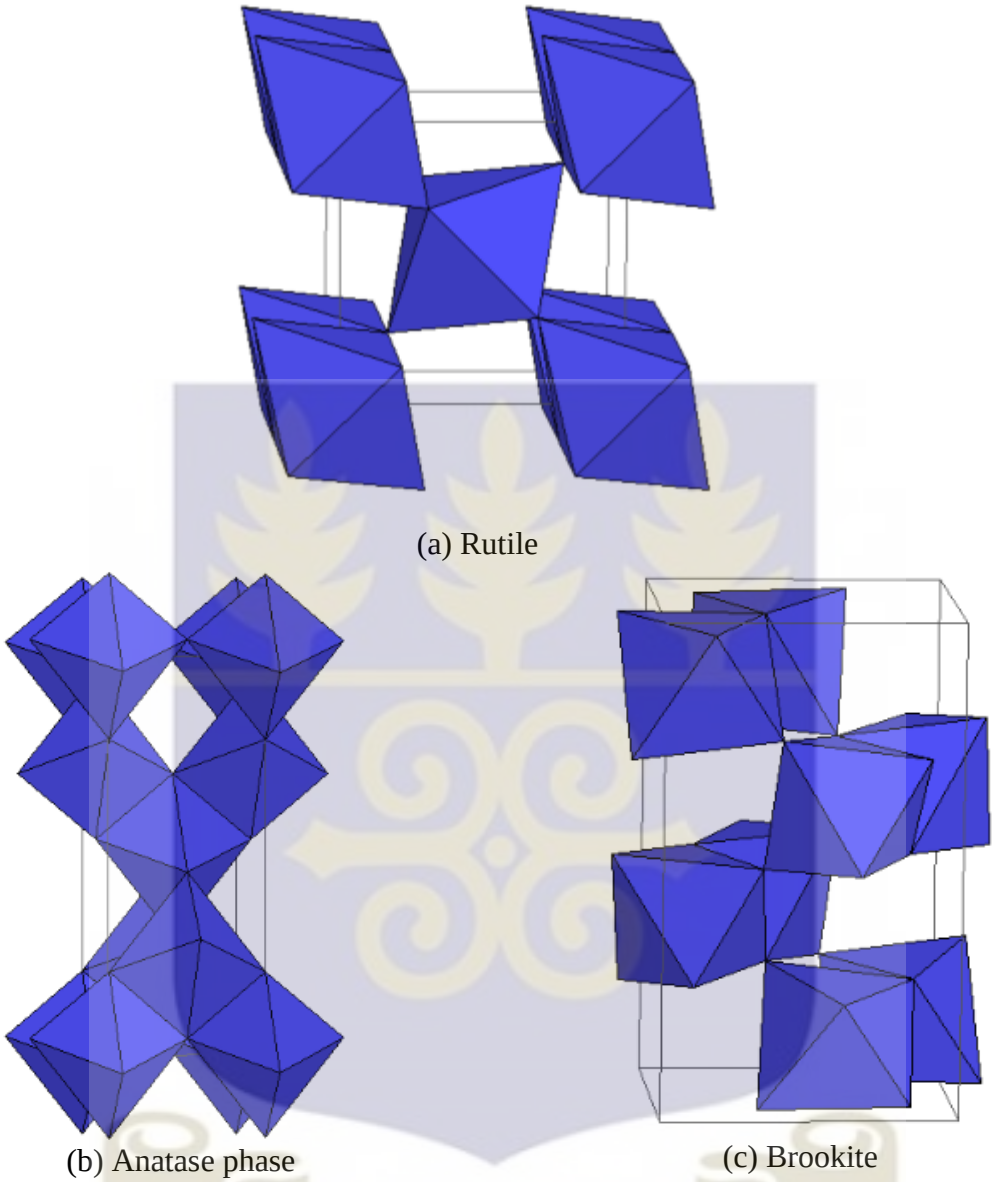

Figure 2.1 Crystal structure of TiO_2: (a) rutile (b) anatase and (c) brookite. [34]

Figure 2.1 shows the crystal structure configurations of rutile, anatase and brookite phase of TiO_2 These three main phases of TiO_2 have high refractive indices (anatase = 2.488, rutile = 2.609, brookite = 2.583), low absorption and low dispersion in visible and near-infrared spectral regions, as well as high chemical and thermal stabilities [31]. Among them, rutile and anatase phases are predominant. Rutile and Anatase phases both exhibit tetragonal crystal structures but

Brookite has an orthorhombic crystal structure. Rutile however, is a more stable phase at high temperature and with an optical energy band gap of 3.0 eV (415 nm), but the anatase phase is mostly formed at relatively lower temperatures and has an optical energy band gap of 3.2 eV (380 nm) [30].

Nanostructured TiO_2 has gained much attention recently in the scientific community due to its wide applications in photocatalysts, solar cells, gas sensors and optoelectronic devices. Sung et al. (2010) emphasized the enormous use of TiO_2 in several applications including photovoltaic applications, water splitting process and hydrogen storage, and many others [33]. These vast applications of TiO_2 emerges due to some interesting properties exhibited, such as crystalline structure, particle size, specific surface area, porosity and thermal stability [21, 33].

Photocatalysis using semiconductor as a catalyst has attracted a great deal of research attention due to its application to solve numerous environmental problems. Among the various semiconductors employed, TiO_2 is good photocatalyst that has been identified for the degradation of environmental contaminants due to its high photocatalytic avtivity, non- toxicity, relatively low cost, and tremendous chemical stability. The excellent photocatalytic property of TiO_2 is attributed to its wide band gap and the long lifetime of photogenerated holes and electrons. TiO_2 photocatalyst when used in photodegradation process generates electron/hole pairs to initiate a series of chemical reactions that eventually detoxify the pollutants [33]. One of the problems normally encountered in photocatalysis process is the recombination of the photogenerated holes and electrons. This problem is relatively reduced to the minimum in the case of TiO_2 and thus, making TiO_2 a suitable catalyst among other semiconductors.

It has also been found through investigations that, the anatase phase of TiO_2 generally possess a better photocatalytic strength than the rutile phase [33].

2.2. Synthesis of TiO_2 nanoparticles

Various properties of TiO_2 nanoparticles including physical, chemical, and photochemical greatly depend on the preparation method. In view of the vast applications of TiO_2, several techniques have been developed over the last decade and can be classified as liquid process sol gel , solvothermal ,hydrothermal , solid state processing routes (mechanochemical alloying/ milling) , thermal hydrolysis, laser evaporation, and ultrasonic synthesis [33].

2.2.1. Sol gel

Sol-gel is the most commonly used method for the synthesis of TiO_2 particles. This technique has been widely adopted for preparing nanostructured TiO_2 particles due to some advantages such as high purity, good uniformity of the microstructure, low temperature synthesis and easily controlled reaction conditions [33].

This method of processing nanostructures begins with nanosize unit and it also undergoes reactions on the nanometer scale hence the material with nanometer features results. The interests about Sol gel processing by scientist are due to the purity of the starting materials as well as generally lower processing temperatures. Also, by adopting this method, the powder size, morphology and surface chemistry are controlled simultaneously [35]. The processing reactions that take place during Sol gel synthesis of TiO_2 nanoparticles are as follows:

i. Hydrolysis to make the reaction active

ii. Condensation polymerization along with further hydrolysis

These reactions result in the increase of molecular weight of the oxide polymer Eventually, the solutions react to a point where the molecular structure can no longer be reversed and it is at this point that the Sol-gel transition occurs [35].

To synthesize TiO_2 nanoparticles with significant properties, several parameters need to be controlled in the sol-gel process. For instance, it is known that the concentration of titanium alkoxide precursor affects the crystallization and related characteristics of the prepared TiO_2 nanoparticles. The size, stability, and morphology of the sol produced from alkoxide are also strongly affected by the hydrolysis and pH. Furthermore, the pH of the prepared solution has a great influence on the final size of TiO_2 nanoparticles. Therefore, a carefully controlled pH and reaction morphology are necessary to optimize the preparation conditions of TiO_2 [33]. These parameters are of great interest since they can be controlled and manipulated to produce the desired nanoparticles.

Nanoparticles synthesis by Sol gel involves initially a homogeneous solution (sol) of the selected alkoxides which are organometallic precursors. Catalysts may also be used to control the pH and the starting reactions.

The Sol gel method was adopted to synthesize TiO_2 nanoparticles by reacting Titanium tetra-isopropoxide (TTIP, $Ti(OCH(CH_3)_2)_4$) and isopropyl alcohol (IPA, C_3H_8O) in the ratio of 1:10 respectively. A second solution was prepared by mixing H_2O and IPA in a molar ratio of 10: 1. This solution was then titrated into the first solution and stirred for 2 h until a uniform colloidal TiO_2 sol was produced. HCl and NH_4OH were used to adjust the pH of the resultant solution to the desired value. [33].

Meng et. al. (2012) also prepared carbon 60 coupled with CdS-TiO_2 system by a sol gel technique and the prepared catalyst was employed in the degradation of Rhodamine B dye. When carbon 60 was added to CdS/TiO_2 system, the catalytic activity was enhanced and this resulted in a degradation of a higher percentage of the dye within a relatively shorter time. The catalytic activity was also enhanced when the content of CdS in C60 and TiO_2 was increased. These observations were associated to the fact that, due to the improved reaction state by CdS, more charges were produced and the rate at which the electron–hole pair recombines were also reduced [15].

2.2.2. Hydrothermal

Hydrothermal method of nanoparticle synthesis is one of the most widely used methods for the preparation of highly crystalline nanostructured TiO_2. Due to the application of elevated temperatures and pressures in an aqueous solution, the conversion of amorphous TiO_2 into crystalline TiO_2 is facilitated and hence the crystallinity of the nanoparticles is increased. Hydrothermal treatment can also be used to alter the morphology, microstructure and phase composition of materials by varying the reaction parameters [28]. The advantages of this method are:

i. Crystallization temperature for phase is below 200 °C.
ii. By changing the process conditions (such as temperature, time, pH, reactant concentration, additives, etc.), various crystalline products with different composition, structure and morphology can be obtained.
iii. Low energy consumption and environmentally friendly process.
iv. Control of reaction conditions is easy and straightforward.

These make hydrothermal synthesis a good method for the preparation of semiconductor photocatalysts such as TiO_2 [28].

In the synthesis of TiO_2 by Pavasupree et al. [36], the hydrothermal technique was adopted by mixing Titanium (IV) butoxide with the same mole of acetyacetone to slowdown the hydrolysis and the condensation reactions. 40 ml was then added to the solution, and the solution was stirred at room temperature for about 5 min. After stirring, 30 ml ammonia aqueous solution (28 %) was added and the solution was put into a Teflon-lined stainless steel autoclave and heated at 130 °C for 12 hours. After the autoclave was allowed to cool to room temperature, the resulting samples were washed with aqueous HCl solution, 2-propanol and distilled water for several times, and then dried at 100 °C for 12 h. The obtained samples were calcined for 4 h at 300-700°C in air condition [36].

2.3. Sudan dyes

Sudan dyes are synthetic fat-soluble azo-compounds, with a building block of chromophoric azo groups (-N=N-) in their molecule [17]. These kind of azo dyes are toxic and have been classified to be carcinogenic. This poses a major risk to the surrounding ecosystem and human health as a result of waste waters originating from their production and application in industries [14].

ETAD carried out a survey which showed that, of a total of approximately 4000 dyes that had been tested, more than 90% showed lethal dose (LD50) values above 2×10^3 mg/kg. The most toxic among these dyes were the group of basic and direct diazo dyes. It appears that exposure to azo dyes by inhalation and contact with the skin by azo dyes is of concern, due to the potential generation of carcinogenic aromatic amines. Certain azo dyes and their biotransformation

products have been proven to be toxic to aquatic life as well as humans. Azo dyes are very stable compounds, and are difficult to destroy or to be decomposed by common treatment in a biological treating station [14].

Sudan dyes are used mostly as colorants in food, cosmetics, waxes, solvents, textiles etc. Sudan I dye has been identified to be carcinogenic in the rat and also found to cause tumours in the liver of mice. Sudan II dye has also been found to cause an increase in the incidence of bladder carcinomas, and Sudan IV increase the risk of formation of local carcomas. As a result, Sudan dyes such as Sudan I, II, and III, Sudan Red 7B, and Sudan Black B reaction products have been declared suspected carcinogens and classified as group 3 compounds by the International Agency for Research on Cancer [17]. The chemical structure of Sudan I, II, III and IV dyes are shown in Figure 2.2.

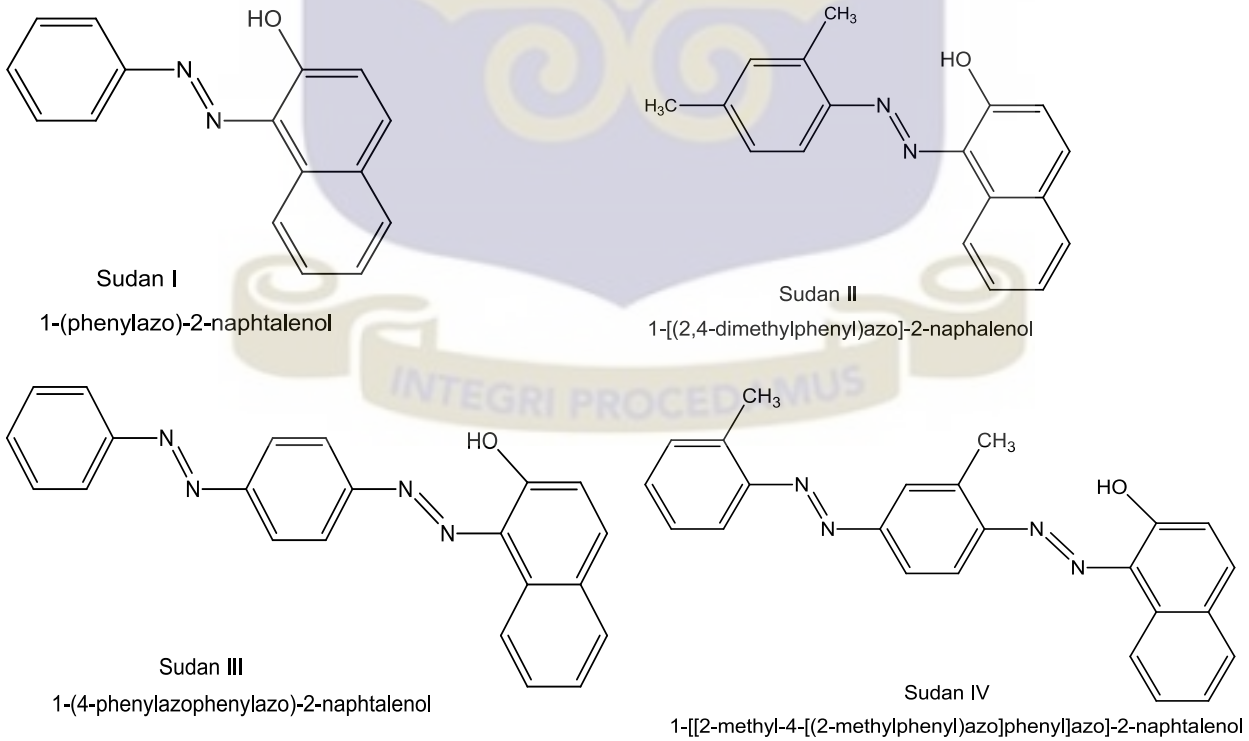

Figure 2.2: Chemical structures of Sudan I, II, III and IV dyes [37]

2.4. Rhodamine B dye

Rhodamine dyes possesses red to violet colour and are normally used as the active medium of tunable laser radiation in the visible region of the light spectrum. The molecular formula of Rhodamine B is $C_{28}H_{31}ClN_2O_3$ and has molecular weight of 479.02 g/mol. It is mostly used as a tracer dye in water in determining the rate and direction of flow and transport. They are used extensively in biotechnology applications such as fluorescence microscopy, flow cytometry and fluorescence correlation spectroscopy [38]. The structure of Rhodamine B dye is presented in Figure 2.3.

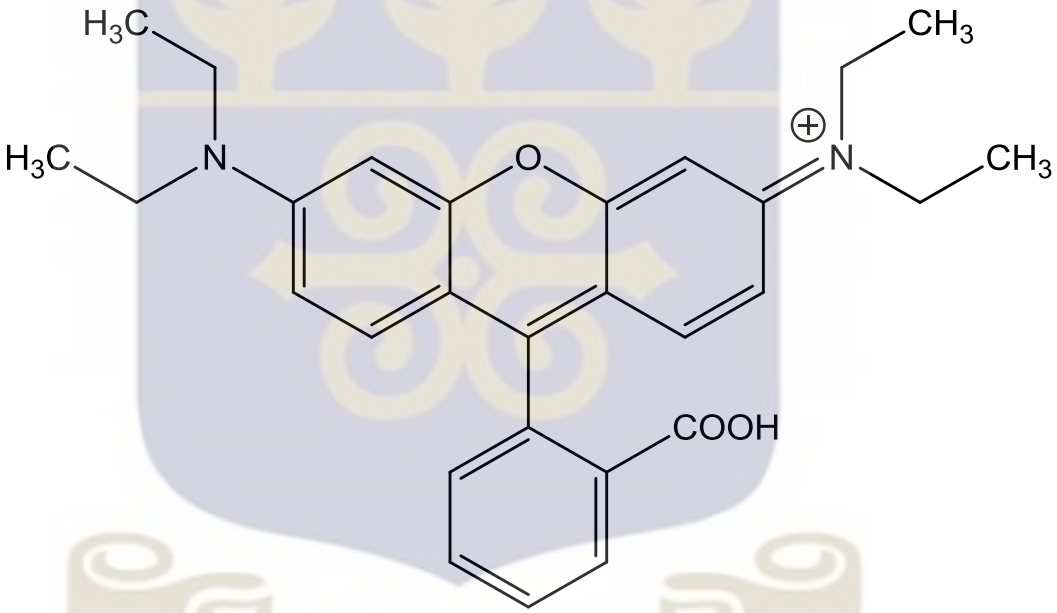

Figure 2.3: Structure of Rhodmine B dye

2.5. Photocatalysis

Semiconductor Photocatalysis involves the use of solid semiconductor such as SnO_2 or TiO_2, oxygen as the electron scavenger and ultraviolet light. The basic principle of the photodegradation of organic dye compounds in water by TiO_2 can be depicted as follows [39]:

i. Once excited by light with energy larger than the band gap energy of TiO_2 (3.2 eV), electron-hole pairs generate and migrate to the surface to react with adsorbed organic dye reactants.

ii. The holes and electrons, together with other oxidizing species such as hydroxyl radicals resulting from the photochemical reactions, oxidize the organic pollutants to carbon dioxide, water and some simple mineral acids.

Photocatalytic oxidation reactions are initiated when a photon of higher energy level or equal to the band gap energy is absorbed by a TiO_2 catalyst which promotes an electron (e^-) from the valence band to the conduction band which simultaneously generates a positive hole (h^+) in the valence band [40].

Increasing the lifetime of the photo-produced pairs by hole and electron transfer between the two coupled semiconductors, has been seen in many cases as the key factor responsible for the improvement of the photoactivity of the reacting species. Photoactivity also strongly depends on other factors such as the bulk and surface physicochemical properties of the photocatalysts. These properties include type of phases, surface hydroxylation, porosity, surface area, adsorption capacity, distribution of the supported photoactive component, and surface acid-base properties [33].

Studies showed that, the degradation of dyes depends significantly on parameters such as catalyst loading, dye concentration, pH, and light intensity [13].

It has also been reported that, there is a general decrease in the rate of photodegradation of the dye with increasing dye concentration [39]. This was because, if the initial concentration of the dye is high, large amount of adsorbed dye would inhibit the reaction between the dye molecules

and the hydroxyl radicals. Furthermore, due to large amount of dye molecules within the solution, they contributes to the scattering of the light and decrease the photons reaching the TiO_2 surface, thus decreasing the photodegradation rate [39].

It is important to study the dependence of the photocatalytic reaction rate on the substrate concentration. It was reported in [13] that, there is general degradation rate increases with the increase in dye concentration to a certain level and then by further increase in dye concentration, a decrease in the degradation rate of the dye resulted.

Also, findings from [41] demonstrated that the rate of photocatalytic degradation of dye was increased on increasing the concentration of azure A up to 3.0×10^{-5} M. This observation may be due to the fact that as the concentration of dye was increased, more dye molecules were available for excitation and energy transfer and as a result, an increase in the rate of degradation of dye was observed. A decrease in rate was observed on increasing the concentration of dye above 3.0×10^{-5} M. This may be that, the dye now will start acting as an internal filter and it will not permit the desired light intensity to reach the surface of the semiconductor present at the bottom of the reaction vessel.

The amount of catalyst to be loaded in the dye solution is one of the main parameter for the degradation studies. The degradation efficiency normally increases with an increase in the catalyst loading up to certain limit. The photocatalytic destruction of many organic pollutants has also been reported to exhibit the same dependency on catalyst loading. The reason for this observation can be explained on the basis that optimum catalyst loading is found to be dependent on initial solute concentration. This is because, with an increase in catalyst loading, the total active surface area increases, hence there is availability of more active sites on catalyst surface.

The availability of active sites increases with the suspension of catalyst loading, but the light penetration is limited, and hence, the photo-activated volume of the suspension shrinks causing a decrease in percentage degradation. Another reason that might contribute to the decrease in percentage degradation may be that, at higher catalyst loading there may be deactivation of activated molecules by collision with ground state molecules [13].

In the study reported by Nan et. al (2014), there was an increase in photoactivity when the TiO_2–zeolite nanocomposites loading was increased and this was attributed to the higher number of active sites and more reactive radicals available for surface reaction [42]. However, the reduction in photoactivity of TiO_2–zeolite nanocomposites observed at higher catalysts loadings was attributed to the increasing cloudiness in the reaction solution that prevented the penetration from UV illumination [42].

Increasing the light intensity also increases the rate of photocatalytic degradation. This is because, as the intensity of light increases, the number of photons striking per unit area of the photocatalyst per unit time also increases [13],[41].

Photocatalytic degradation of dye increases with increase in pH up to a pH value of 7.5 and then decreases again with increase in pH above 7.5. This behaviour may be due to the increased availability of OH^- at higher pH values. By combining with holes, OH^- ions will generate more hydroxyl radicals (•OH), which are considered be one of the major species responsible for the photocatalytic degradation [13]. But above a pH value of 7.5, the increased number of OH^- ions may compete with the electron rich dye. Therefore, the OH^- ions will render the surface of the semiconductor negatively charged and as a result of repulsive force between the negatively charged species (OH^-) ions and the electron rich dye; the approach of dye molecules to the

semiconductor surface will be retarded. This will result in a decrease in the rate of photocatalytic degradation of dye [13],[41] .

CHAPTER THREE

3.0. Experimental Methods

3.1. Chemicals

All the reagents used in this work were of analytical grade and were used without any further purification. The reagents used in this work were Rhodamine B dye, Sudan III dye, Titanium tetrachloride ($TiCl_4$), Titanium isopropoxide (TTIP), isopropyl alcohol (IPA) and ethanol.

3.2. TiO_2 nanoparticles Synthesis

Sol gel and Hydrothermal methods were adopted to synthesize TiO_2 nanoparticles by using different metal alkoxide precursors.

3.2.1. Sol gel technique

In a typical synthesis of the nanoparticles (Figures 3.1 and 3.2), the precursor solution consisting of ($TiCl_4$) and absolute ethanol in the ratio of 1: 10 respectively, were subjected to vigorous stirring at 1200 rpm for 4 hours at room temperature to enhance the homogeneity and stability of the slurry.

The sol formed was aged at room temperature for 18 hours, ultrasonicated for 30 minutes and dried at 120°C for 7 hours. The as-prepared powder was then calcined at elevated temperatures of 200°C, 300°C, 400°C, 500°C, and 600°C for 2 hours to obtain the TiO_2 nanoparticles for analysis.

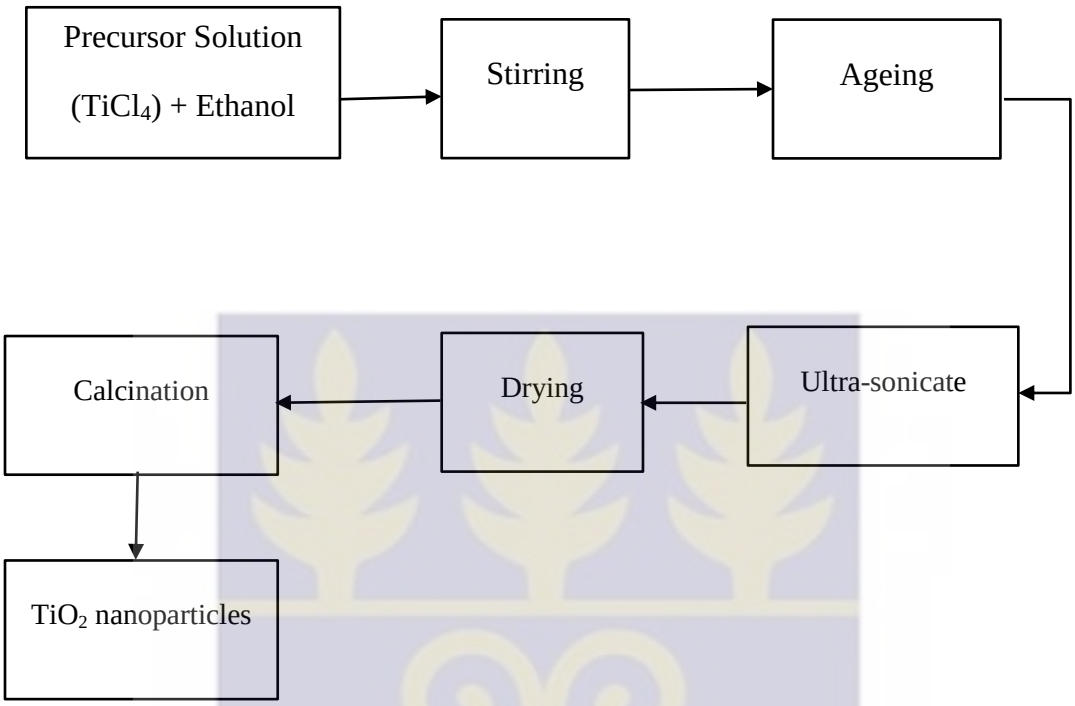

Figure 3.1: Preparation of TiO_2 nanoparticles via Sol gel method

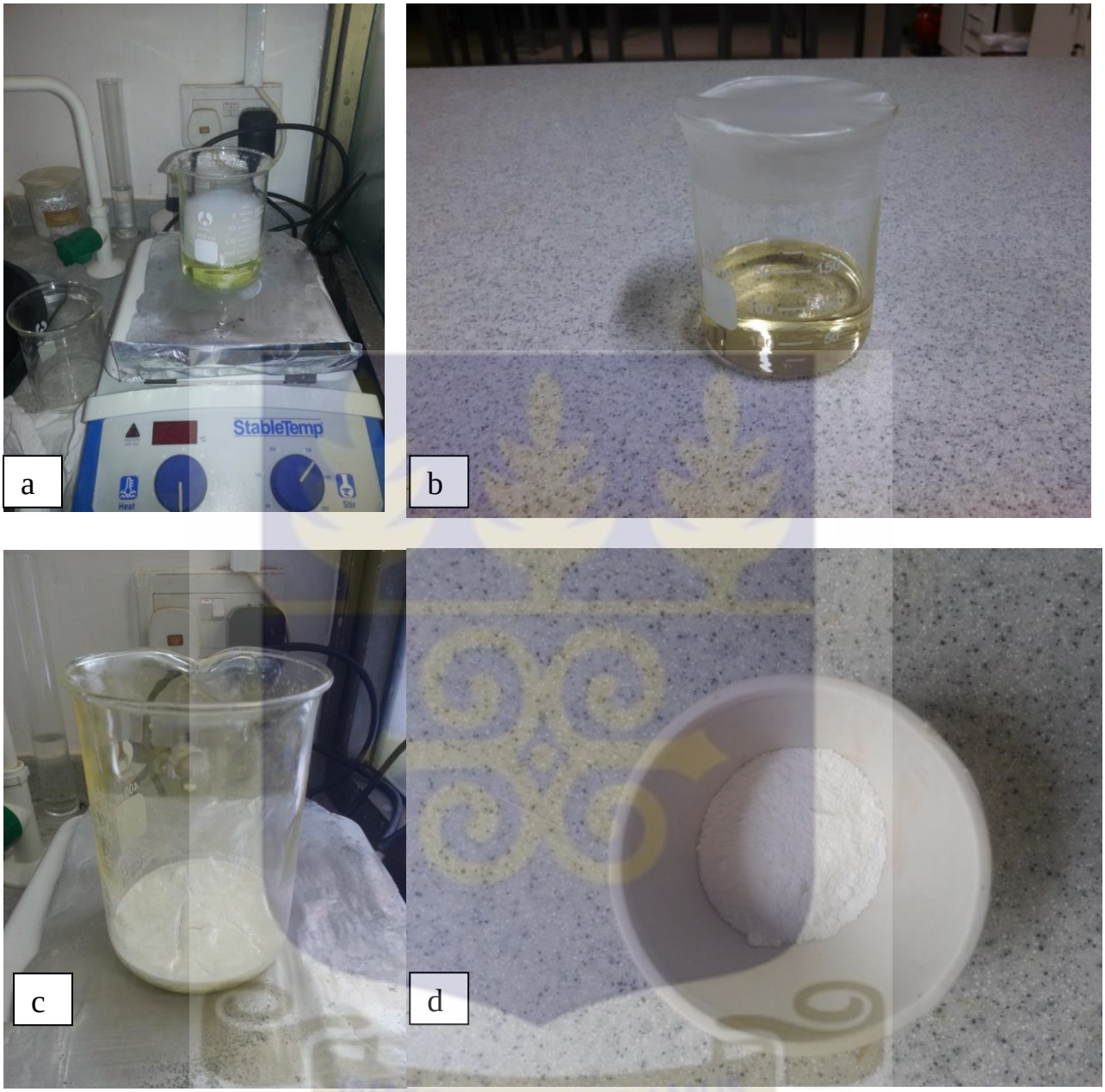

Figure 3.2: TiO_2 nanoparticles synthesis (a) Stirring process (b) Ageing process (c) As-prepared sample obtained after drying (d) Final calcined TiO_2 nanoparticles

3.2.2. Hydrothermal technique

In the synthesis of TiO_2 nanoparticles by the hydrothermal technique as demonstrated in Figure 3.3, 10 ml of TTIP was added to 100 ml of isopropyl alcohol and was subjected to a room

temperature stirring at 1200rpm. 10ml of distilled water was added slowly at a rate of 2 ml/min and the solution was subsequently stirred at 1200 rpm for 10 min.

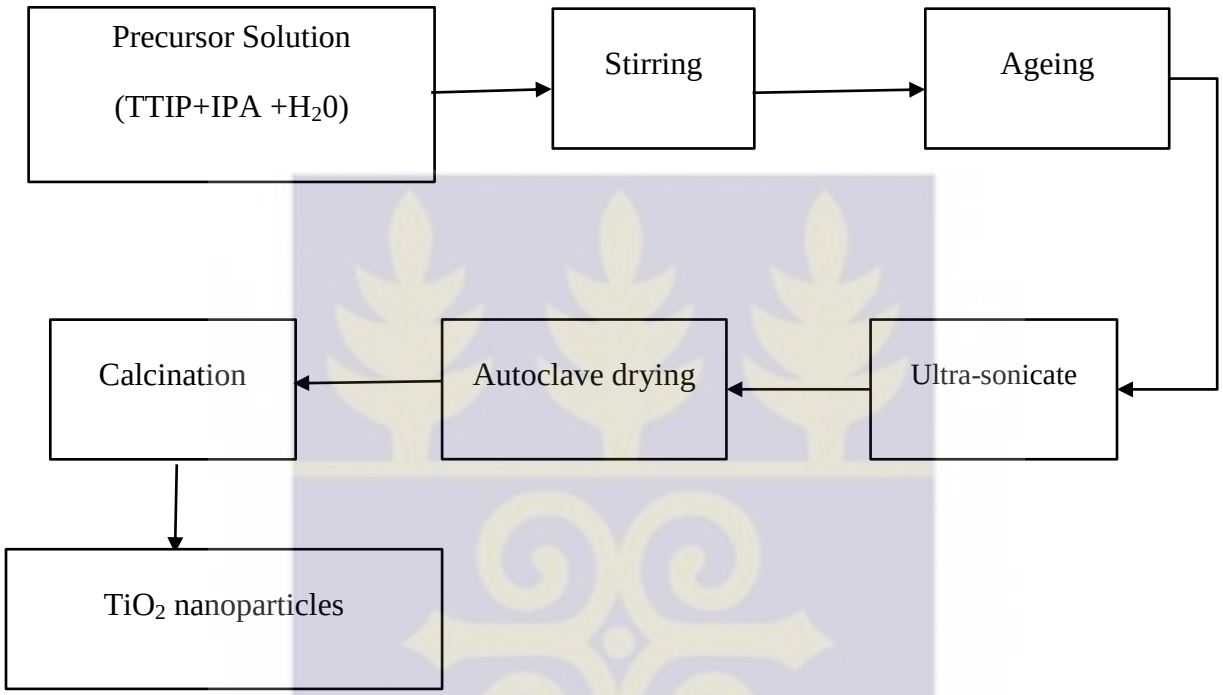

Figure 3.3: Preparation of TiO_2 nanoparticles via Hydrothermal method

The solution was then aged at room temperature for 24 hours. After ultrasonicating the sol for 10min it was transferred to Teflon steel autoclave at 15psi, 120°C for 8 hours. After cooling to room temperature, the as prepared TiO_2 nanoparticles was calcined at 200 °C, 300 °C, 400 °C, 500 °C and 600 °C for 2 hours to obtain the TiO_2 nanoparticles.

3.3. Characterization of TiO_2 nanoparticles

The as-produced nanoparticles are then characterized by X-Ray Diffraction (XRD), Scanning Electron Microscopy (SEM), Fourier Transform Infra-Red (FTIR), Brunauer–Emmett–Teller (*BET*) surface area analysis for their crystal structure, optical, microstructure, porosity and surface properties.

3.3.1. X-Ray Diffraction

To determine the phases present and the microstructure of the TiO_2 nanoparticles, X-ray powder diffraction (XRD) patterns were collected on an Empyrean diffractometer (Panalytical BV, Netherlands) with theta/theta geometry, operating Cu Kα radiation tube (λ = 1.5418 Å) at 40 kV and 45 mA as seen in Figure 3.4. The XRD patterns of all the randomly oriented powder specimens were recorded in the 20°- 70° 2θ range with a step size of 0.017°.

Figure 3.4: X- Ray Diffractometer

The diffraction patterns were matched against the ICSD's PDF database and qualitative phase analysis conducted using the X'Pert Highscore plus search match software (Panalytical, Netherlands). The instrumental resolution function was characterized with the NIST SRM 640d (Si) standard [43] and all peak profiles were simultaneously fitted with symmetrical pseudo-Voigt functions whose width and shape were constrained according to the Caglioti et al. (1958) formulae [44]. Microstructural analysis was performed using the Whole Powder Pattern Modelling (WPPM) method [45], with the aid of the PM2K software [46].

3.3.2. Scanning Electron Microscopy (SEM)

A high resolution Zeiss Ultra plus 55 field emission scanning electron microscope (FESEM) as shown in Figure 3.5 operated at 2.0 KV was used in the surface morphological investigations of the as-produced particles. Prior to the SEM analysis, the samples were metallized with carbon coating to render it conductive and were inserted into the sample place holder. They were then bombarded with a primary electron beam accelerated to 10 keV and the secondary electrons obtained were used to visualise the microstructure of the samples. The captured images were stored on the computer.

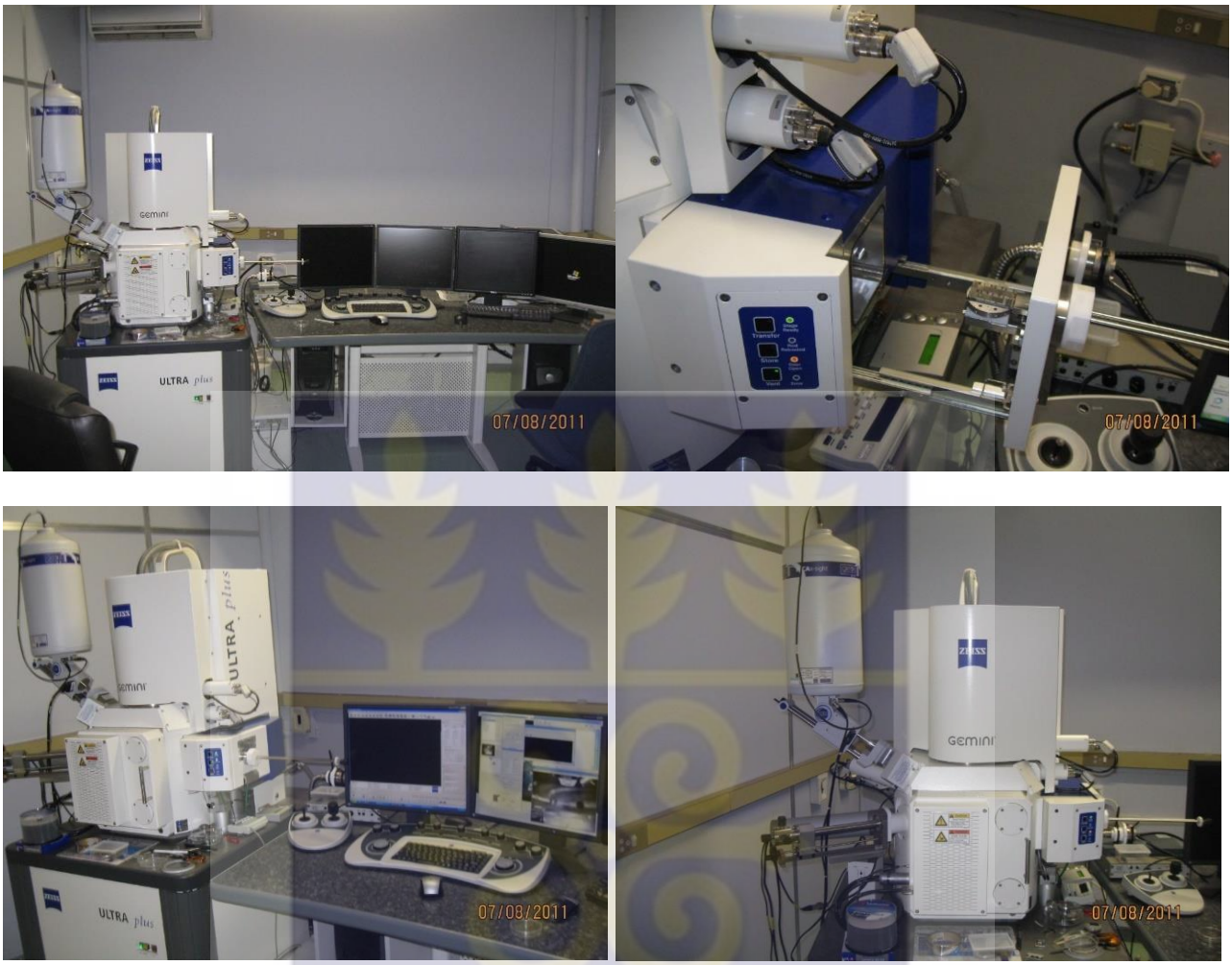

Figure 3.5: Field emission scanning electron microscope (FESEM)

3.3.3. Raman Spectroscopy

Raman spectroscopy data were collected on a Jobin Yvon Horiba TX 6400 micro-Raman spectrometer equipped with a triple monochromator system and LabSpec (Ver. 5.78.24) analytical software as shown in Figure 3.6. All the samples were analyzed with a 514 nm Argon excitation laser through an X 50 objective with acquisition time of 120 seconds and a resolution of 2 cm^{-1}.

Figure 3.6: Raman Spectroscopy

3.3.4. Brunauer Emmett Teller (BET) Characterization

Specific surface area (SSA) and porosity of the powders synthesized were measured by nitrogen chemisorption using and Accelerated Surface Area and Porosimetry System, model ASAP 2010 (Micromeritics Instrument Corporation) seen in Figure 3.7. The ASAP 2010 (Accelerated Surface Area and Porosimetry System) provides versatility in gas selection and high vacuum for

high-resolution low surface area measurements. It uses the principle of physical adsorption to obtain adsorption and desorption isotherms and information about the surface area and porosity of a solid material. It performs surface area analyses plus pore size and pore volume distributions, using nitrogen as the standard gas. The observations are interpreted following the model of Brunauer, Emmett and Teller (BET Method), or Langmuir, to calculate the surface areas, the average and total pore volume, the BJH pore size distribution and performs micro-pore analysis. Before the analysis all the samples (about 0.2 g) were outgassed at 300 °C in vacuum for 24 h. The data of the adsorption and desorption isotherms were used to evaluate the porosity of the samples.

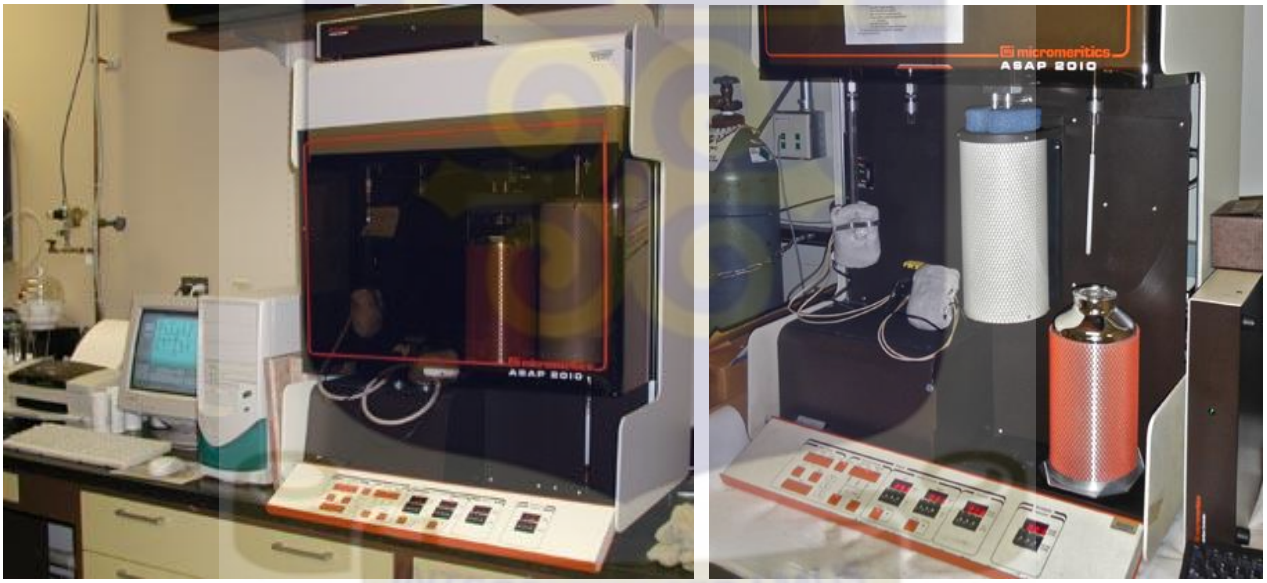

Figure 3.7: BET (ASAP system)

3.3.5. FTIR

Transmission FTIR spectra were recorded on a Vertex 70v (Bruker) spectrometer shown in Figure 3.8 in the 4000-400 cm^{-1} range with 4 cm^{-1} resolution. Sample compartment was

evacuated during acquisition and the contact between the sample and the diamond ATR crystal is 2 mm diameter. Spectra were recorded and analysed with the Opus software.

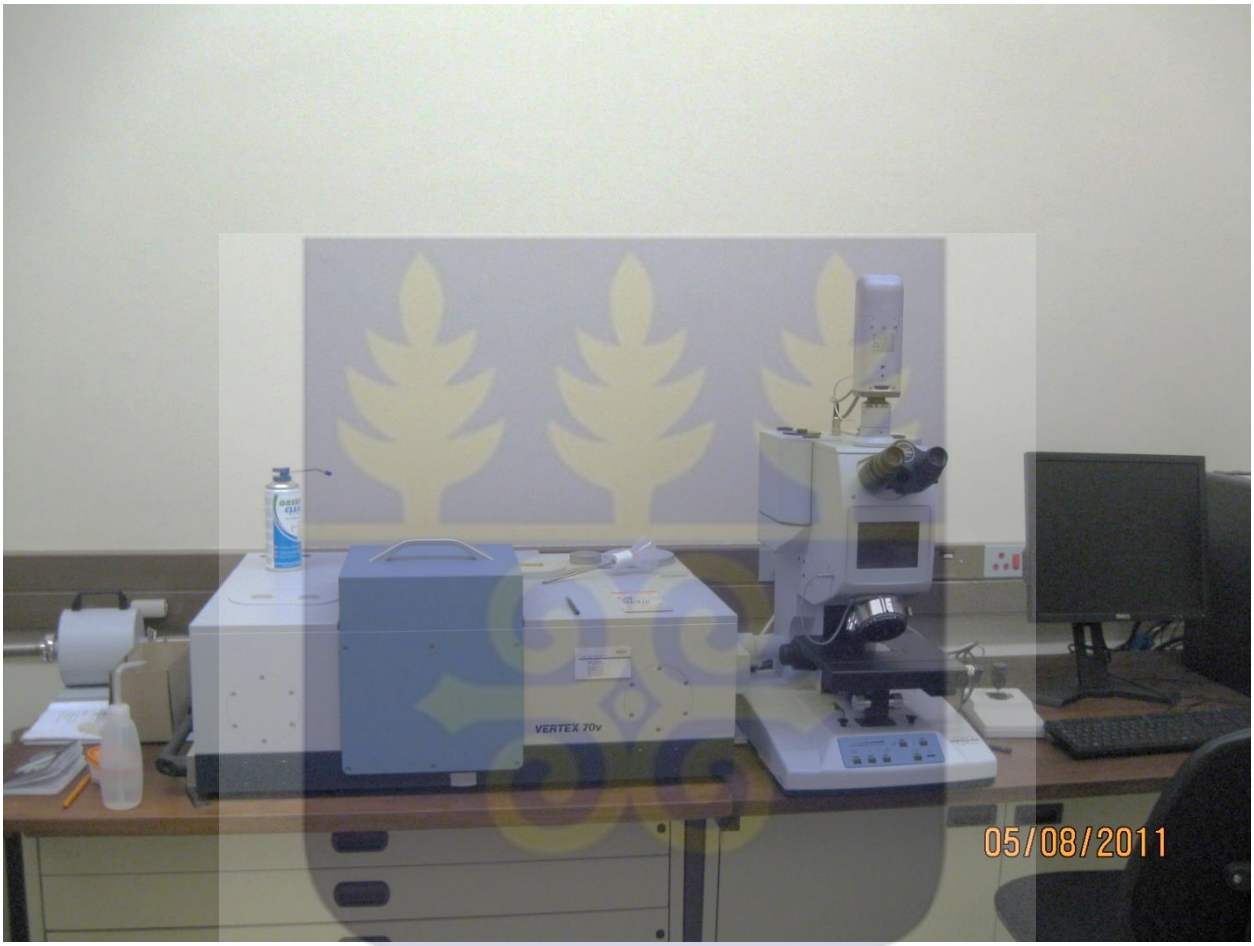

Figure 3.8: FTIR Spectrometer

3.4. Photocatalytic Experiment

The photocatalytic experiment was carried out according to the schematic diagram demonstrated in Figure 3.9.

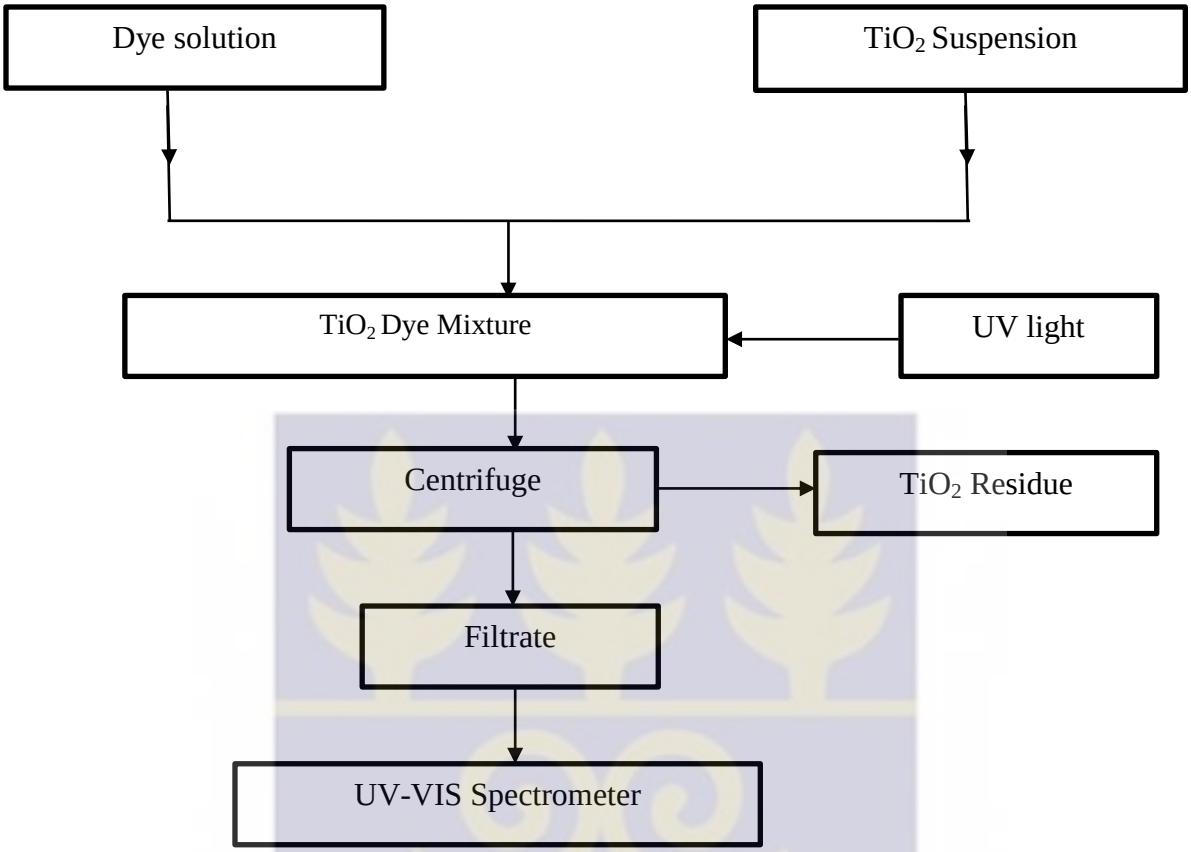

Figure 3.9:Photocatalytic Experimental Process

3.4.1. Rhodamine B dye Degradation

The Rhodamine B dye degradation experiment was carried out as follows:

i. 0.01 g of the Rhodamine B dye was mixed with 200ml of distilled water to obtain the dye solution.

ii. 0.1 g of TiO_2 was also mixed with 50ml of distilled water in a different beaker to obtain the TiO_2 suspension.

iii. 30 ml of the dye solution was then added to the prepared TiO_2 suspension.

iv. Prior to UV irradiation, the suspension was stirred in the dark room at 1000 rpm for 30 minutes for optimum adsorption.

v. After the 30minutes stirring in the dark room, it was then exposed to a UV light source. A benchtop UV transluminator with power rating of 330W was used as the UV light source in this work.

vi. Whiles this suspension was exposed to the UV light, 5 ml was withdrawn with syringe every 30 minutes.

vii. The aliquot was centrifuged at 5000 rpm for 10 minutes. This is necessary to ensure that any excess TiO_2 particles are separated from the dye solution.

viii. The supernatant was transferred into a cuvette and analyzed by a PelkinElmer Lambda 850 UV-Vis spectrometer to determine the absorbance over a wavelength range of 200 nm – 800 nm.

The various exposure times observed in this work were 0, 30, 60, 90, 120 and 150 minutes.

The concentration of the Rhodamine B dye solution was decreased and the photocatalytic procedure repeated as described above. In this case,

i. A mixture was obtained by mixing 0.01 g of the Rhodamine B dye with 400 ml of distilled water to obtain the dye solution.

ii. 0.1 g of TiO_2 was also mixed with 50 ml of distilled water in a different beaker to obtain the TiO_2 suspension.

iii. This was followed by the addition of 10 ml of the Rhodamine B dye solution to the 50 ml TiO_2 suspension.

iv. Prior to UV irradiation, the suspension was stirred in the dark room at 1000 rpm for 30 minutes.

v. After the 30 minutes stirring in the dark room, it was then exposed to a UV light operating at 330 W power.

vi. The described steps (steps vi, vii and viii) were repeated at this dye concentration to obtained the UV spectrum of the solution at different exposure times.

The parameters involved in the photocatalytic degradation of Rhodamine B dye solution are summarized in Table 3.1.

Table 3.1: Rhodamine B dye degradation parameters

Concentration of Rhodamine B dye solution (mol/dm^3)	**pH**	**Volume of Rhodamine B dye solution (ml)**	**Mass of TiO_2 catalyst (g)**	**Method of catalyst preparation**
3.8×10^{-5}	3.49	80	0.1	Sol gel
8.5×10^{-6}	4.02	60	0.1	Sol gel
3.8×10^{-5}	3.49	80	0.1	Hydrothermal
8.5×10^{-6}	4.02	60	0.1	Hydrothermal

3.4.2. Sudan III Dye Degradation

In Sudan III dye degradation experiment,

i. Sudan III dye solution was prepared by dissolving 0.8g of Sudan III dye in 400 ml isopropanol solution.

ii. Since sudan III is not completely soluble in isopropanol, the mixture was filtered and the filtrate was used as the dye solution for the photodegradation experiment.

iii. 50 ml of the prepared Sudan III dye solution was taken and mixed with 0.1 g of TiO_2 catalyst to obtain Sudan III – TiO_2 supension.

iv. Prior to UV irradiation, the suspension was stirred in the dark room at 1000 rpm for 30 minutes.

v. It was then exposed to a UV light with power rating of 330 W.

vi. Whiles this suspension was exposed to UV light, 5ml was withdrawn with syringe every 30 minutes

vii. The aliquot was centrifuged at 5000 rpm for 10 minutes.

viii. The supernatant was transferred into a cuvette and analyzed by a PelkinElmer Lambda 850 UV-vis spectrometer to determine the absorption over a wavelength range of 200nm – 800nm.

The various exposure times observed in this work were 0, 30, 60, 90, 120 and 150 minutes.

In another batch, 20ml of the prepared Sudan III dye solution was taken and mixed with 0.1ml of TiO_2 catalyst, and 30 ml isopropanol to obtain Sudan III – TiO_2 suspension. Procedures (iv - viii) were repeated to obtain the UV spectrum at different exposure times.

The concentration of the prepared Sudan III dye solution was further reduced and the experiment repeated. In this case, 5ml of the prepared Sudan III dye solution was taken and mixed with 0.1 g of TiO_2 catalyst, and 50 ml isopropanol to obtain Sudan III – TiO_2 suspension. Procedures (iv - viii) were repeated to obtain the UV spectrum at different exposure times.

The parameters involved in the photocatalytic degradation of Sudan III dye solution are summarized in Table 3.2.

Table 3.2: Sudan III dye degradation parameters

Concentration of Sudan III dye solution (mol/dm^3)	**pH**	**Volume of Sudan III dye solution (ml)**	**Volume of Isopropanol (ml)**	**Mass of TiO_2 catalyst (g)**	**Method of catalyst preparation**
5.7×10^{-3}	8.25	50	0	0.1	Sol gel
2.3×10^{-3}	4.5	20	30	0.1	Sol gel
5.2×10^{-4}	4.0	5	50	0.1	Sol gel
5.7×10^{-3}	8.25	50	0	0.1	Hydrothermal
2.3×10^{-3}	4.5	20	30	0.1	Hydrothermal
5.2×10^{-4}	4.0	5	50	0.1	Hydrothermal

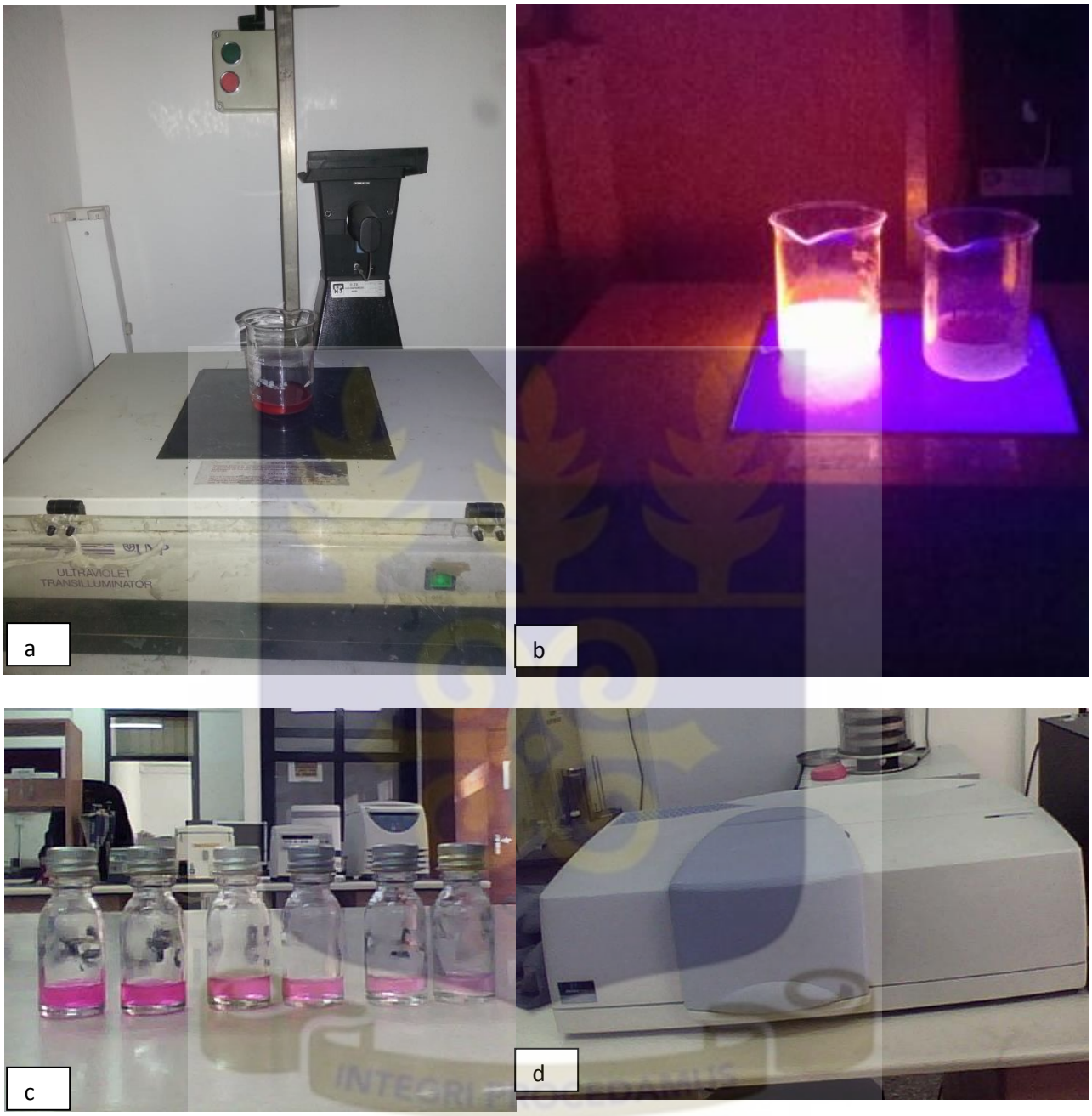

Figure 3.10:Photocatalytic Experiment: (a)Dye and TiO_2 suspension before exposing to UV light (b) Exposing to UV Light (c) degraded dye over time from 0 minute to 150 minute (d) UV-vis Spectrometer

CHAPTER FOUR

4.0. Results and Discussions

4.1. TiO_2 nanoparticles Preparation

In synthesis of TiO_2 nanoparticles by Hydrothermal techniques, alkoxides were hydrolysed in the presence of water and subsequently polymerized to obtain a three-dimensional oxide network. A colourless solution was obtained when the Titanium tetraisopropoxide (TTIP, $Ti(OCH(CH_3)_2)_4$) solution was reacted with isopropanol (IPA) but a white precipitate was formed when water was added dropwise. The reactions are presented as follows in Equations 4.1 - 4.3, starting from the reactions between the Titanium alkoxide (TTIP and IPA) and water.

$$Ti(OCH(CH_3)_2)_4 + 4H_2O \rightarrow Ti(OH)_4 + 4(CH_3)_2CHOH \quad (4.1)$$

$$Ti(OH)_4 \rightarrow TiO_2.xH_2O + (2-x)H_2O \quad (4.2)$$

$$TiO_2xH_2O \xrightarrow{heat} TiO_2 \quad (4.3)$$

Equations 4.1. and 4.2 shows the hydrolysis and condensation reactions respectively [33]. Calcining the samples at various temperatures gave the resultant TiO_2 nanoparticles as illustrated by Equation 4.3.

In the Sol gel processing of TiO_2 nanoparticles, the reaction kinetics are described in Equations 4.4 and 4.5. The hydrolysis reaction was initiated when the Titanium tetrachloride precursor was reacted with absolute ethanol to form the sol. In this process hydrochloric acid gas was seen expelled from the reaction mixture (Figure 3.2 (a)) and a yellow suspension was seen after 2

hours. After the Titanium organic compound obtained was heat treated, white powdered TiO_2 nanoparticles were obtained as the hydrocarbon components were expelled through the heat treatment process.

$$TiCl_4 + 4C_2H_5OH \rightarrow Ti(C_2H_5O)_4 + 4HCl \quad (4.4)$$

$$Ti(C_2H_5O)_4 \xrightarrow{heat} TiO_2 + hydrocarbons \quad (4.5)$$

4.2. XRD Analysis

XRD pattern of the samples at various calcination temperatures are presented. Whole Powder Profile Modelling using PM2K software was used to analyze the TiO_2 nanoparticles prepared.

The grain sizes of the prepared TiO_2 nanoparticles at various treatments were obtained by XRD as the particle size is related to the broadening of the diffraction peak [30]. This technique was also used in the determination of the crystalline phases of the nanoparticles at various temperature treatments.

The XRD patterns (Figure 4.1(c)) of the TiO_2 nanoparticles synthesized by sol gel showed that Anatase phase of TiO_2 nanoparticles were produced. The as-prepared nanoparticles had broader peaks but when it was calcined at 200°C, 300°C, 400°C, 500°C and 600°C, the peaks became narrower with increasing calcination temperature. However, the as-prepared nanoparticles without any temperature treatment were amorphous, hence distinct crystalline peaks were not seen in the XRD pattern obtained (Figure 4.1(a)). The as-prepared TiO_2 nanoparticles also showed broader peaks as a result of smaller grain sizes.

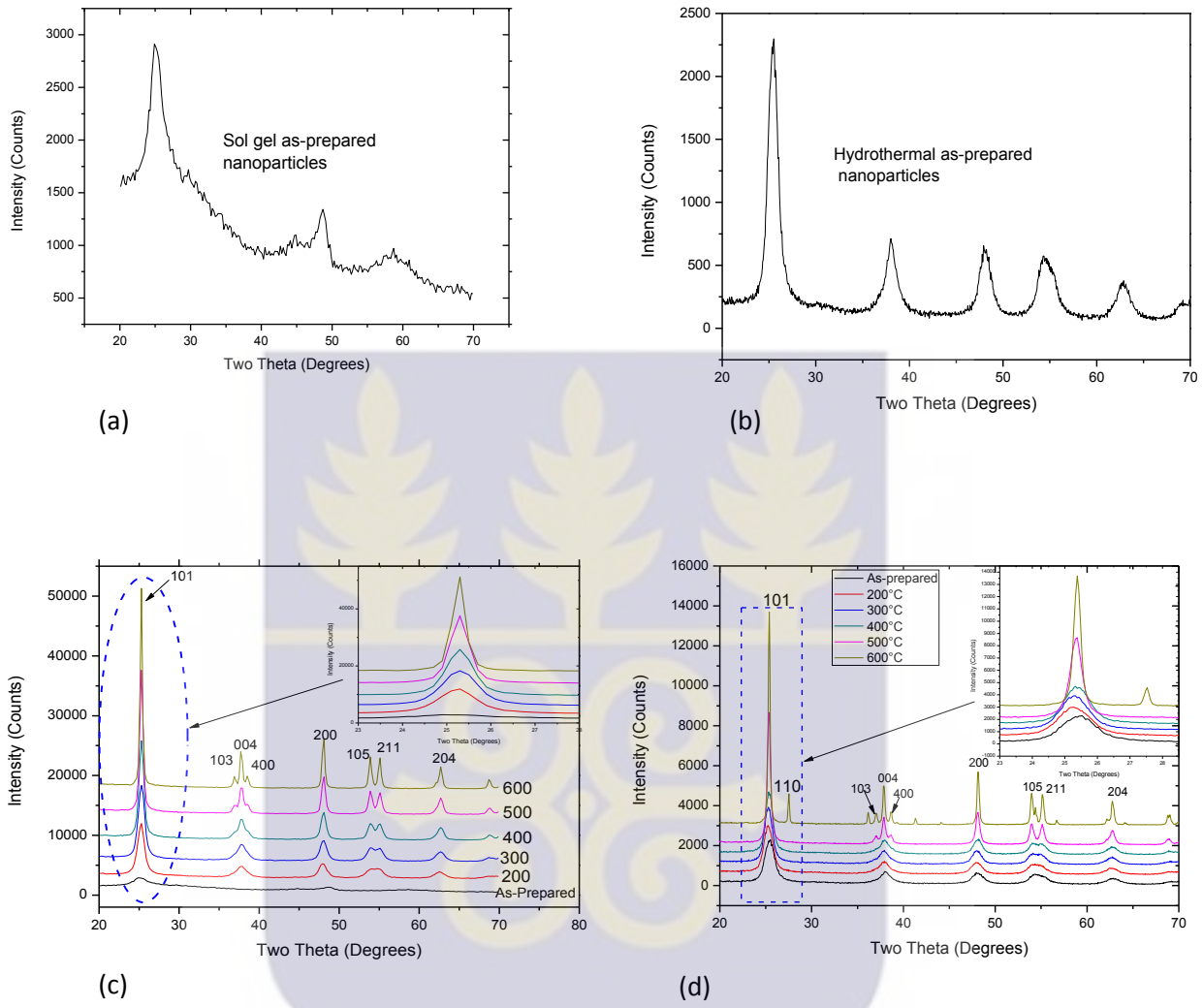

Figure 4.1: XRD Pattern (a) Sol gel as-prepared nanoparticles (b) Hydrothermal as-prepared nanoparticles (c) Stacked plot of TiO_2 nanoparticles prepared by sol gel method (d) Stacked plot of TiO_2 nanoparticles prepared by Hydrothermal method

It was seen that the major peaks were sharper as the calcination temperature was increased and this shows that the crystallinity of the TiO_2 was higher with increasing temperature [30].

The peaks in [101] direction of the prepared nanoparticles as highlighted in Figure 4.1(a) showed no distinct crystalline peak, in the as-prepared nanoparticles. But at 200°C (Figure 4.1(c) and Figure 4.1(d)) a broad distinct peak was seen and this peak became narrower and sharper as the

temperature treatment was increased further up to 600°C. This observation could be attributed to the crystalline behavior of the nanoparticles introduced into the structure of the nanoparticles by temperature. This effect also affects the particle sizes as crystallinity and crystallite size of the nanoparticles increased as a function of temperature [30]

The strong and intense diffraction peaks identified at 25.3° and 48.1° in the direction of [101] and [200] confirms that an Anatase TiO_2 structure is formed. The intense and sharp XRD peaks of the nanoparticles also showed that the formed TiO_2 nanoparticles are crystalline and broad diffraction peaks indicates small crystallite size [31]. Also, there was no peak identified in the [110] direction when the nanoparticles were synthesized by Sol gel method and this confirmed that the TiO_2 nanoparticles synthesized by this method with the stated temperature treatments produced a pure Anatase phase of TiO_2 nanoparticles.

Figure 4.1(b). shows broad distinct peaks in the as-prepared TiO_2 nanoparticles. These peaks were seen becoming narrower and sharper when the calcination temperature was increased as seen in Figure 4.1 (d). Analyzed results of TiO_2 nanoparticles synthesized by the Hydrothermal technique showed that Anatase phase was obtained in the as-prepared powder as well as the samples calcined at 200°C, 300°C, 400°C and 500°C However, when the calcination temperature was increased to 600°C, rutile phase, confirmed by the diffraction peak in [110] direction, which is a more stable phase at high temperatures was seen (Figure 4.2). This was seen as the peaks labelled **R**, whereas the Anatase phase direction is labelled as **A**. This observation was in agreement with Ba-abbad et. al (2012) [40]. It was expected that, the rutile phase peaks would increase in intensity with increasing annealing temperature since temperature increases the stability of the rutile phases of TiO_2.

These rutile phase peaks were not seen when the as-prepared TiO_2 nanoparticles were calcined at 200°C, 300°C, 400°C, and 500°C. This was because, those temperatures were not high enough to initiate the rutile phase formation.

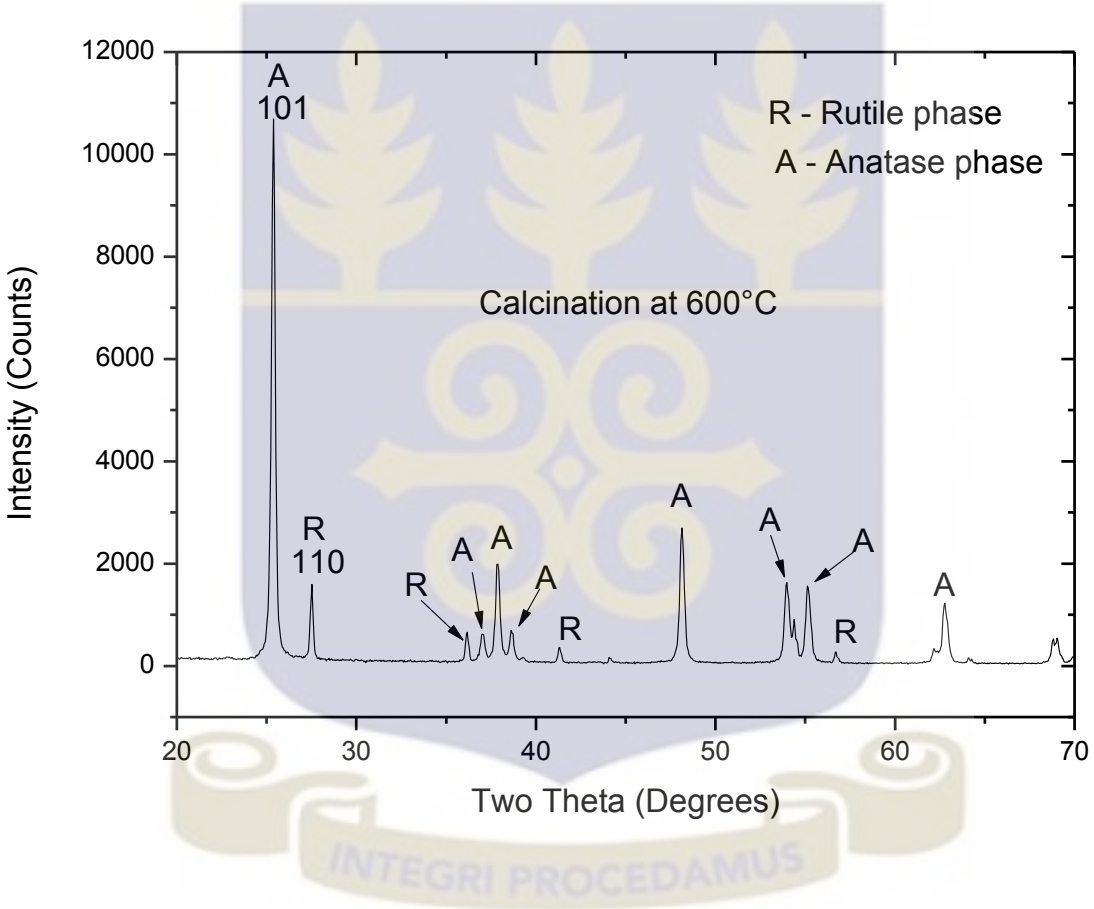

Figure 4.2: XRD diffraction pattern Hydrothermal prepared TiO_2 calcined at 600°C showing Rutile and Anatase phases

The amount of anatase and rutile phases of TiO_2 nanoparticles prepared by hydrothermal route and calcined at 600 °C was calculated using Equation 4.6:

$$X_A = \frac{100}{1+(1.265 I_R / I_A)} \quad (4.6)$$

Where X_A is the weight fraction of anatase phase, I_A and I_R are intensities of anatase (101) and rutile (110) diffraction, respectively [40].

Table 4.1 summarizes the prepared TiO2 nanoparticles parameters and the resulting average grain sizes and phases.

Table .4.1: Summary of prepared TiO_2 nanoparticles properties

Sample ID	**Annealing Temperature**	**Grain size (nm)**	**Anatase phase (%)**	**Rutile phase (%)**
HT_As	As-prepared	4.95	100	0
HT_200	200°C	5.87	100	0
HT_300	300°C	7.14	100	0
HT_400	400°C	11.49	100	0
HT_500	500°C	14.98	100	0
HT_600	600°C	30.58	**85**	**15**
SG_As	As-prepared	2	100	0
SG_200	200°C	5.40	100	0
SG_300	300°C	7.25	100	0
SG_400	400°C	9.87	100	0

SG_500	500°C	14.84	100	0
SG_600	600°C	22.58	100	0

From Table 4.1, all the samples prepared by both Sol gel and Hydrothermal techniques were pure anatase (ie. 100 % anatase phase) except the sample synthesized by Hydrothermal method and heat treated at 600 °C which had 85 % of anatase phase present and 15 % of rutile phase present according to Equation 4.6. It was expected that, by further elevating the calcination temperatures, the rutile phase would have increased since this phase is more stable at higher temperatures.

XRD patterns obtained fitted well when modelled by Whole Powder Pattern Modelling (WPPM) method with the aid of the PM2K software. The modelled XRD patterns of the synthesized samples by Hydrothermal and Sol gel methods are shown in Figures 4.3 and Figure 4.4, respectively

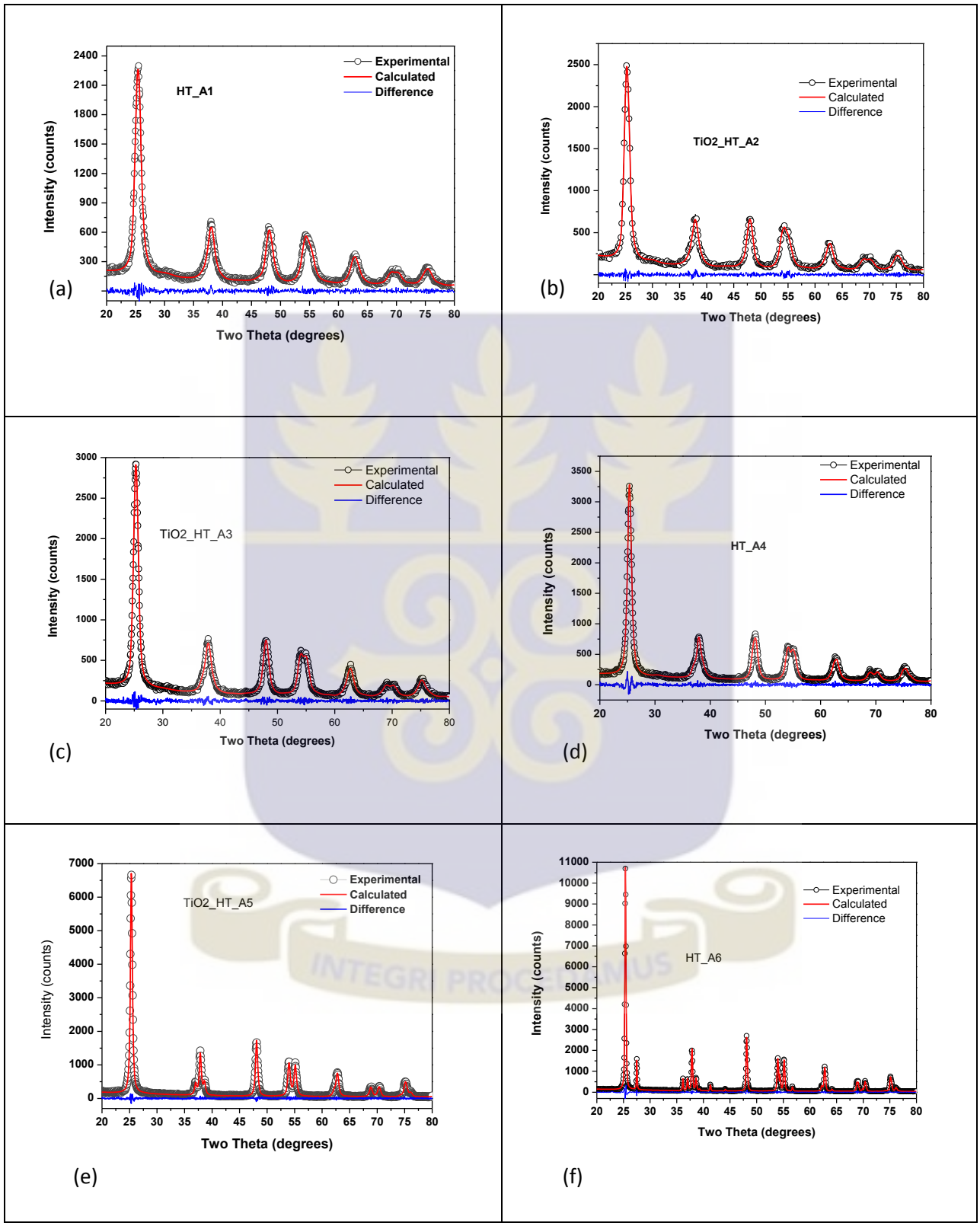

Figure 4.3: Modelled XRD of TiO_2 nanoparticles synthesized by Hydrothermal method (a) as-prepared (b) calcined at 200 °C (c) calcined at 300 °C (d) calcined at 400°C (e) calcined at 500 °C (f) calcined at 600°C

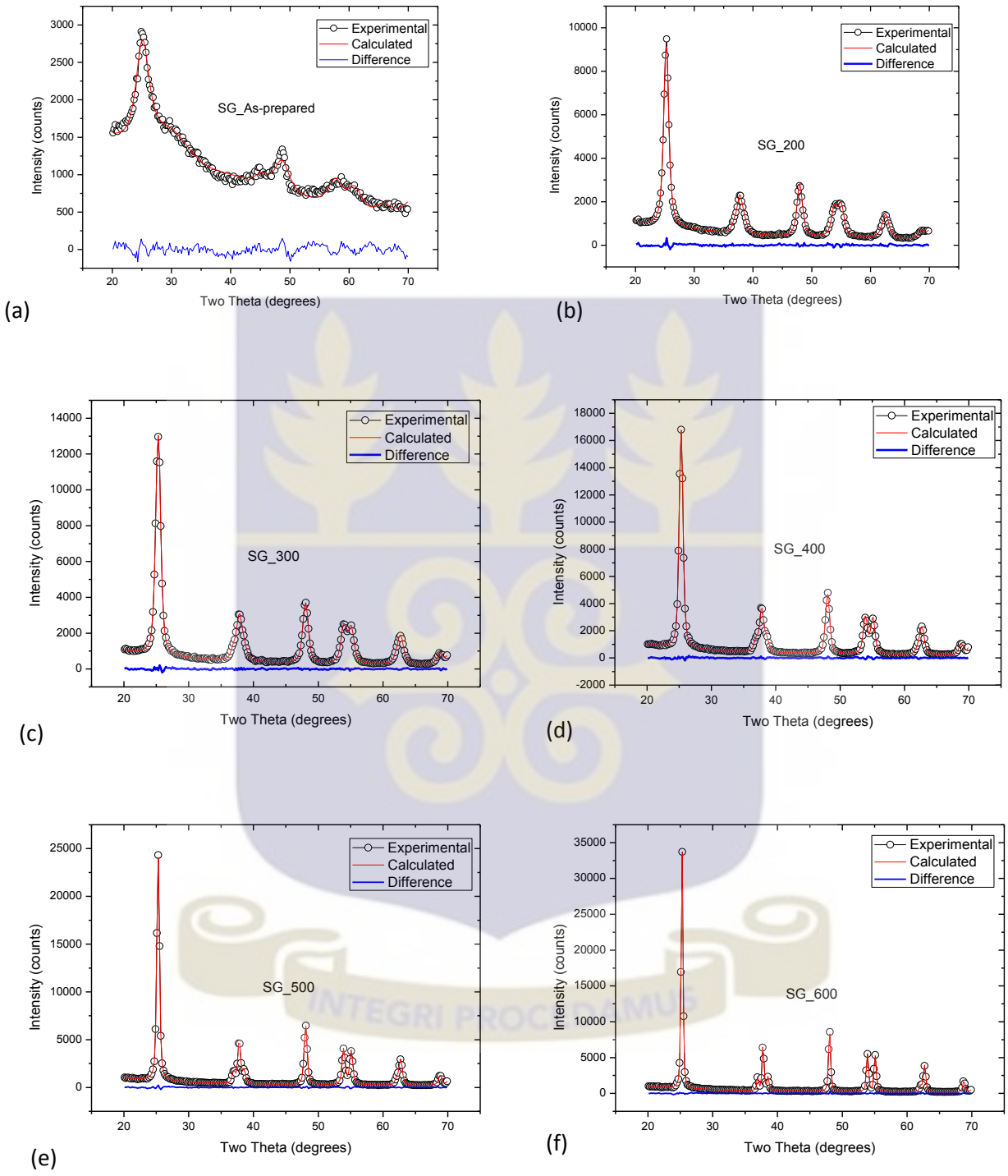

Figure 4.4: Modelled XRD of TiO_2 nanoparticles synthesized by Sol gel method (a) as-prepared (b) calcined at 200 °C (c) calcined at 300 °C (d) calcined at 400 °C (e) calcined at 500 °C (f) calcined at 600°C

4.3. Particle Size analysis

The XRD data obtained on the synthesized TiO_2 nanoparticles were modelled and the particle sizes of the prepared TiO_2 nanoparticles were investigated. The grain size as a function of annealing temperature for the Sol gel and Hydrothermal prepared TiO_2 nanoparticles are shown in Figure 4.5 and Figure 4.6 respectively.

By using Whole Powder Pattern Modelling (WPPM) method with the aid of the PM2K software to estimate the average grain sizes at the respective calcination temperatures, the as-prepared TiO_2 nanoparticles synthesized by the sol gel method obtained an average grain size of 2nm (Figure 4.5). This grain size increased to approximately 5nm when it was annealed at 200°C. There was a gradual increase in grain size when the annealing temperature was increased up to 400°C. However, there was a dramatic increase in grain size when the annealing temperature was elevated further as it can be seen in the sample annealed at 600°C. This may be due to the enhanced grain growth resulting from this temperature treatment.

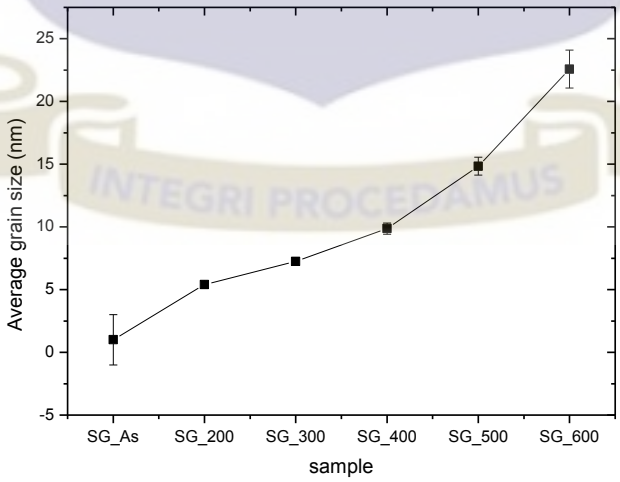

Figure 4.5: Average grain size as a function of temperature of TiO_2 catalyst prepared by Sol gel route

In the case of the TiO_2 nanoparticles synthesized by the Hydrothermal method, the as-prepared nanoparticles grain was approximately 5nm. The grain size increased gradually when it was annealed at 200 °C, 300 °C, 400 °C and 500 °C as seen in Figure 4.6. At 600 °C annealing temperature, the grain size increased to 31nm. Comparing the average grain size of the samples annealed at 500 °C which is about 15nm, and 600 °C which is about 31 nm there was about 100 % increase in grain size between these annealing temperatures. This observation could be attributed to grain growth as a result of increase in annealing temperature as well as the phase transformation from the anatase phase to the rutile phase at 600 °C.

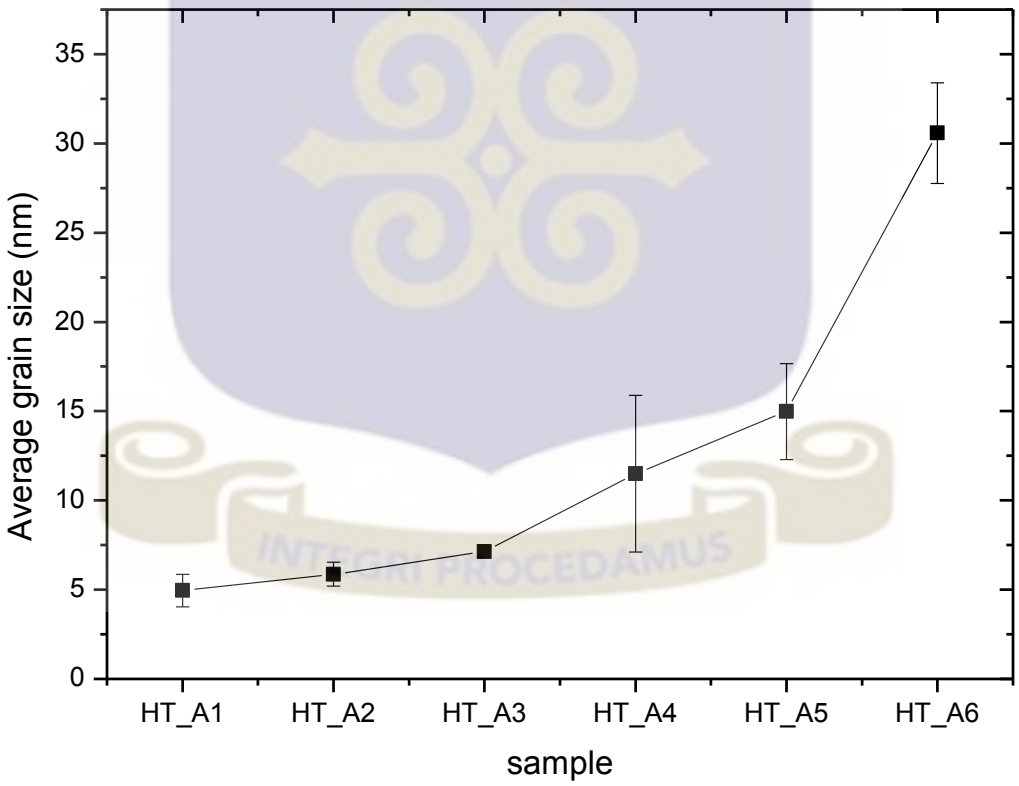

Figure 4.6:Average grain size as a function of temperature of TiO_2 catalyst prepared by Hydrothermal route

4.3.1. Particle Size Distribution

The Figure 4.7 shows the lognormal size distribution of TiO_2 nanoparticles prepared via the hydrothermal technique.

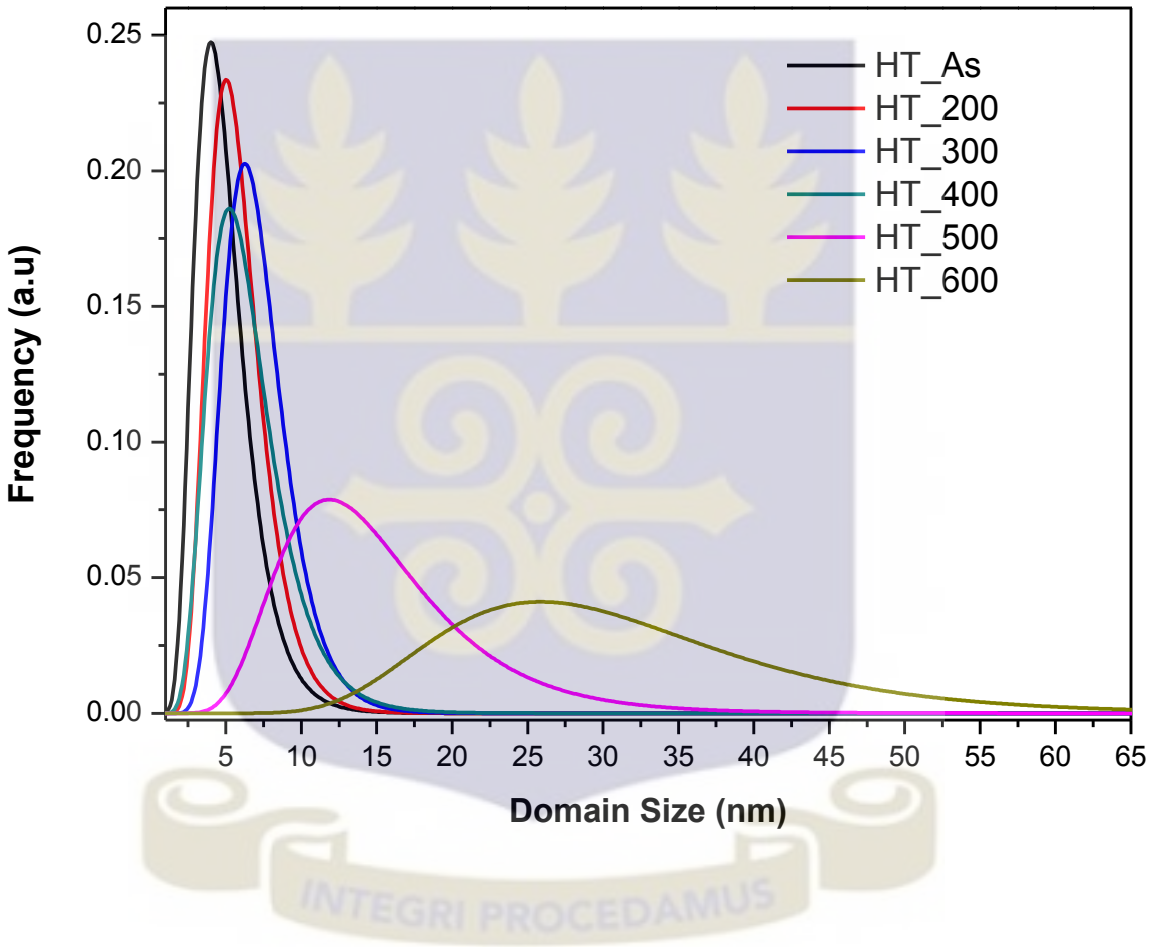

Figure 4.7: Lognormal size distribution of Hydrothermal synthesized TiO_2 nanoparticles

It shows clearly a narrow frequency peak around 5nm domain size for the as-prepared TiO_2 nanoparticles**.** The domain size increased and broadened slightly as the calcination temperature was raised up to 400 °C with the domain size distribution revealed to be between 1 – 15nm. However, the domain size increased and broadened drastically over a wide particle size

distribution when the calcination temperatures were increased to 500°C and 600°C respectively. It was therefore proven that the there was a wide particle size distribution as the temperature was increased as well as a general increase in particle size with temperature

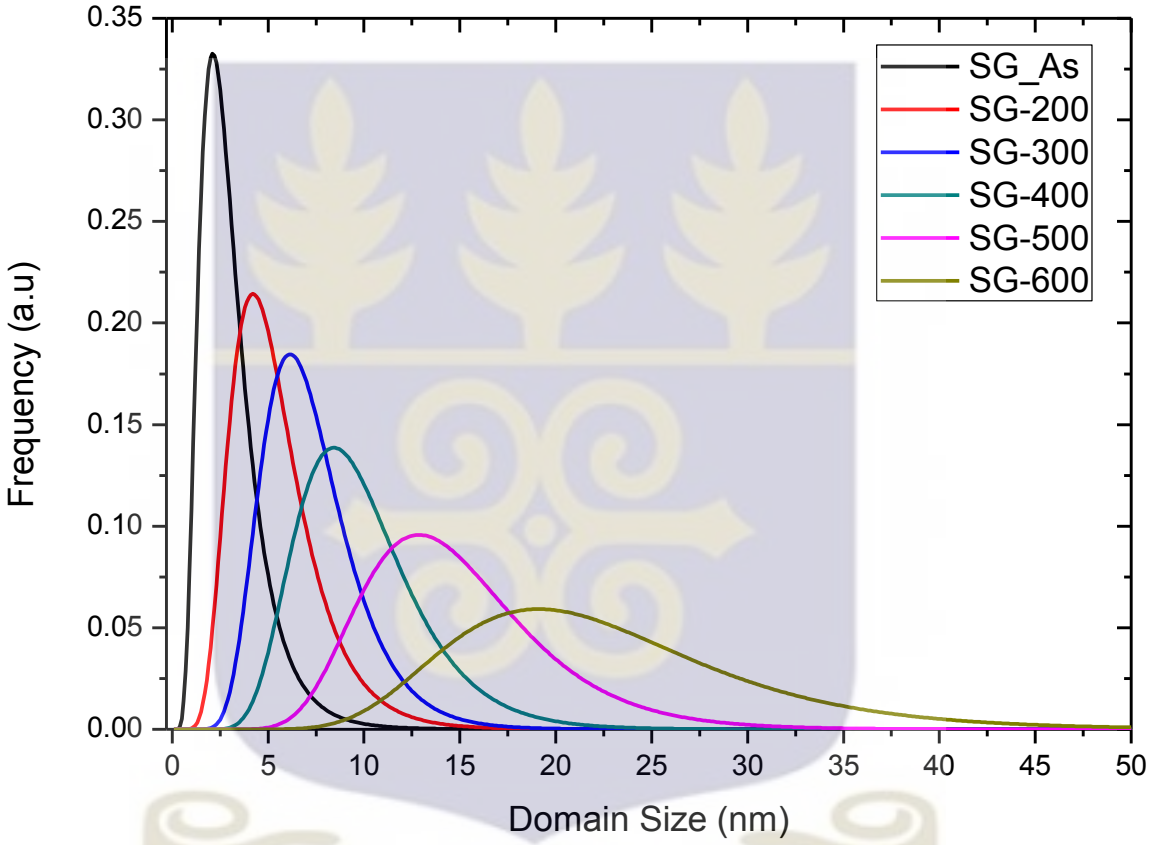

Figure 4.8: Lognormal size distribution of Sol gel synthesized TiO_2 nanoparticles

The Lognormal size distribution of the nanoparticles synthesized by Sol gel as shown in Figure 4.8 also demonstrates a general widening of particle size distribution with increasing temperature. The peak of each distribution normal gives the average grain size of the synthesized TiO_2 nanoparticles. It was also clearly demonstrated that the average grain size was increased as

the calcination temperature was increased. The as prepared TiO_2 nanoparticles which exhibited a highly amorphous nature (confirmed by XRD Figure 4.1(a)) showed an average grain size of 2nm. The grain size increased gradually as well as broadening of the particle size distribution with increasing calcination temperature

4.3.2. Shift in Lattice Parameters (a, b and c) size as a Function of Grain Size Growth

The lattice parameters (a, b and c) of TiO_2 crystal structure prepared by Hydrothermal method changed in size at different temperature treatment as seen in Figures 4.9.

There was a general decrease in lattice parameter, ***a***, as the particle size increased and this observation was in agreement with Gamarnik et. al (1992). However, there was a general increase in lattice parameters, b and c size as the particle size of the TiO_2 nanoparticles increased. The change and crystal lattice parameters could be attributed to surplus or deficit in the internal stress and intracrystalline pressure (IP) which occurs when the particles get smaller. This phenomenon introduces deformations into the crystal structure resulting in the changes in lattice parameters as the particle size changes[47].

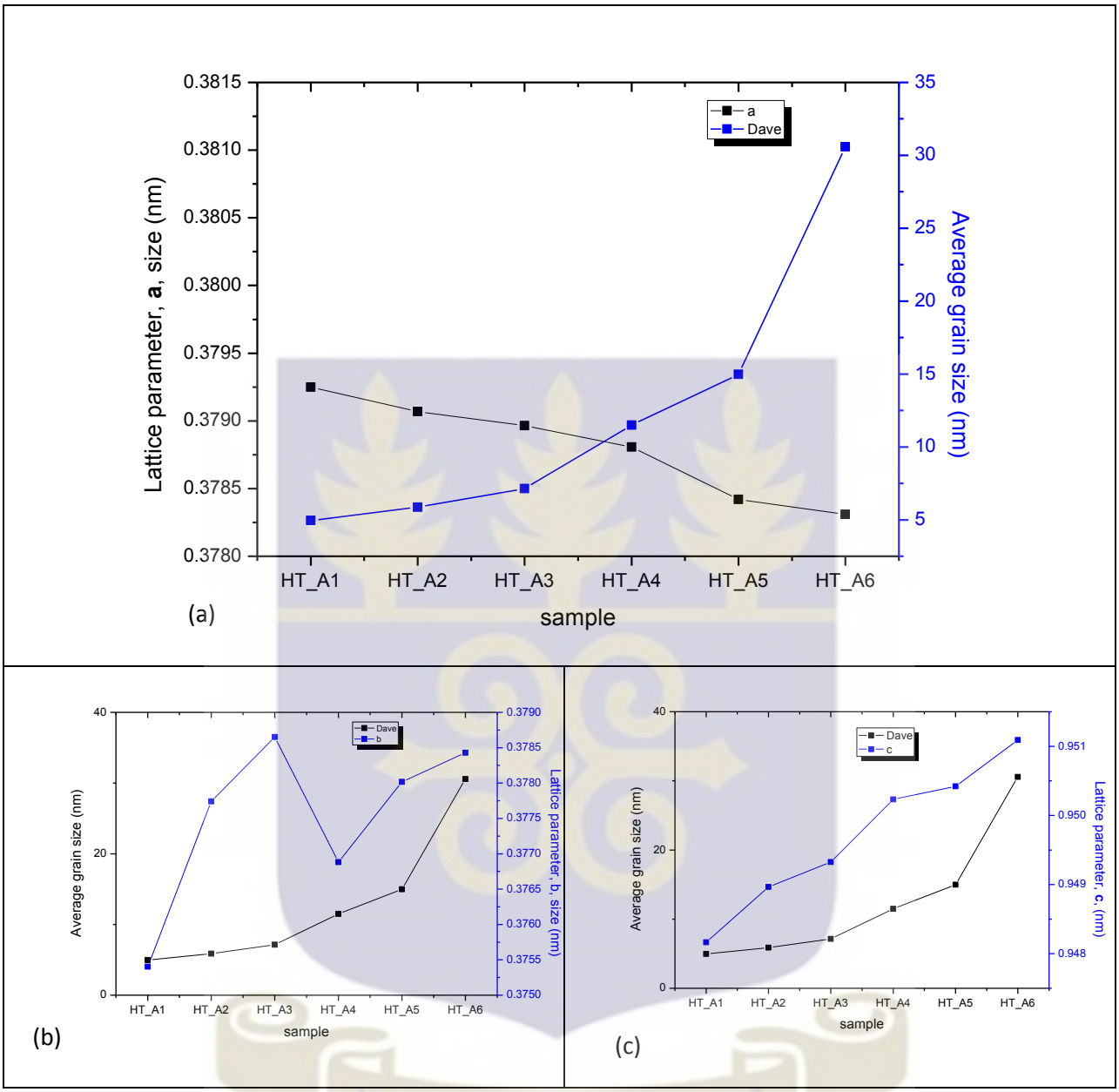

Figure 4.9: Size change in lattice parameters at different calcination temperatures of TiO_2 catalyst prepared by hydrothermal route (a) Lattice parameter, a (b) Lattice parameter, b (c) Lattice parameter, c

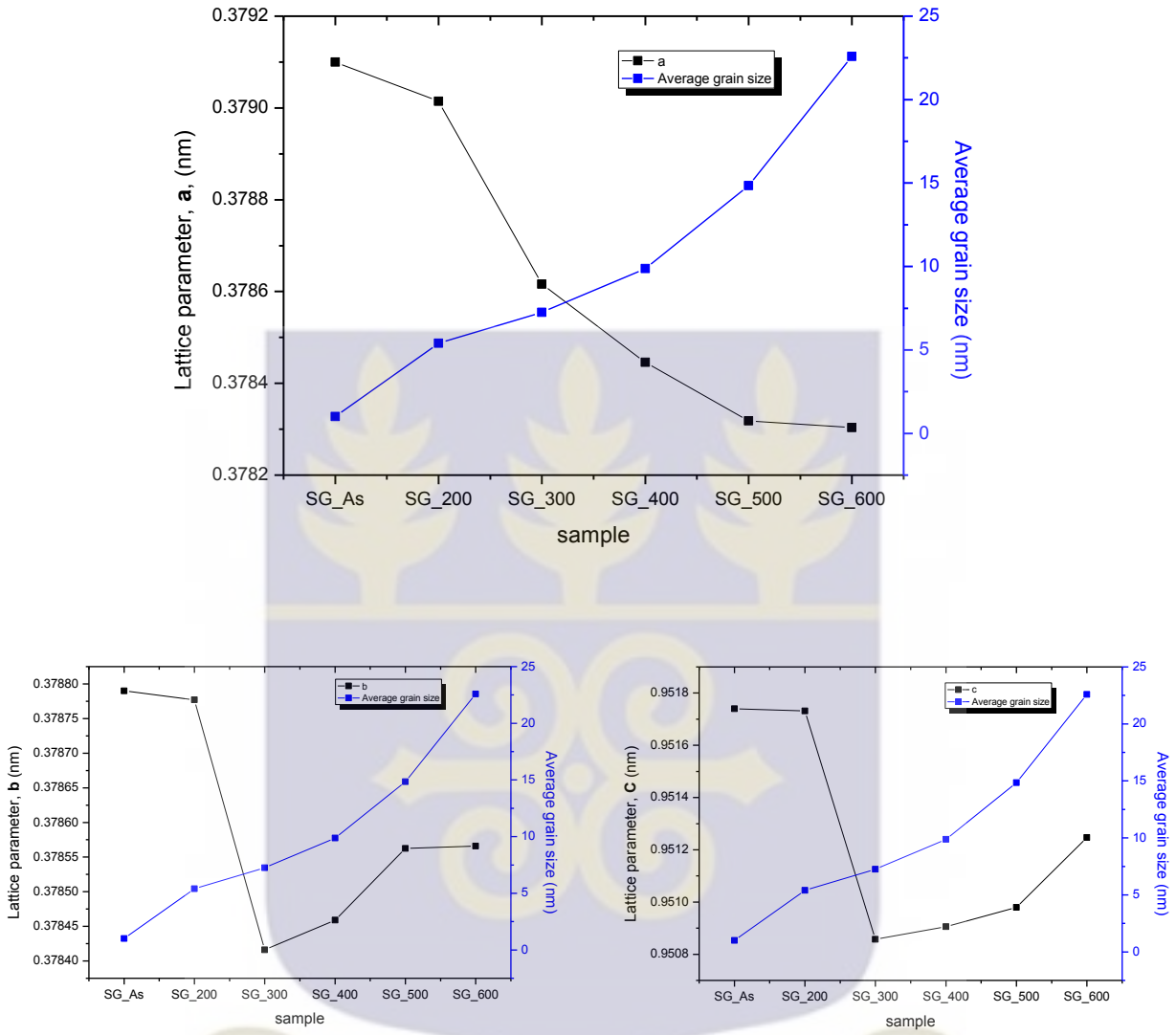

Figure 4.10: Size change in lattice parameters at different calcination temperature of TiO_2 catalyst prepared by Sol gel route (a) Lattice parameter, a (b) Lattice parameter, b (c) Lattice parameter, c

TiO_2 nanoparticles synthesized by Sol gel method showed a decrease in lattice parameter, ***a***, as the grain size increased as a result of increase in calcination temperature and grain size as seen in Figure 4.10. Lattice parameter, ***b*** and ***c***, showed a decrease in size when calcined up to 300° but

increased in size gradually when the calcination temperatures were increased to 400°C, 500°C and 600°C.

4.4. Fourier Transform Infra-Red Analysis

Fourier Transform Infra – Red spectroscopy was conducted on the synthesized nanoparticles to estimate the absorption of the incident light rays with respect to the wavelength of the incident beam. High energy spectrum was bombarded onto the sample to cause bending and stretching within the material.

Fourier Transform Infra-Red spectrum on the TiO_2 prepared by Sol gel method (Figure 4.11) showed a broad band around 3228cm^{-1} which is attributed to O-H stretching mode of the surface and adsorbed water molecules. The other peaks at 1635 cm^{-1} were indicated to the stretching of titanium carboxilate, which were formed from $TICl_4$ and ethanol precursors. The band between 800 and 414cm^{-1} was as a result of Ti-O bond stretching mode of the anatase polymorph of the TiO_2 [48].

After calcining the TiO_2 nanoparticles at different temperature, almost all the peaks of the hydroxyl and the carboxilate disappeared. Only the strong absorption between 800 and 410 cm^{-1} remained, which were attributed to obtained TiO_2 nanoparticles [40] .

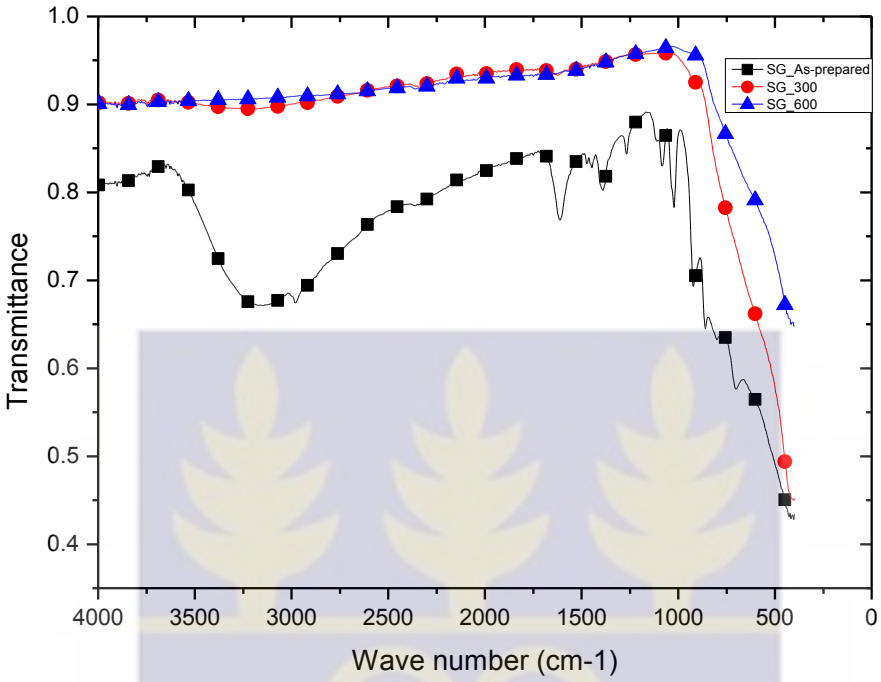

Figure 4.11: FTIR spectra of TiO_2 nanoparticles prepared by Sol gel method

4.5. Raman Spectroscopy

Better insight into the synthesized nanostructured TiO_2 was gained by Raman spectroscopy. The TiO_2 nanoparticles synthesized by the Sol gel method showed intense raman peaks at 395 cm^{-1}, 515 cm^{-1} and 638 cm^{-1}. The observed Raman spectra indicates that the TiO_2 nanoparticles prepared and calcined at 200 °C, 300 °C, 400 °C, 500 °C and 600 °C were of anatase phase in accordance with XRD results in Figure 4.12 [49].

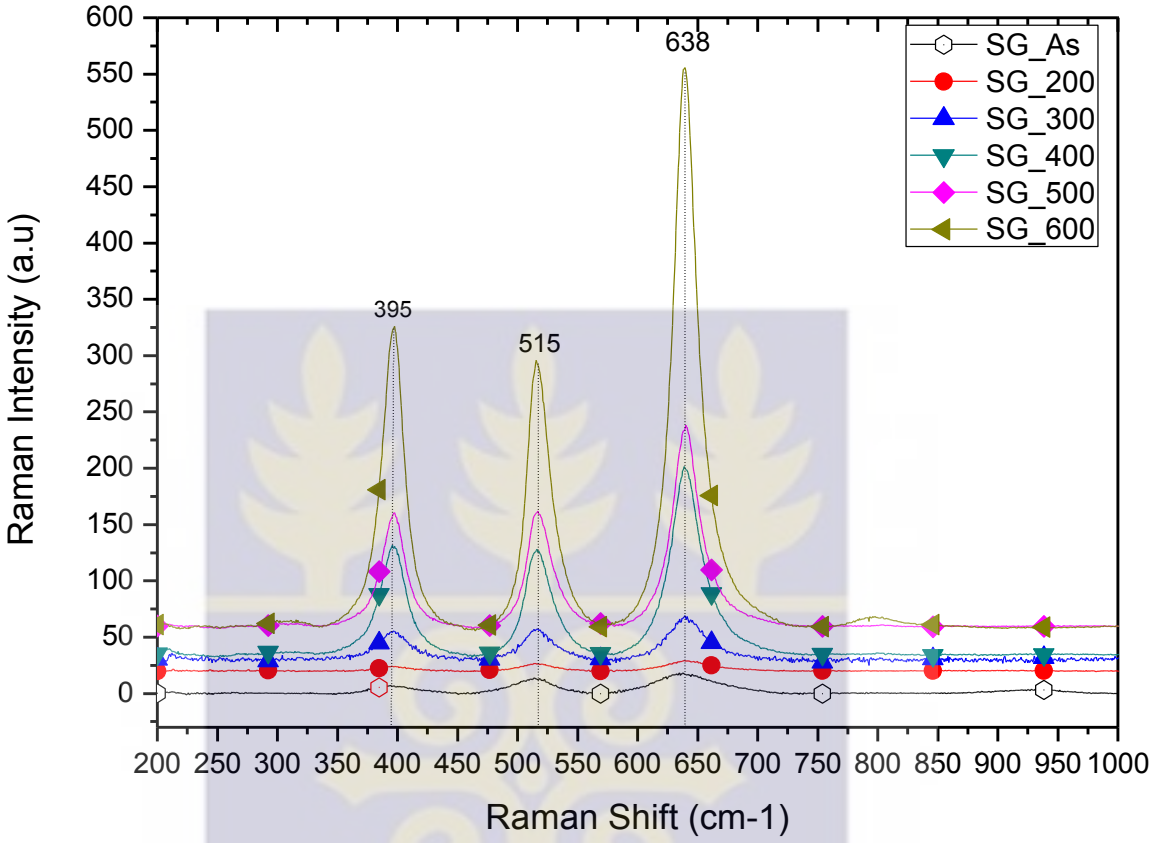

Figure 4.12: Raman Spectra of TiO_2 nanoparticles synthesized by sol gel method

The Raman spectra shown in Figure 4.13 revealed Raman peaks around 141 cm^{-1},380 cm^{-1}, 510 cm^{-1}, 640 cm^{-1} and 1261cm^{-1} when the samples were prepared by the Hydrothermal technique. Temperature treatment played an important role as in it can be seen that, the Raman peaks generally became more distinct and intense with increasing temperature. However, there was not much significant difference in the Raman peaks as it increased gradually when the samples were calcined up to 500 °C. But when the sample was calcined at 600 °C, the Raman peaks intensified

significantly especially at 141 cm^{-1}. This observation may be due to phase transformation from anatase to rutile at this temperature treatment in accordance to the XRD result.

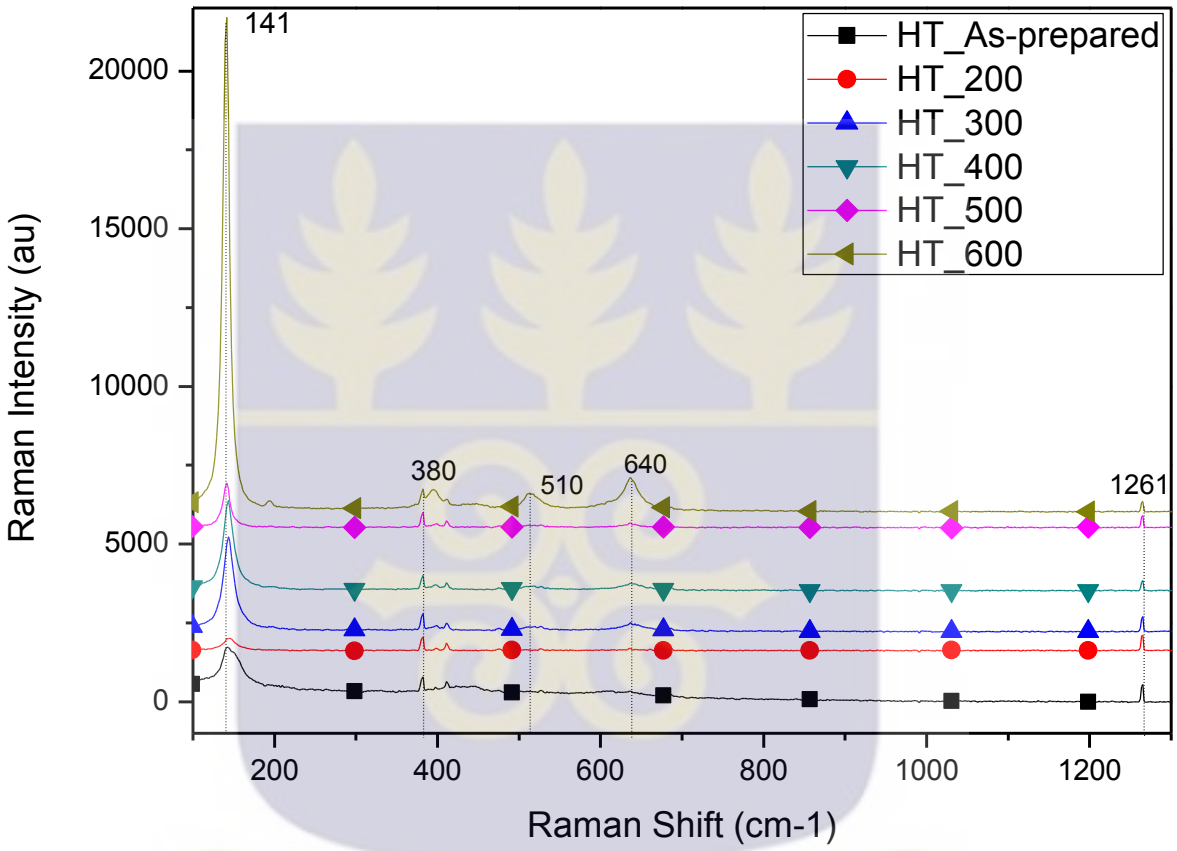

Figure 4.13: Raman Spectra of TiO_2 nanoparticles synthesized by Hydrothermal method

4.6. Surface Area and Porosity Analysis

The states of the surfaces played an important role in nanoparticles. There is a general increase in surface to volume ratio when the particle sizes get smaller. Specific Surface Area is a material property and a derived scientific value that can be used to determine the type and properties of a material. Generally, the specific surface area and surface to volume ratio increases as the size of

material decreases. The large surface area of TiO_2 nanoparticles facilitates the reaction between TiO_2 based devices and the interacting media. These reactions occur mainly on the surfaces or at the interfaces and hence are strongly dependent on the surface area of the material [31].

4.6.1. Adsorption and Desorption Isotherms

The adsorption isotherms of nitrogen on TiO_2 nanoparticles at an increasing relative pressure were analyzed to determine the BET surface area, pore size and pore volume. The adsorption and desorption isotherms were seen not to follow the same path for a specified region of relative pressures. This phenomenon is known as a hysteresis loop and is commonly exhibited in mesoporous adsorbents.

From Figure 4,14, the Isotherm Linear plot of the as-prepared TiO_2 nanoparticles synthesized by Sol gel method as well as samples calcined at 200 °C, 300 °C and 400 °C revealed a stepwise adsorption and desorption branch at wide range of pressure (P/Po) and were classified as Type IV isotherm in accordance with the IUPAC isotherm classifications [42, 50].. This showed that mesoporous TiO_2 nanoparticles were produced at these temperature treatments. At 500 °C and 600 °C calcination temperatures, a stepwise adsorption and desorption branch was not observed and were classified as Type III isotherms according to IUPAC isotherm classifications. .

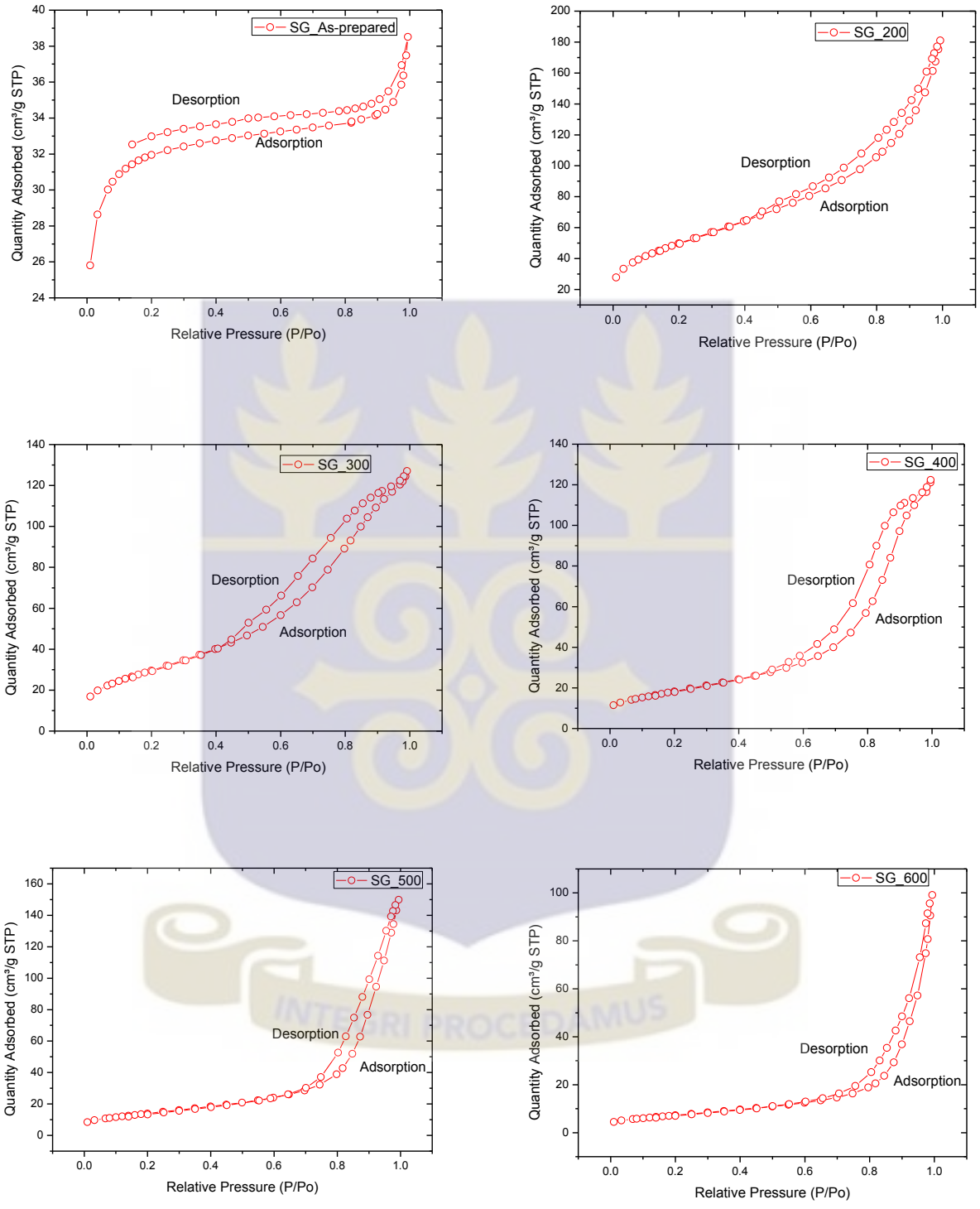

Figure 4.14: Isotherm linear plot of TiO_2 nanoparticles synthesized by Sol gel method

The linear isotherm plots of TiO_2 nanoparticles prepared by hydrothermal method are presented in Figure 4.15. As prepared TiO_2 nanoparticles as well as sample calcined at 200 °C, 300 °C, 400 °C, and 500 °C isotherms exhibit typical type IV pattern with hysteresis loop, characteristic of mesoporous material, according to the classification of IUPAC. There was also a sharp increase in adsorption volume of N_2 that was observed and located in the P/P_o range of 0.6-0.8. This sharp increase can be imputable to the capillary condensation, which indicates a good homogeneity of the sample and fairly small pore size since the P/P_o position of the inflection point is related to the pore dimension [36]. Sample calcined at 600 °C exhibited a Type III isotherm and in this case a hysteresis loop with a stepwise adsorption and desorption branch was not observed [50].

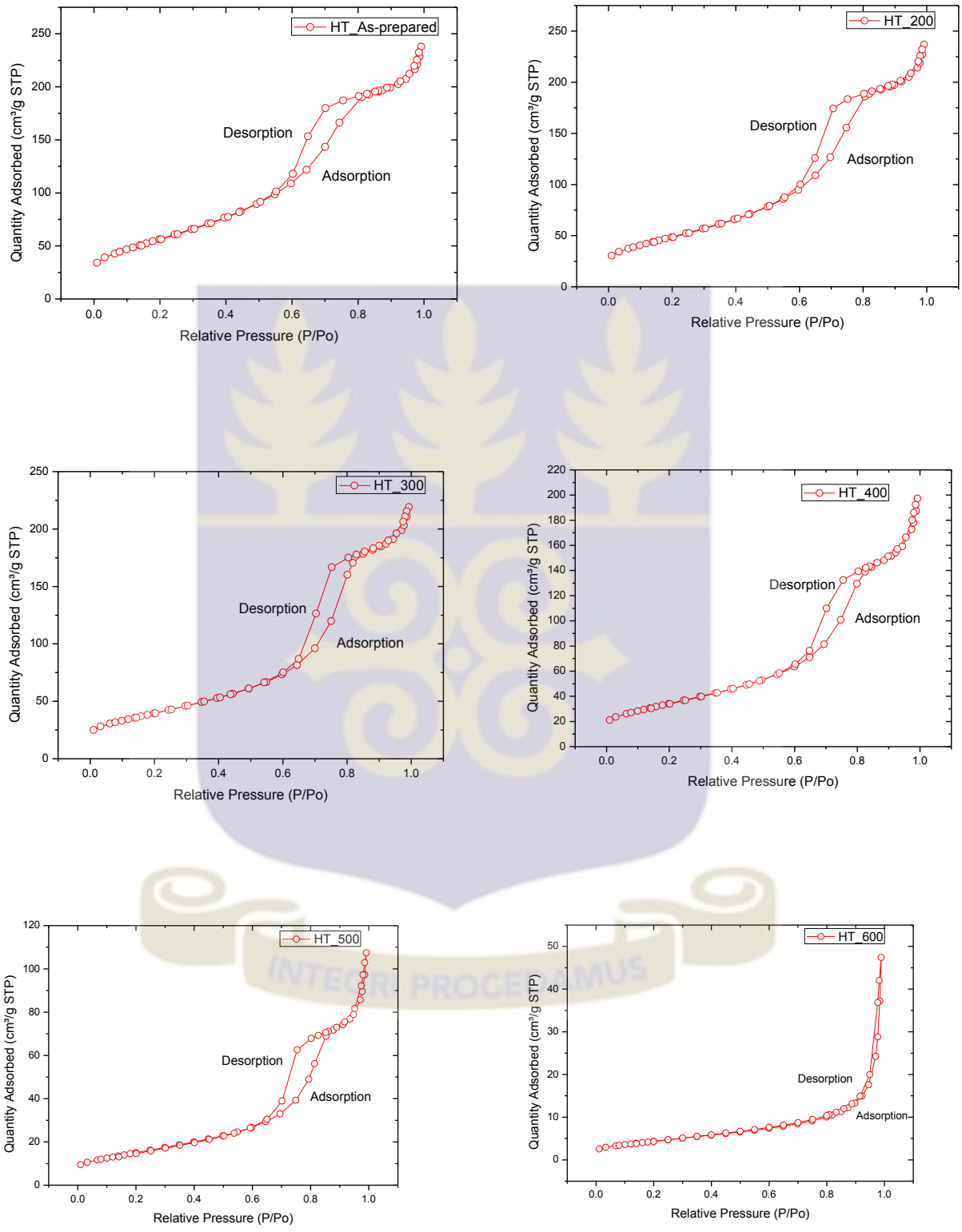

Figure 4.15: Isotherm linear plot of TiO_2 nanoparticles synthesized by Hydrothermal method

4.6.2. Effect of Surface Area and porosity with Temperature

For samples synthesized by the Sol gel technique, there was an initial increase in BET surface area (Figure 4.16) when the as-prepared TiO_2 nanoparticles were calcined at 200°C but was subsequently reduced when the calcination temperature was increased further. At 200°C calcination temperature, the reported BET surface area was **181.6 m^2/g**. Also, there was a general decrease in BET surface area when the calcination temperature was increased.

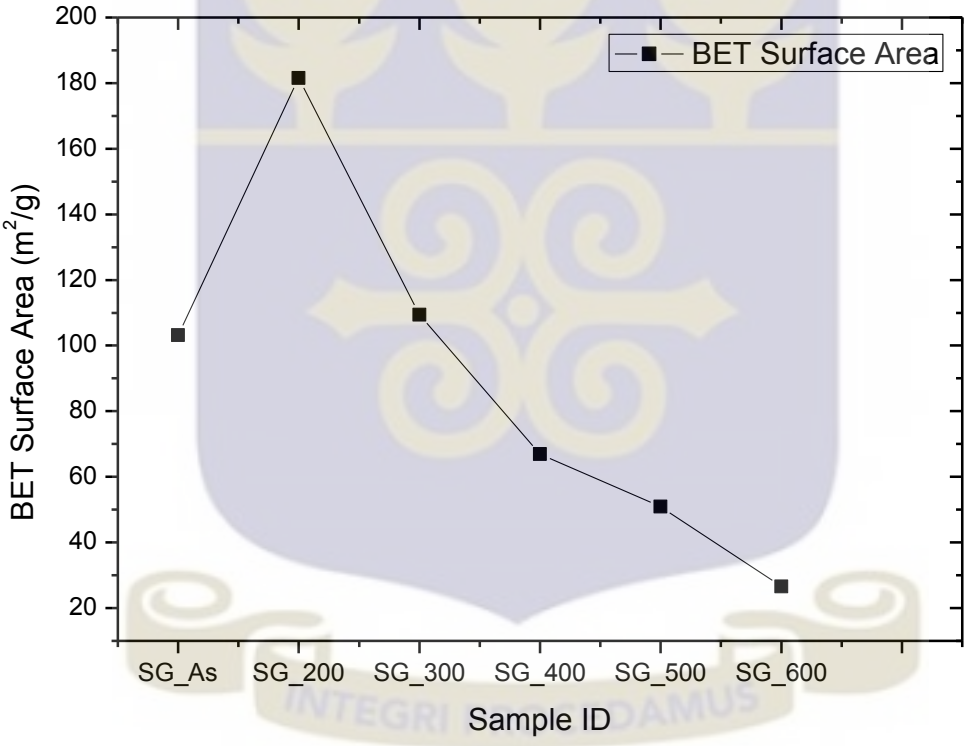

Figure 4.16: BET Surface area of TiO_2 nanoparticles synthesized by Sol gel method

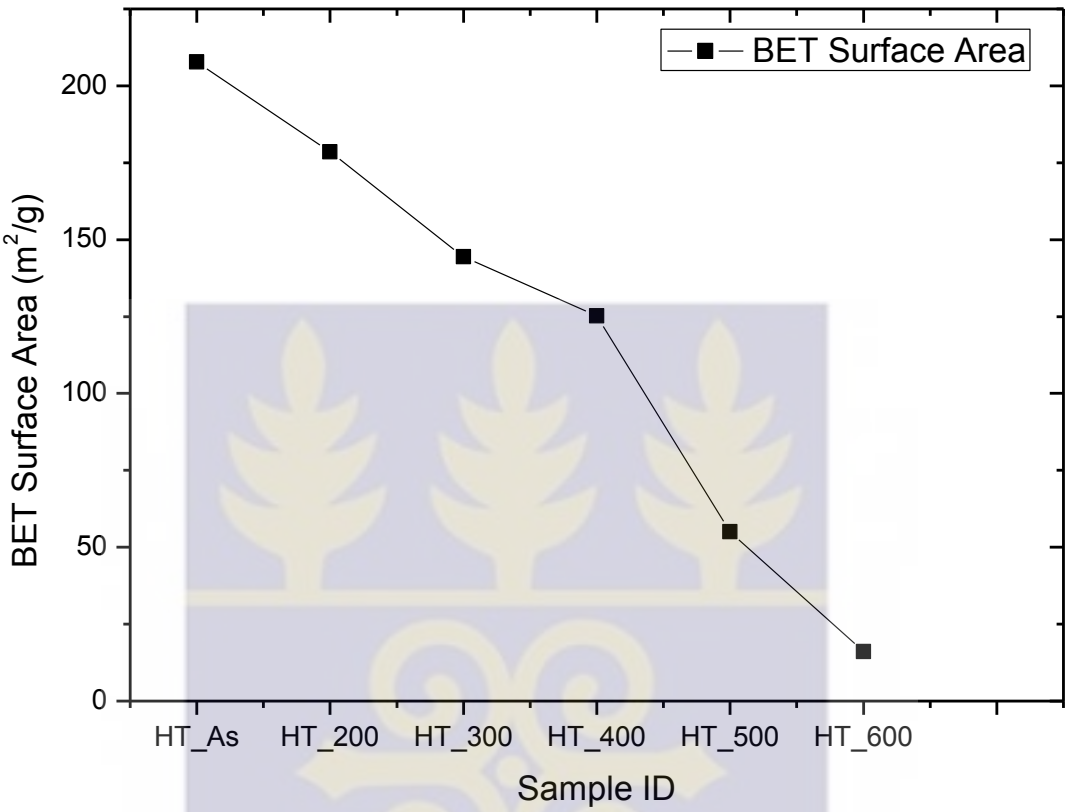

Figure 4.17: BET Surface area of TiO_2 nanoparticles synthesized by Hydrothermal method

There was a general decrease in BET surface area in the samples synthesized by Hydrothermal method (Figure 4.17) when the calcination temperature was increased since the grains grow in size with temperature, hence resulting in a material with reduced surface area. The highest BET surface area was reported to be **207.7 m^2/g** which was assigned to the as-prepared nanoparticles synthesized by Hydrothermal method. The least BET surface area was at 600°C to be **16m^2/g**.

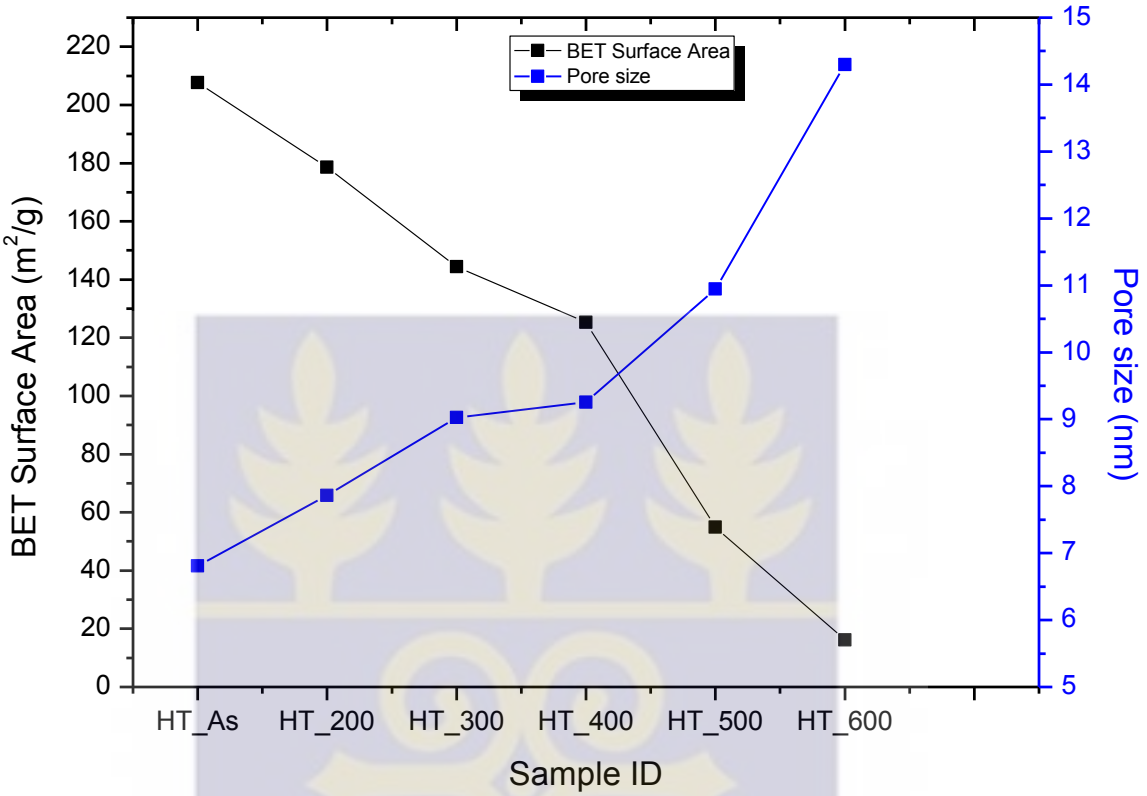

Figure 4.18: Pore size of Hydrothermal prepared TiO_2 nanoparticles as a function of calcination temperature

As seen in Figure 4.18 and Figure 4.19, there was a general increase in pore size in both Sol gel and Hydrothermal prepared TiO_2 nanoparticles when the calcination temperatures were increased. The reason for this observation could be that, since the grain size increases with temperature, the voids created in between the particles were also enhanced and this could have accounted for the increase in pore size when the calcination temperatures were increased.

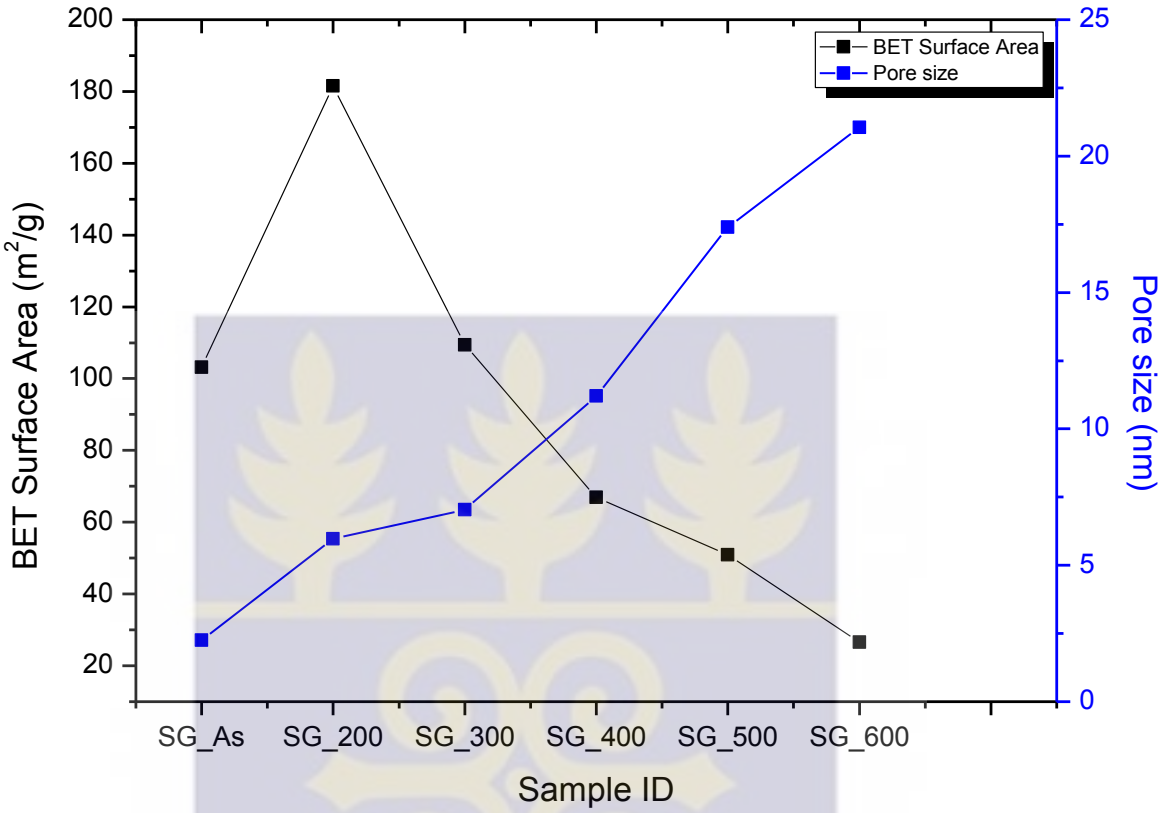

Figure 4.19: Pore size of Sol gel prepared TiO_2 nanoparticles as a function of calcination temperature.

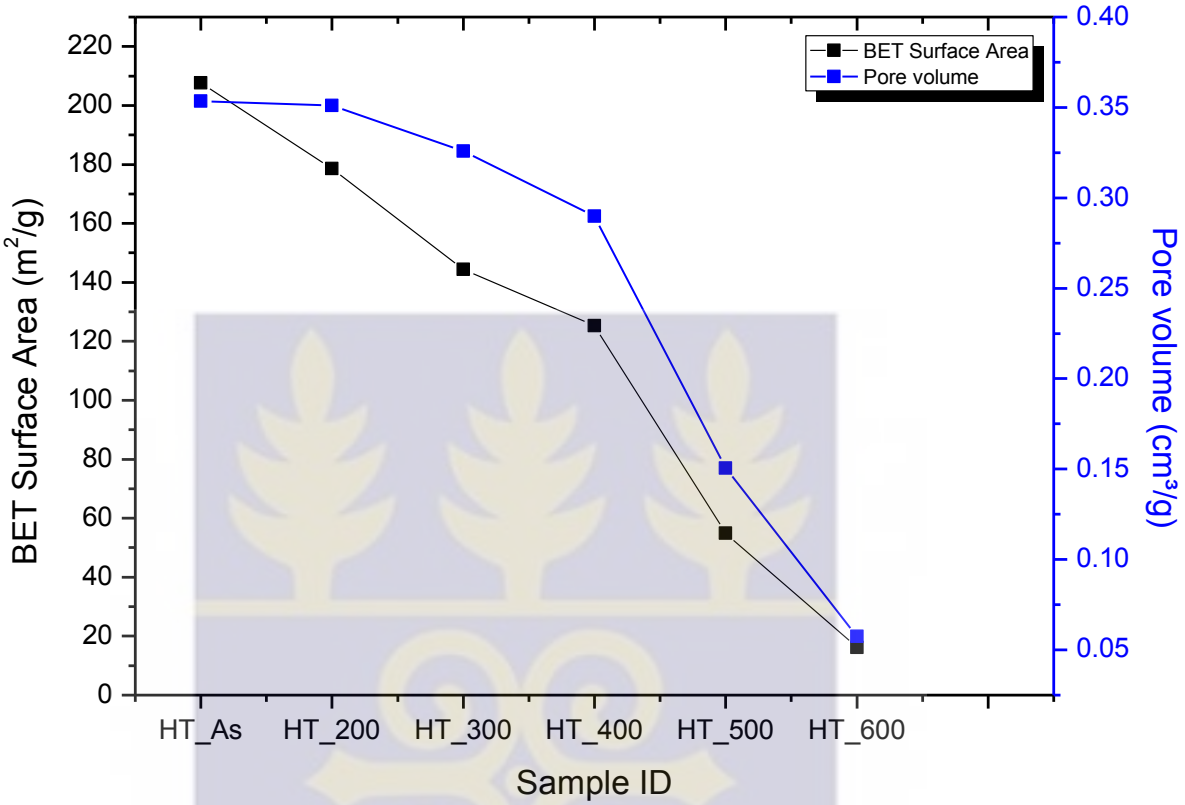

Figure 4.20: Pore volume of Hydrothermal prepared TiO_2 nanoparticles as a function of calcination temperature

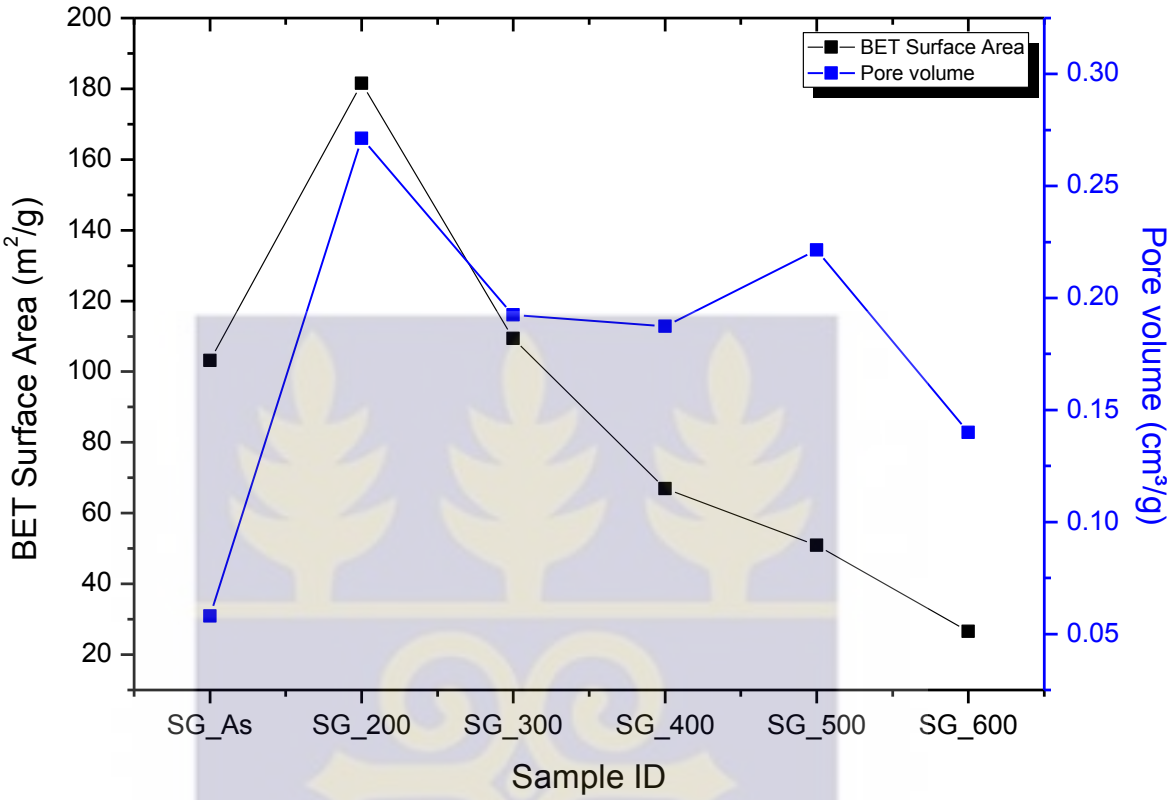

Figure 4.21: Pore volume of Sol gel prepared TiO_2 nanoparticles as a function of calcination temperature

As shown in Figure 4.20 and Figure 4.21, there was a general decrease in pore volume as the calcination temperature increased. This was because, as the grains increase in size and the surface area decreases, the number of pores within the material also diminishes since some of the particles fuse into each other as a result of agglomeration. Samples prepared by Sol gel method showed a slight deviation from this pattern

Table 4.2 summarizes BET parameters of the synthesized TiO_2 nanoparticles.

Table 4.2: Summary of surface area parameters of the prepared TiO_2 nanoparticles

Sample Name	Sample Mass (g)	BET Surface Area (m^2/g)	Pore size **(nm)**	Pore volume **(cm^3/g)**
HT_As-prepared	0.143	207.701	6.806	0.353
HT_200	0.189	178.588	7.864	0.351
HT_300	0.273	144.366	9.025	0.326
HT_400	0.184	125.238	9.255	0.290
HT_500	0.212	54.973	10.947	0.150
HT_600	0.247	16.086	14.297	0.057
SG_As-prepared	0.161	103.120	2.249	0.058
SG_200	0.208	181.551	5.975	0.271
SG_300	0.251	109.354	7.040	0.192
SG_400	0.219	66.880	11.205	0.187
SG_500	0.242	50.920	17.399	0.221
SG_600	0.250	26.619	21.043	0.140

4.7. Microstructural Analysis

SEM micrographs shown in Figure 4.22 and Figure 4.23 demonstrated that, nearly spherical nanoparticles were produced. Also, the agglomeration was enhanced when the calcination temperature of the samples was increased.

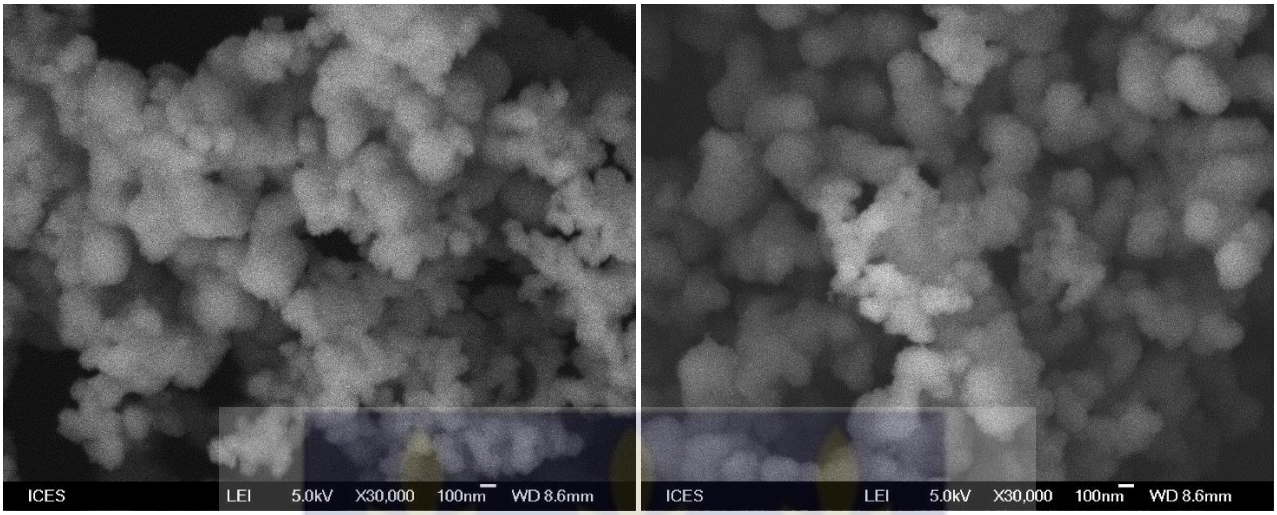

(a) (b)

Figure 4.22:SEM images of TiO_2 nanoparticles prepared by hydrothermal method (a) as-prepared (b)calcined at 300°C

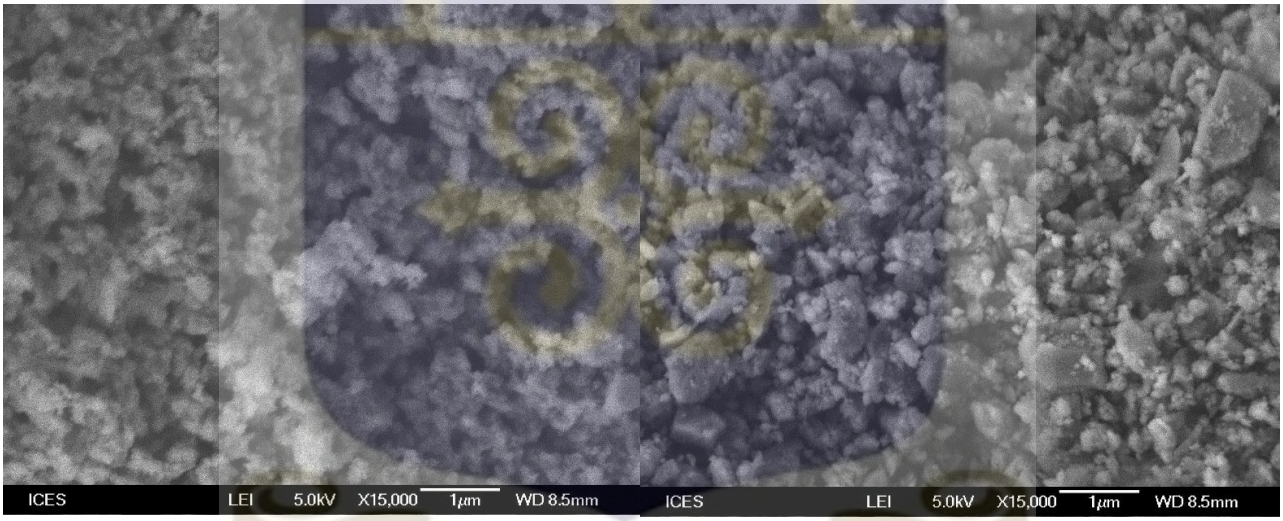

Figure 4.23: SEM images of TiO_2 nanoparticles prepared by Sol gel method (a) calcined at 300°C (b)calcined at 600°C

Energy dispersive X-ray spectrometry (EDX) (Figure 4.24 and Figure 4.25) analysis of prepared TiO_2 nanoparticle showed peaks for Ti and O elements. No trace of any other impurities or elements was seen within the detection limit of the EDX. This confirms that TiO_2 nanoparticles with high purity were prepared.

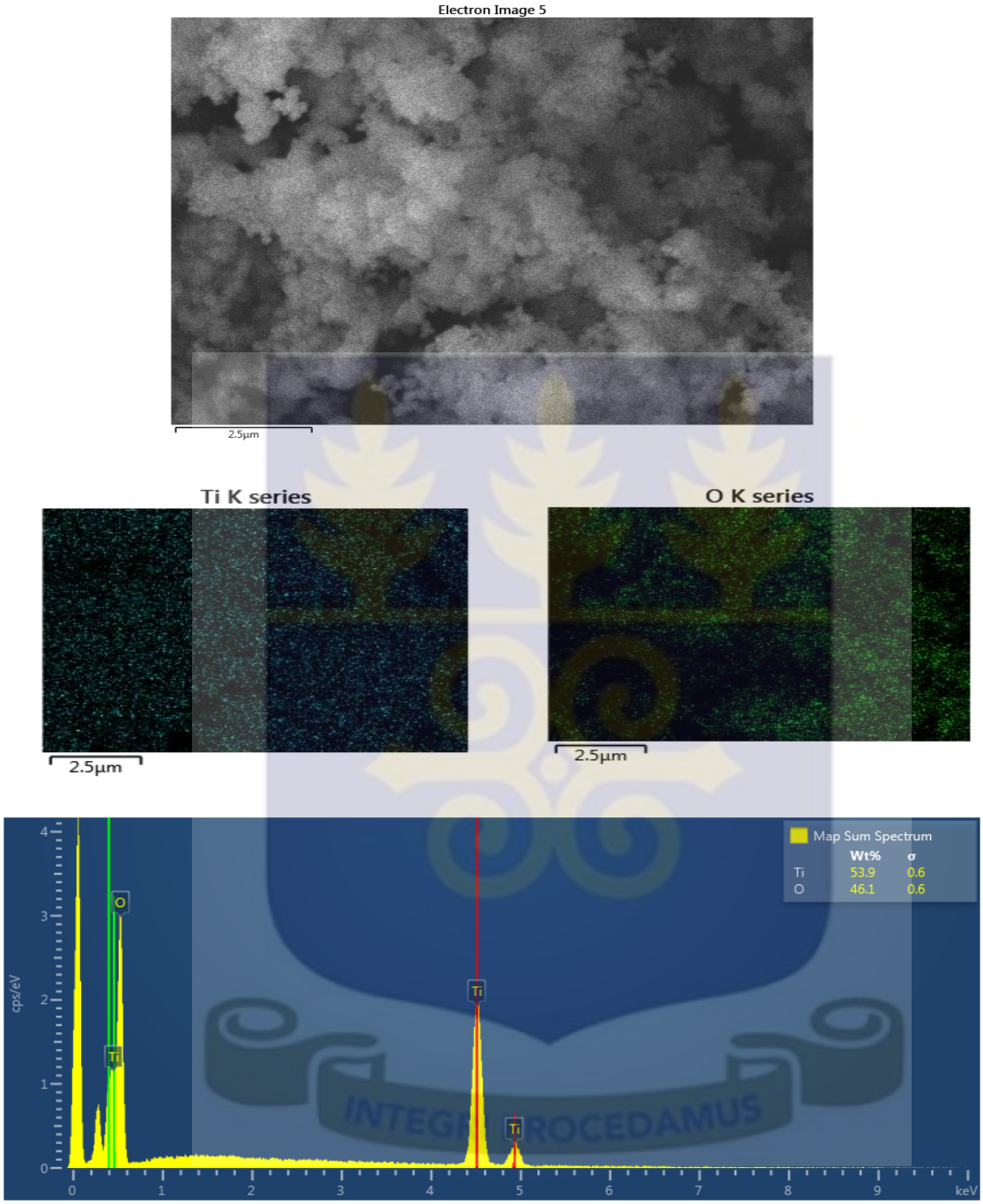

Figure 4.24: EDX of TiO_2 nanoparticles prepared via hydrothermal method

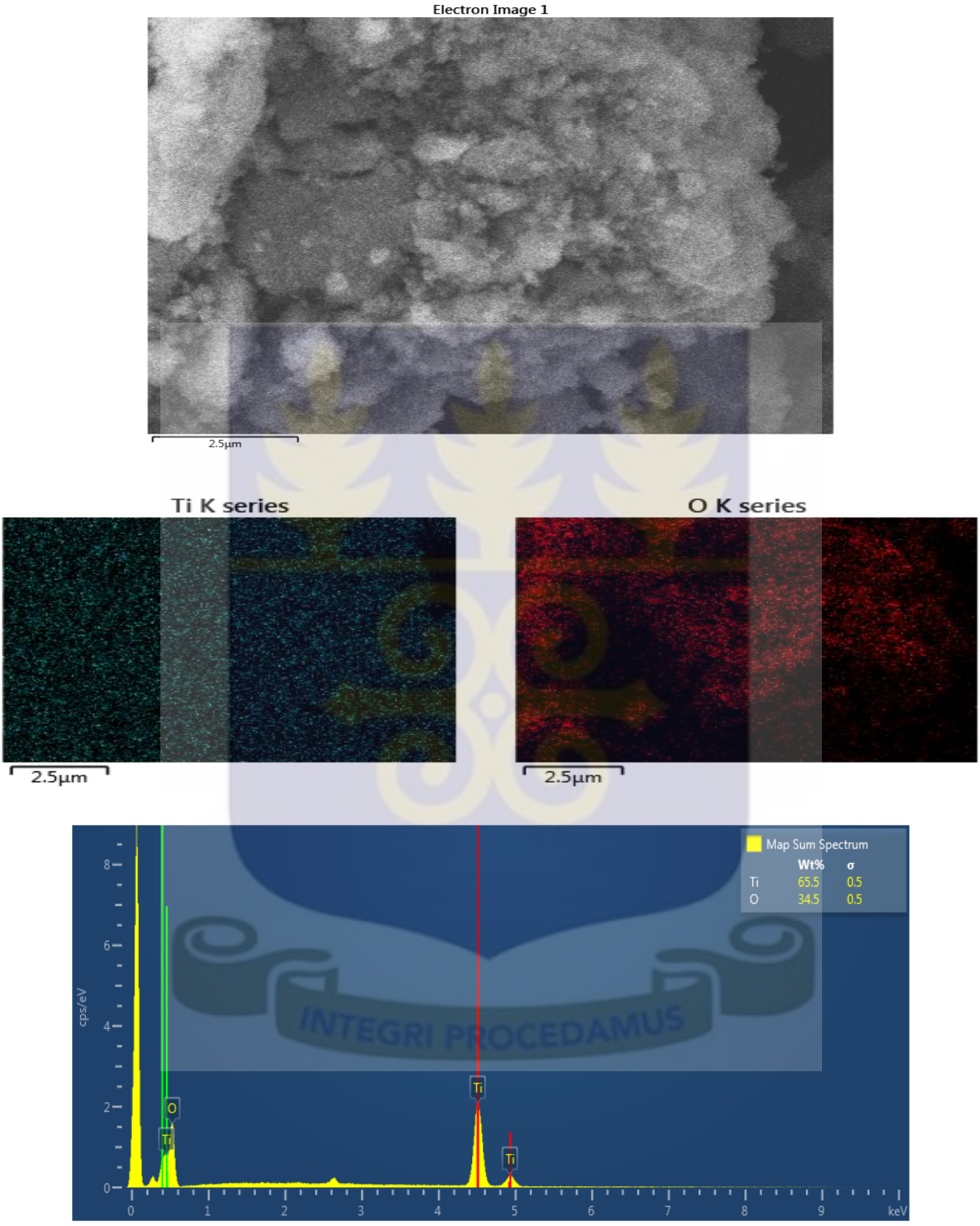

Figure 4.25: EDX of TiO_2 nanoparticles prepared via Sol gel method

4.8. Photodegradation

The photocatlytic degradation of Rhodamine B dye and Sudan III under ultraviolet light irradiation assisted by TiO_2 nanoparticles as catalyst is demonstrated in the flow chat (Figure 4.26) and summarized as follows [39]:

i. TiO_2 adsorbed ultraviolet photons and the electrons in the valence band and were excited to the conduction band to create a highly reactive electron and hole pairs **(Equation 4.7)** which migrates to the TiO_2 surface to initiate the photocatalytic reaction

ii. The photo-generated holes were trapped by hydroxyl groups attached on the surface to form hydroxyl radicals **(Equation 4.8).**

iii. The electrons were trapped by oxygen to form oxygen species **(Equation 4.9).**

iv. The holes, together with hydroxyl radicals and oxygen species, oxidize the Rhodamine B and Sudan III dyes to carbon dioxide, water and some simple mineral acids.

$$TiO_2 + h\nu \rightarrow TiO_2 + (e^- + h^+) \quad \text{..... 4.7}$$

$$h^+ + OH^- \rightarrow \bullet OH \quad \text{.....4.8}$$

$$e^- + O_2 \rightarrow \bullet O_2^- \quad \text{..... 4.9}$$

Hydroxyl ions played an important role in the photocatalytic degradation of the dye by adsorbing a photo-generated hole to form the highly oxidative •OH. The superoxide radicals formed also contributed positively to the photocatalytic degradation of the dye [39].

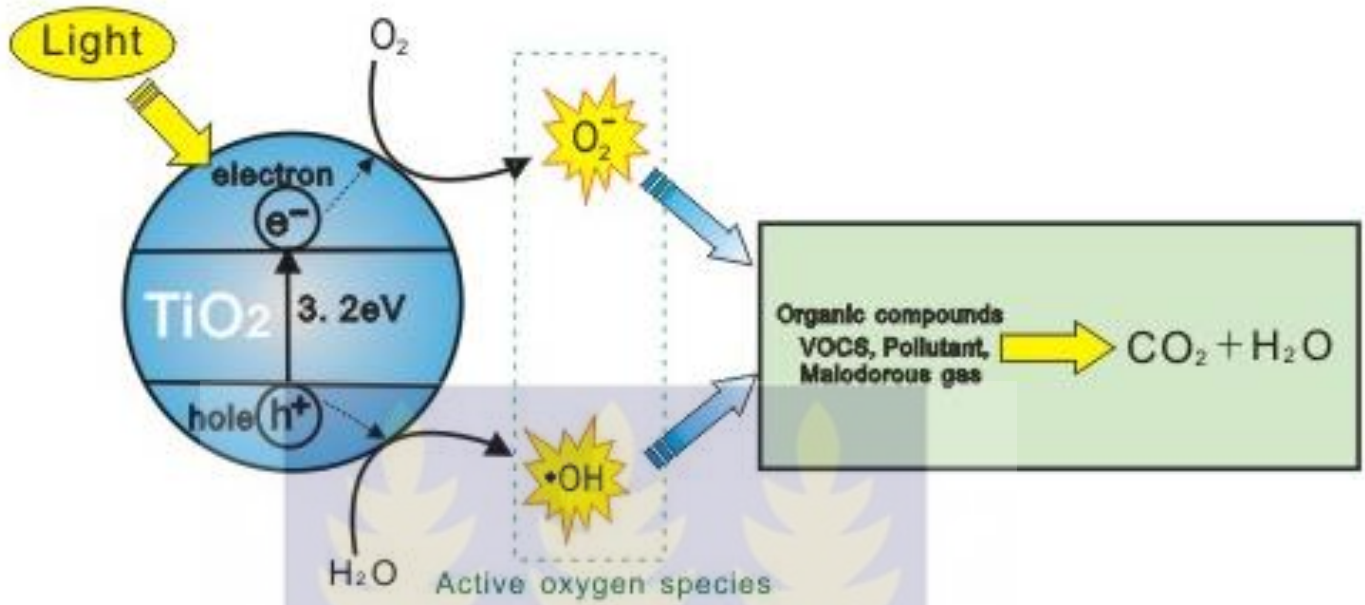

Figure 4.26: Photodegradation Process[51]

4.8.1. Rhodamine B dye

At a characteristic wavelength of 554nm, the absorbance peak was recorded at various exposure times for Rhodamine B dye solutions. A control experiment with rhodamine B dye solution without TiO_2 catalyst showed no or negligible degradation when illuminated by ultraviolet light over 150 minutes exposure. Also Rhodamine B dye solution with TiO_2 catalyst without Ultraviolet light illumination also showed no or negligible degradation over 150 minutes period. This showed that both the TiO_2 catalyst and ultraviolet are required to initiate the photocatalytic reaction to cause the degradation of the dye solution.

At initial Sudan III dye concentration of 3.8×10^{-5},the absorption spectrum was studied and reported as seen in Figures 4.27, 4.28 and 4.29.

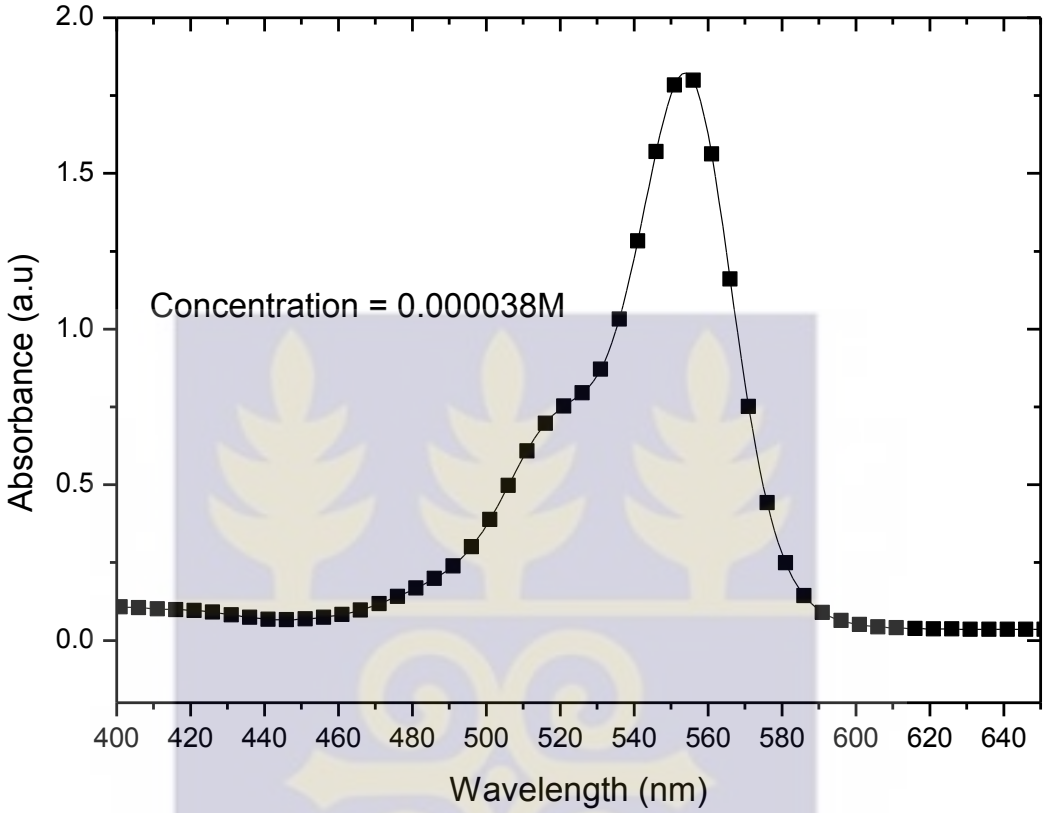

Figure 4.27: Absorption Spectrum of Rhodamine B dye solution without TiO_2 catalyst

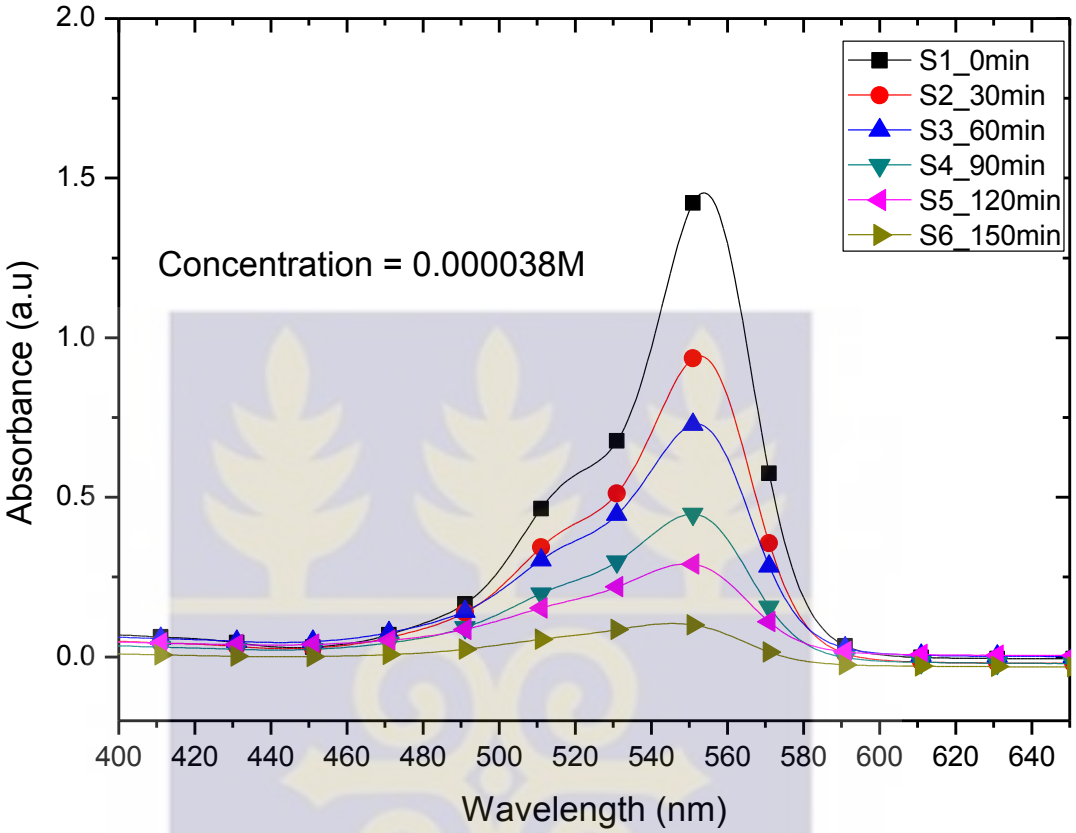

Figure 4.28: Absorption Spectrum of rhodamine B dye solution degraded by TiO_2 catalyst prepared via sol gel route

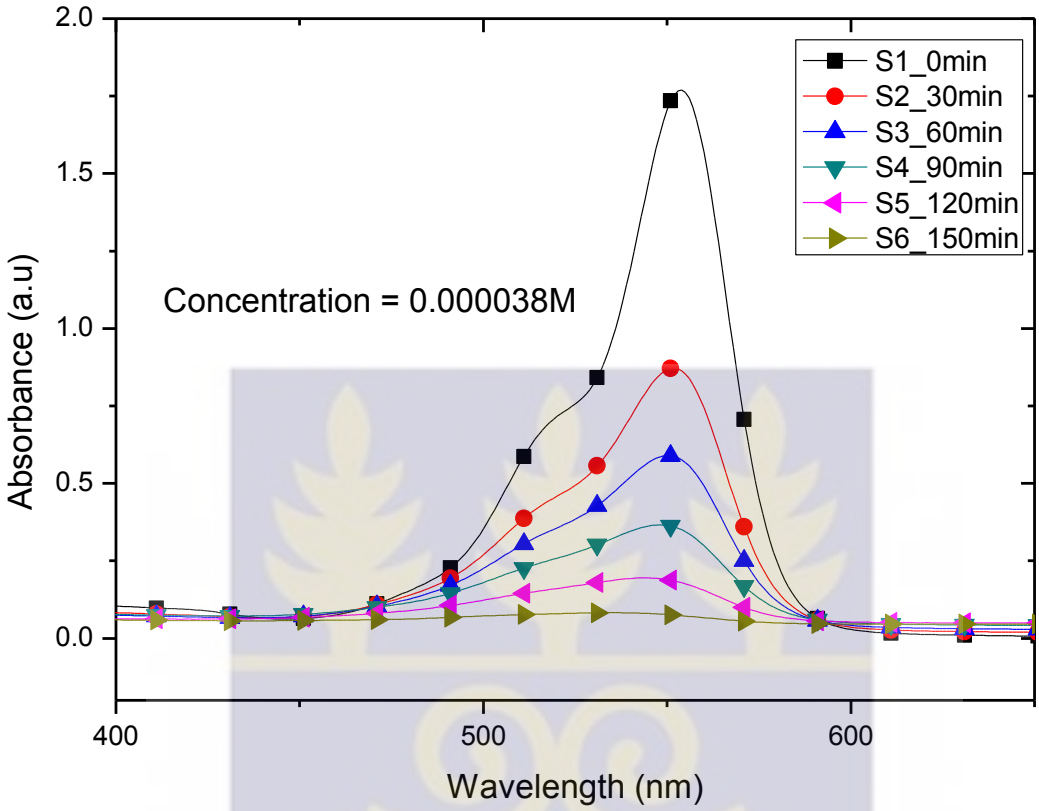

Figure 4.29*: Absorption Spectrum of rhodamine B dye solution degraded by TiO_2 catalyst prepared via hydrothermal route*

At initial Rhodamine B dye concentration of 8.5×10^{-6} ,the absorption spectrum was studied and reported as seen in Figures 4.30, 4.31 and 4.32.

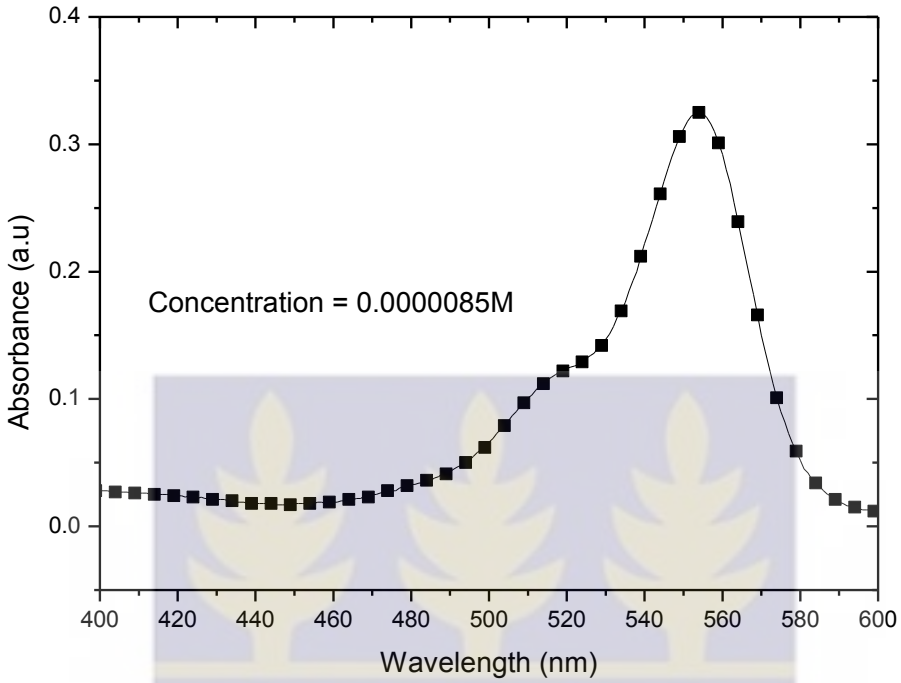

Figure 4.30: Absorption Spectrum of Rhodamine B dye without catalyst

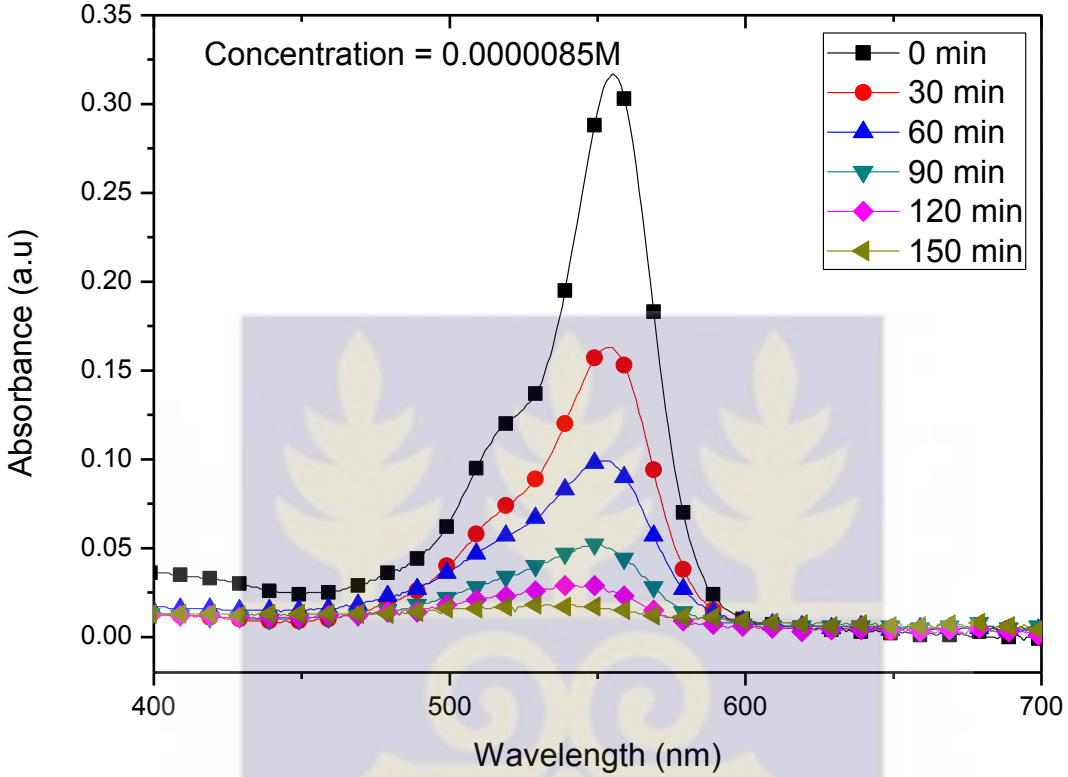

Figure 4.31: Absorption Spectrum of Rhodamine B dye degraded by sol gel prepared catalyst

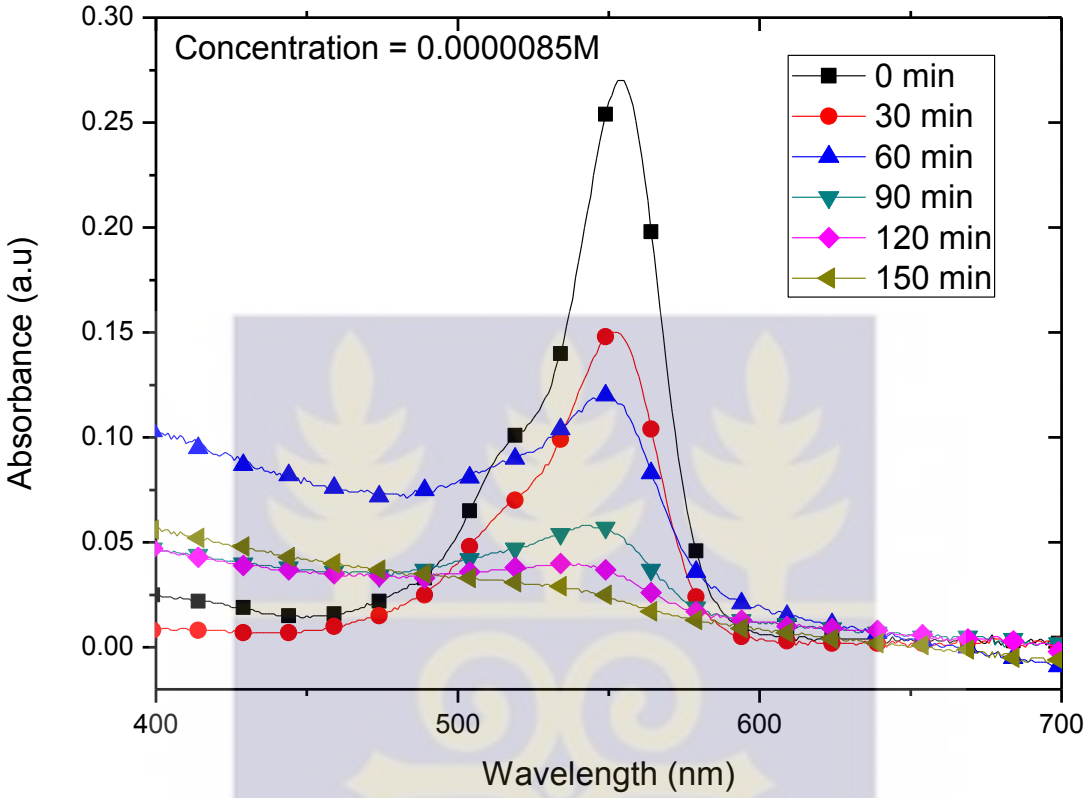

Figure 4.32 : Absorption Spectrum of Rhodamine B dye degraded by Hydrothermal prepared catalyst

Exposing rhodamine B dye to the UV light showed no decrease in absorbance over time. The dye was not degraded because there was no TiO_2 catalyst present to initiate degradation reaction.

4.8.2. Sudan III Dye

At a characteristic wavelength of 507nm, the absorbance of Sudan III dye was monitored and evaluated as it was degraded by the prepared TiO_2 catalyst. Sudan III dye exposed to UV light

without any TiO_2 catalyst showed no or negligible degradation over 150 minutes period. Also, the Sudan III dye with catalyst but not exposed to UV light showed no or negligible degradation.

At initial Sudan III dye concentration of $5.2\times10^{-4}M$,the absorption spectrum was studied and reported as seen in Figures 4.33, 4.34 and 4.35

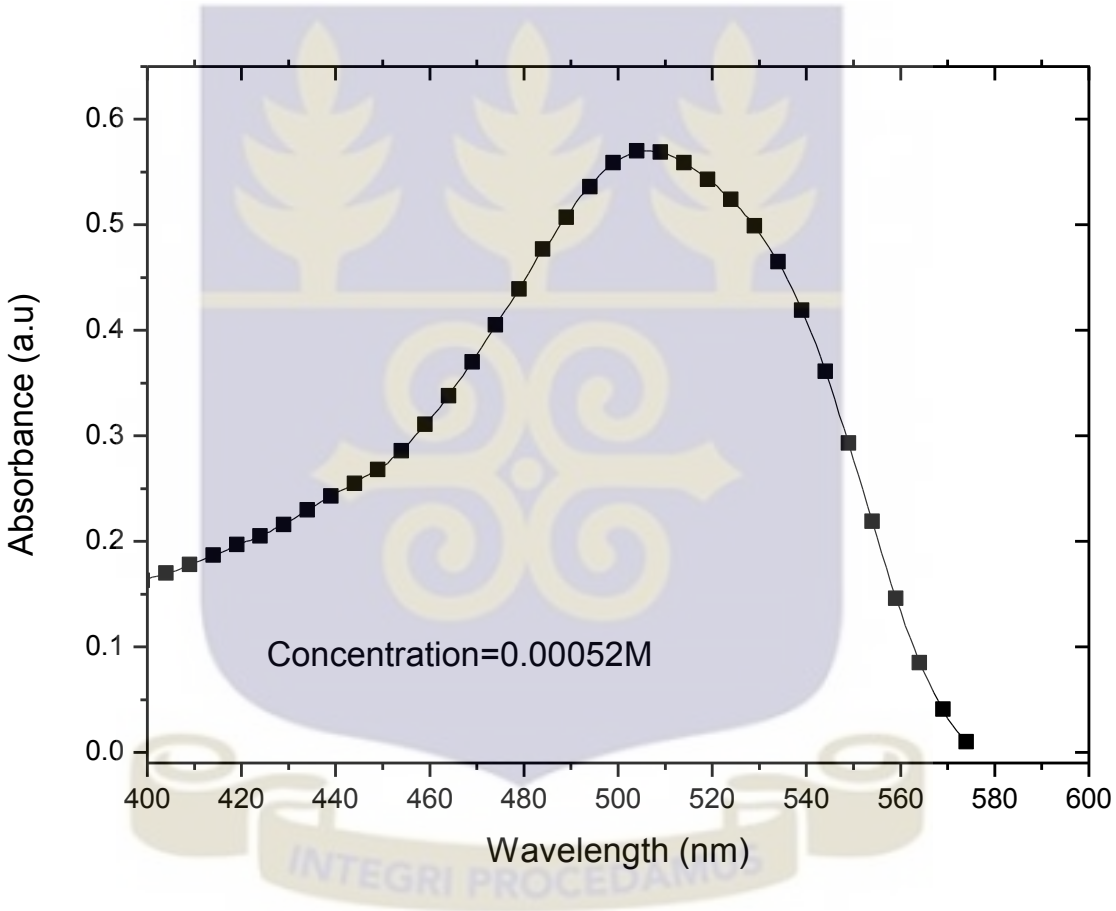

Figure 4.33: Absorption Spectrum of Sudan III dye without catalyst

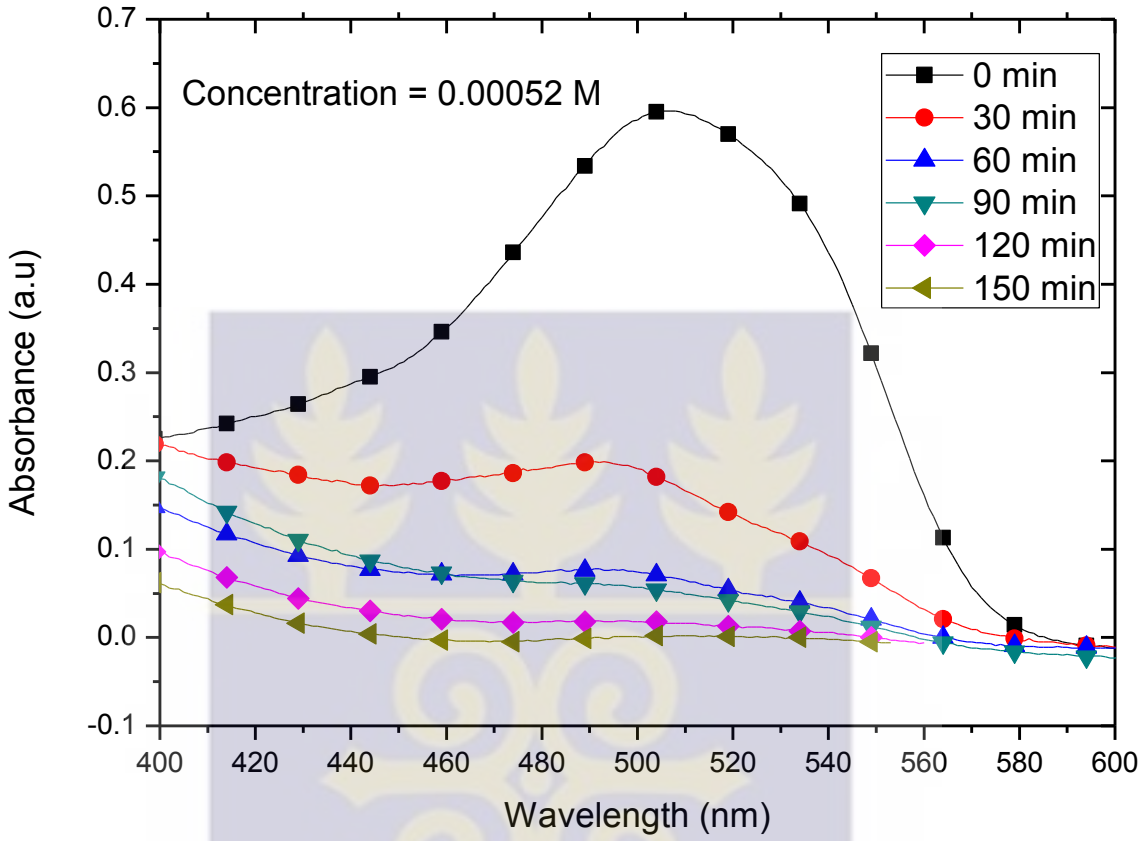

Figure 4.34: Absorption Spectrum of Sudan III dye degraded by Hydrothermal prepared TiO_2 catalyst

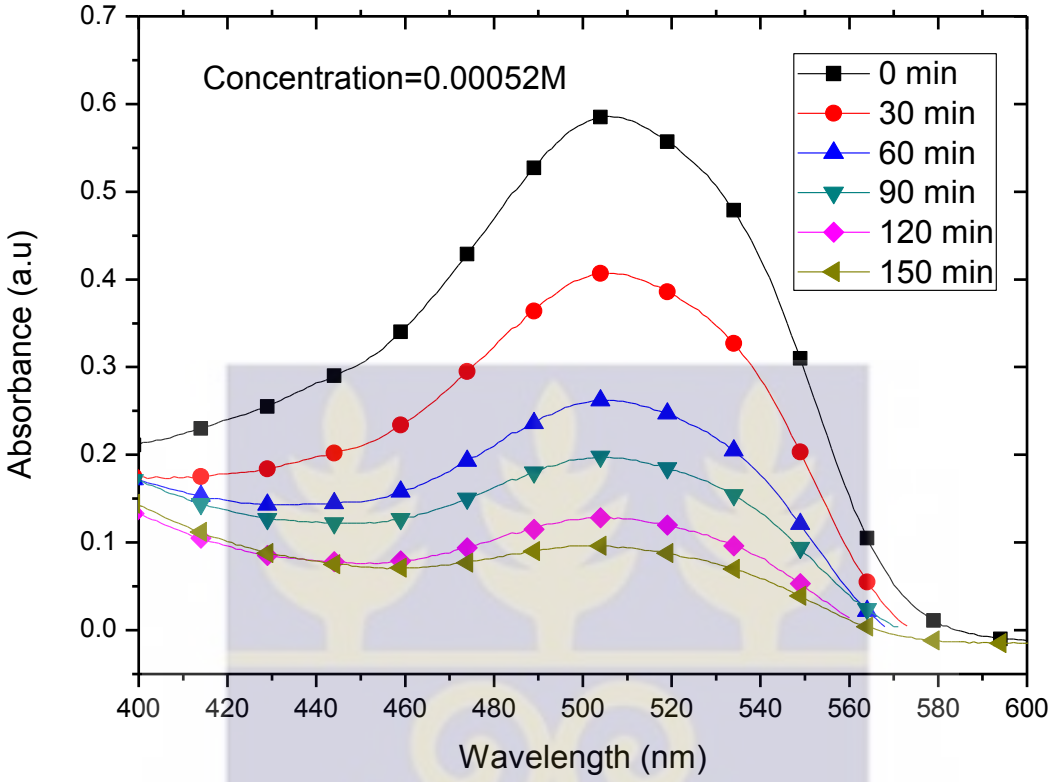

Figure 4.35: Absorption Spectrum of Sudan III dye degraded by Sol gel prepared TiO_2 catalyst

At initial Sudan III dye concentration of $2.3\times10^{-3}M$, the absorption spectrum was also studied and reported as seen in Figures 4.36 and 4.37.

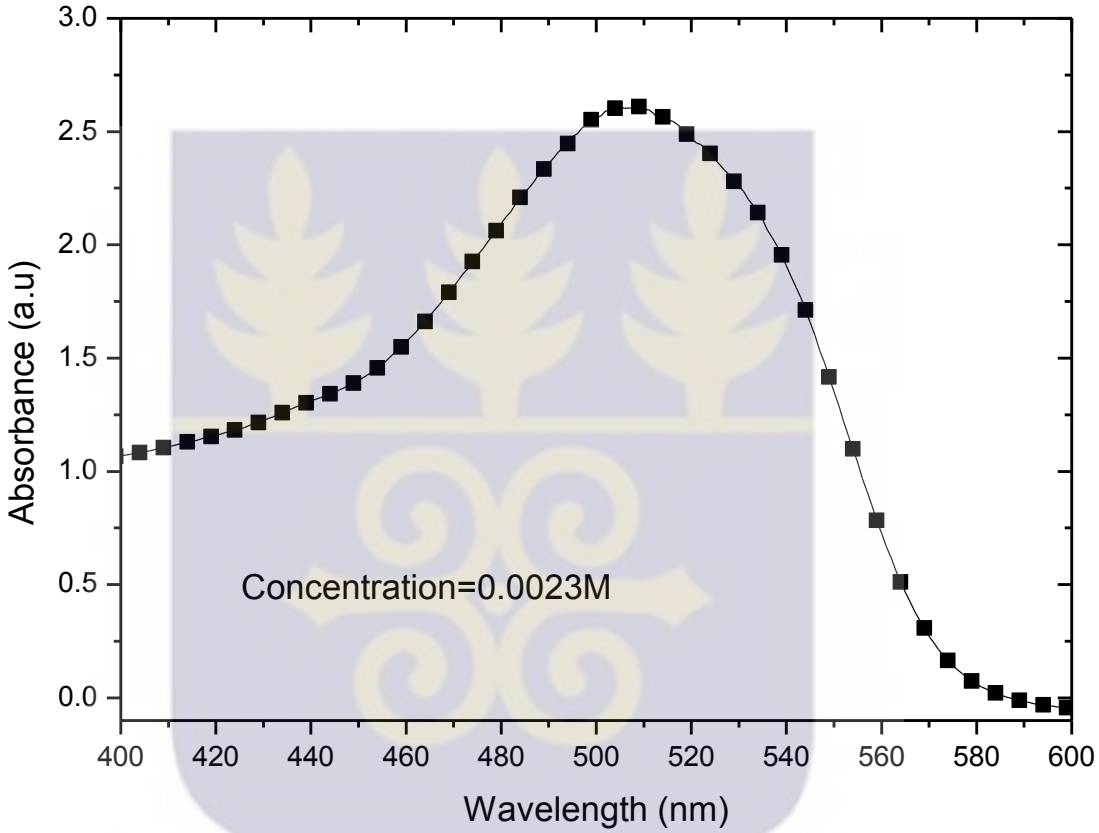

Figure 4.36: Absorption Spectrum of Sudan III dye without catalyst

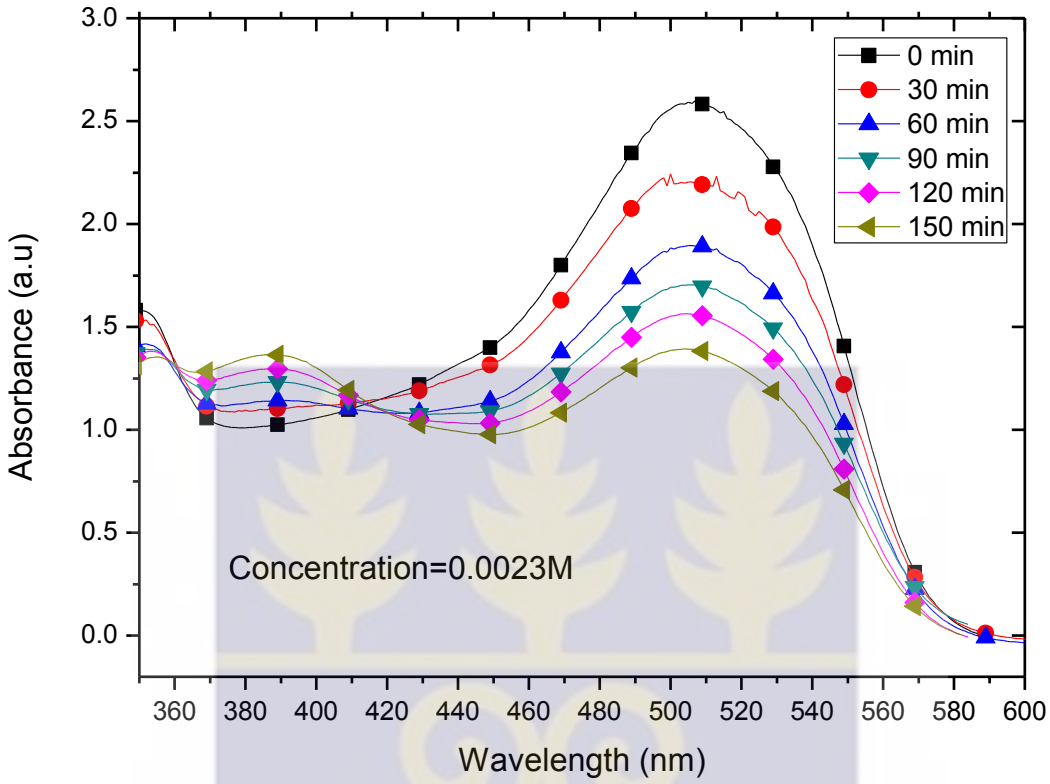

Figure 4.37: Absorption Spectrum of Sudan III dye degraded by sol gel prepared catalyst

From Figure 4.37, There was a gradual degradation of the of the Sudan III dye at this concentration. However there was still a significant amount of Sudan III dye molecules remaining owing to the high initial dye concentration.

At initial Sudan III dye concentration of $5.7\times10^{-3}M$, the absorption spectrum was also studied and reported as seen in Figures 4.38 and 4.39.

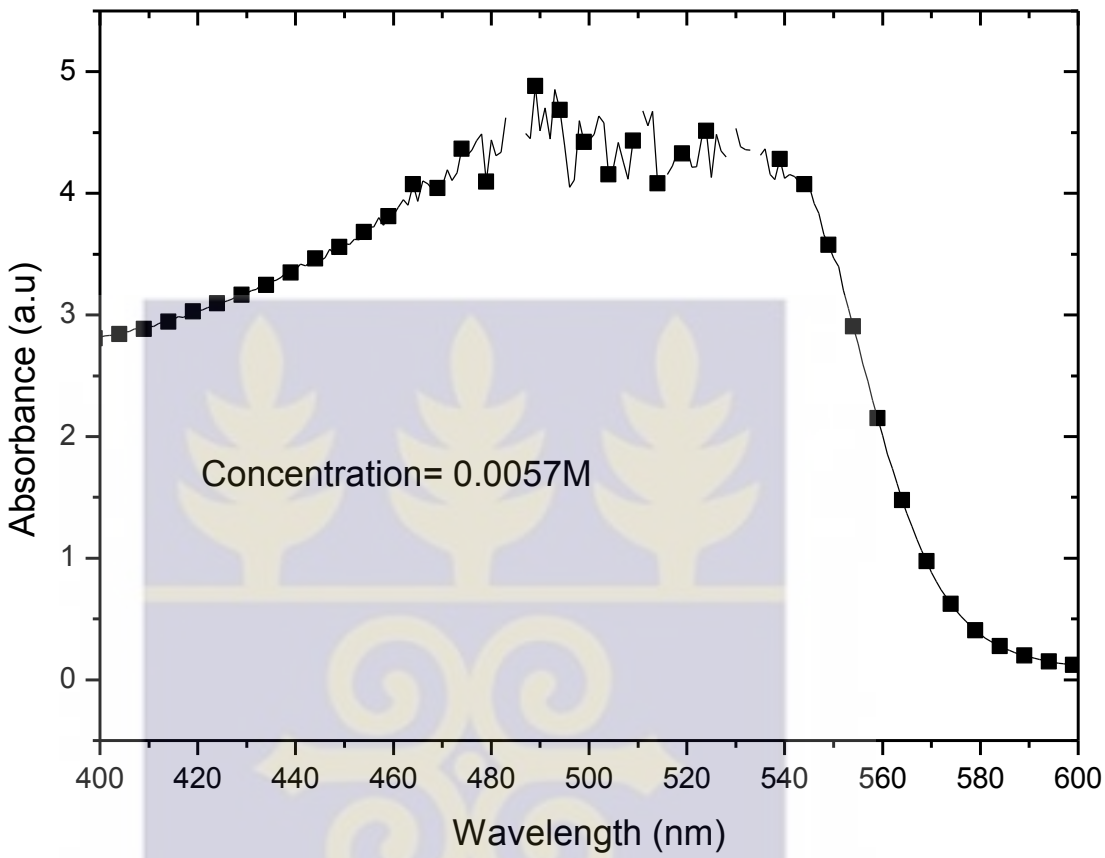

Figure 4.38: Absorption Spectrum of Sudan III dye without catalyst

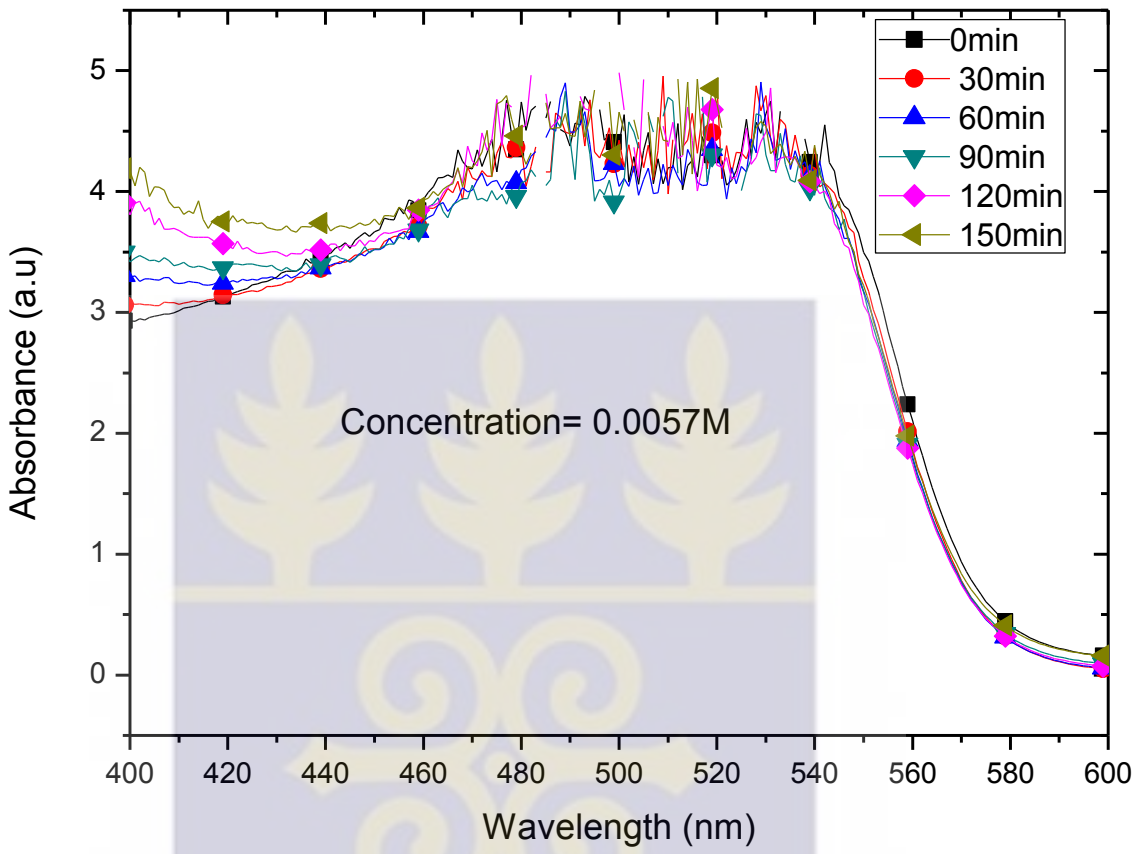

Figure 4.39 : Absorption Spectrum of Sudan III degraded by Sol gel prepared catalyst

From Figure 4.39, there was a negligible degradation of the Sudan III dye solution when the dye solution concentration was increased to 0.0057 M whiles keeping the catalyst loading constant. This is because, the active surface on the catalyst available for reaction is very crucial for the degradation to take place, but as the dye concentration was increased and the catalyst amount was kept constant, a fewer active sites for their reaction resulted. As the dye molecules were increased, the solution became more intensely coloured and the path length of photons entering the solution decreased thereby only fewer photons reached the catalyst surface. As a result, the

production of degradation species and radicals were limited and therefore, the path length was further reduced and the photodegradation was found to be negligible [13].

4.8.3. Effect of irradiation Time on Photodegradation of the Dyes

There was a general percentage degradation increase with increasing irradiation time for both Rhodamine B and Sudan III dyes assisted by TiO_2 nanoparticles (Figures 4.40 and 4.42). This is because, formation of •OH and $•O_2^-$ radicals increased with increasing irradiation time [13]. Since the photocatalytic degradation of the dye occurs on the surface of catalyst where •OH and $•O_2^-$ radicals are available for photocatalytic degradation, the OH• radicals were strong enough to break the different bonds in the dye molecules adsorbed on the surface of catalyst, which led to the formation of carbon dioxide, water and inorganic ions.

The percentage of dye degraded was calculated as follows:

$$Degradation(\%) = \frac{C_{initial} - C_{final}}{C_{initial}} \times 100 \quad \text{..... (4.10)}$$

Where C_{intial} is the initial concentration of the dye solution and C_{final} is the concentration at time intervals of the irradiation time.

TiO_2 nanoparticles synthesized by Sol gel method showed a higher degradation rate in Rhodamine B dye solution than that of the TiO_2 nanoparticles synthesized by Hydrothermal method. There was about **50%** degradation caused by Sol gel prepared catalyst compared to the **44%** degradation caused by Hydrothermal prepared catalyst. After 30 minutes of UV light irradiation, the degradation occurred at a reducing pace After 150 minutes, the Rhodamine B dye solution at $\mathbf{8.5\times10^{-6}M}$ was **94%** degraded by Sol gel prepared catalyst and **89%** degraded by Hydrothermal prepared catalyst.

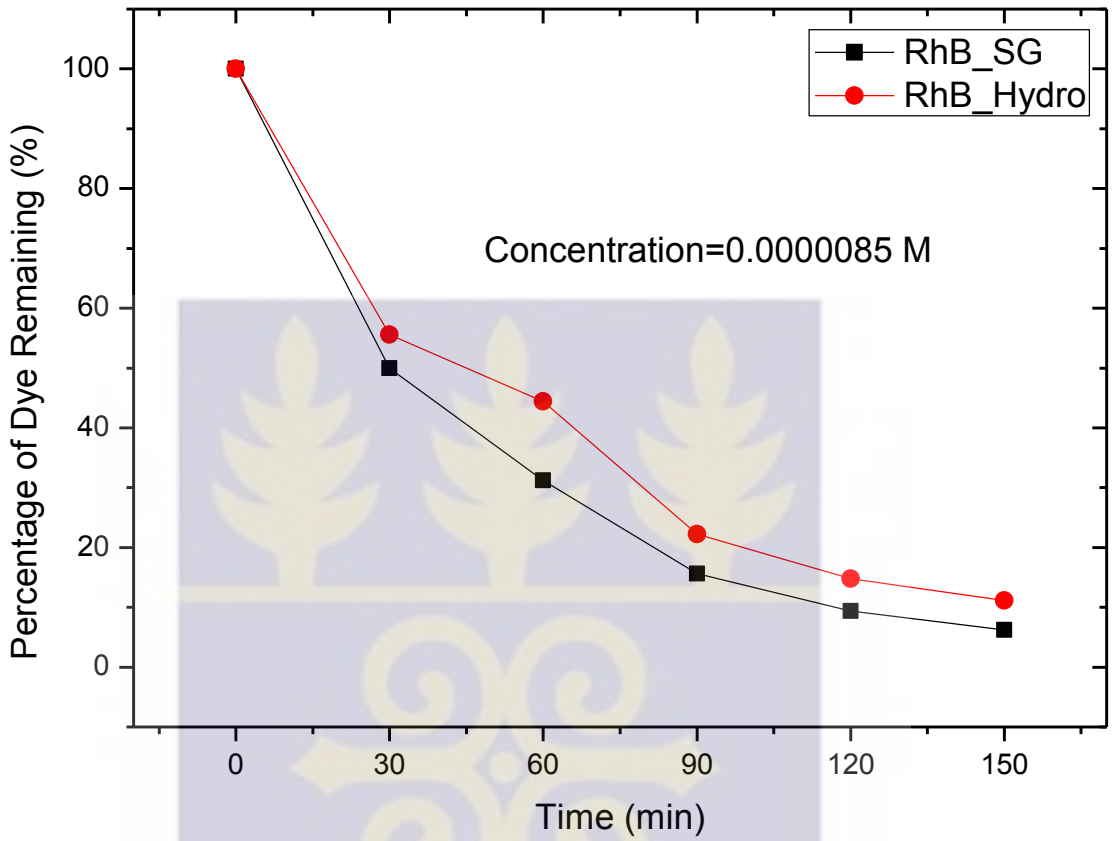

Figure 4.40: Percentage Degradation of Rhodamine B dye at different exposure times

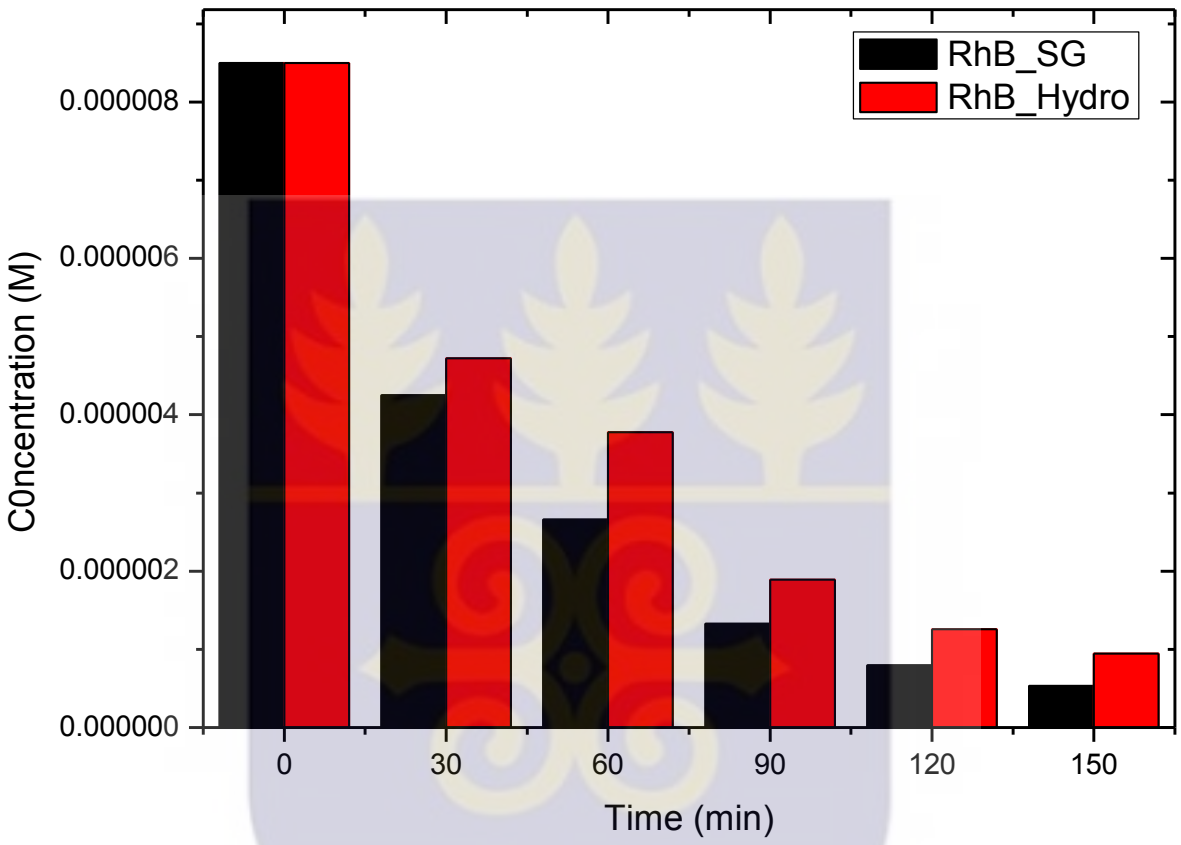

Figure 4.41: Concentration of Rhodamine B dye solution at different exposure times

From Figure 4.41**,** the initial concentration of Rhodamine B dye solution (**8.5×10^{-6} M**) was seen to be reducing with time upon UV light irradiation and after 150 minutes exposure, the concentration reduced to **5.3×10^{-7}M** when Sol gel prepared catalyst was used and for Rhodamine B dye degradation assisted by Hydrothermal prepared catalyst, the concentration after 150 minutes was **9.4×10^{-7}M**.

Therefore, TiO_2 catalyst prepared by Sol gel showed a higher photocatalytic activity in Rhodamine B dye than Hydrothermal prepared catalyst.

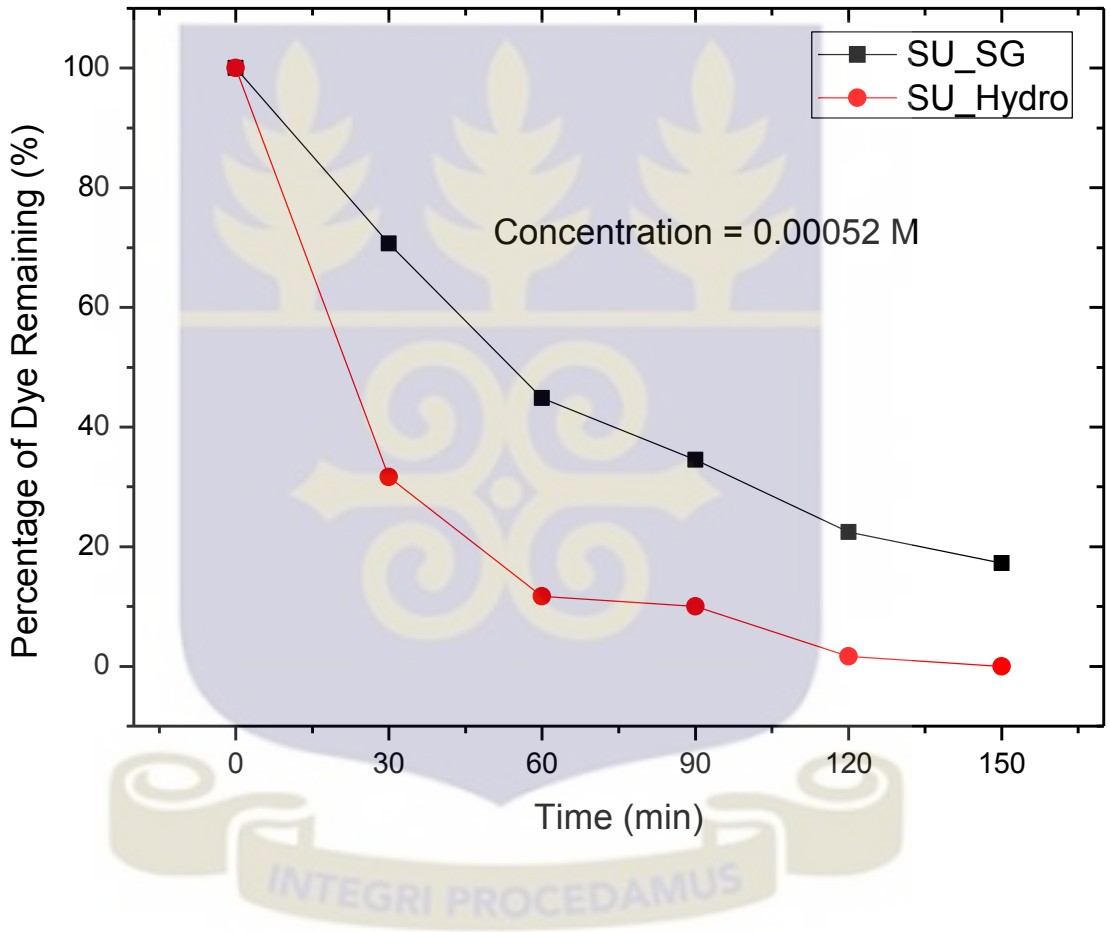

Figure 4.42: Percentage degradation of Sudan III dye at different exposure times

At **5.2×10^{-4} M** concentration of Sudan III dye solution, a high percentage degradation (**68%**) was seen in the first 30 minutes when the photodegradation was assisted by the Hydrothermal prepared catalyst whiles the photodegradation assisted by Sol gel prepared catalyst reported only

29 %. There was **83 %** degradation after 150 minutes when TiO_2 catalyst prepared by Sol gel method was used and **100 %** degradation was observed after 150 minutes when the Hydrothermal prepared TiO_2 nanoparticles was used as the catalyst.

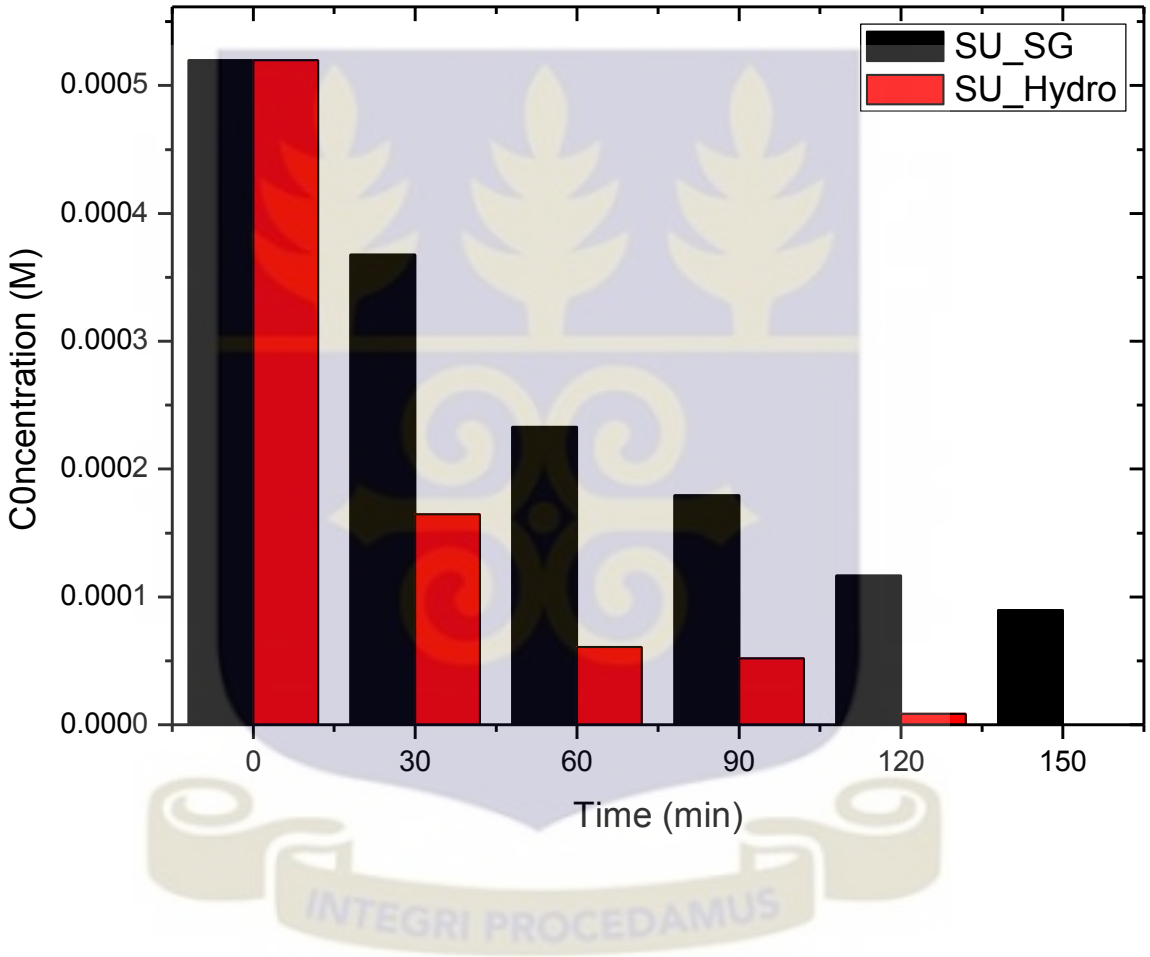

Figure 4.43: Concentration of Sudan III dye solution at different exposure times

As seen in Figure 4.43, the initial concentration of Sudan III dye solution (**5.2×10^{-4} M**) was also seen reducing with time upon UV light irradiation and after 150 minutes exposure, the concentration reduced to **9×10^{-5} M** when Sol gel prepared catalyst was used and for Sudan III

dye degradation assisted by Hydrothermal prepared catalyst, the concentration was **0 M**, indicating a **100 %** degradation after this time. As a result, TiO_2 nanoparticles catalyst synthesized by Hydrothermal method showed higher photocatalytic activity in Sudan III dye that Sol gel prepared catalyst.

CHAPTER FIVE

5.0. Conclusions and Recommendations

In this present work, TiO_2 nanoparticles were synthesized by sol gel and hydrothermal routes and characterized by XRD, BET, FTIR, Raman Spectroscopy and SEM techniques. Analysis from the XRD and Raman confirmed that the synthesized particles were pure tetragonal anatase phase TiO_2 except the sample prepared by Hydrothermal method and calcined at 600°C which showed **15%** rutile phase and **85%** anatase phase.

A BET surface area reported to be 207.7 m^2/g, was observed in the as-prepared TiO_2 nanoparticles synthesized by the Hydrothermal technique. The samples also revealed stepwise adsorption and desorption branch isotherms of a typical type IV pattern with hysteresis loop, characteristic of mesoporous material according to the classification of IUPAC.

The synthesized catalysts were employed in the photocatalytic degradation of Rhodamine B and Sudan III dyes. The photocatalytic degradation of Rhodamine B and Sudan III dyes were studied at various exposure times to the UV light. The photocatalytic activity of the synthesized TiO_2 was evaluated by determining the decrease in concentration of the respective dye solutions over time when TiO_2 was used as the catalyst. It was demonstrated that Rhodamine B and Sudan III dyes were degraded within a short time. Sol gel prepared catalyst showed a higher photocatalytic activity in Rhodamine B dye solution and Hydrothermal prepared catalyst showed a higher photocatalytic activity in Sudan III dye solution.

A high photacatalytic activity of 94% degradation of Rhodamine B dye was observed after 150 minutes irradiation of UV light when TiO_2 catalyst synthesized by Sol gel technique was

employed and a 100% degradation was seen after 150 minutes UV light irradiation in Sudan III dye when Hydrothermal prepared catalyst was used.

The SEM micrographs' EDX results obtained also showed that nearly spherical TiO_2 nanoparticles with high purity were produced. They were highly crystalline with grain size ranging from 2 nm to 30 nm. These synthesized TiO_2 nanoparticles can be applied in the degradation of wide range of dye pollutants.

Using TiO_2 films for photocatalysis is recommended since it would be ideally compared to TiO_2 powders in terms of applicability. This is because, recovering the TiO_2 particle suspension from the reaction mixture could be a nuisance. Also, doping the TiO_2 nanoparticles with other transition metals would be helpful to increase the degradation power of the catalyst.

References

[1] M. Lazar, S. Varghese, and S. Nair, "Photocatalytic Water Treatment by Titanium Dioxide: Recent Updates," *Catalysts*, vol. 2, no. 4, pp. 572–601, 2012.

[2] V. Žunič, "Photocatalytic discoloration of the azo dye methylene blue in the presence of irradiated TiO_2/Pt nano-composite," *Ipssc.Mps.Si*.

[3] M. Omaish, M. M. Khan, and S. Ali, "Polythiophene Nanocomposites for Photodegradation Applications : Past , present and future," *J. Saudi Chem. Soc.*, vol. 19, no. 5, pp. 494–504, 2015.

[4] K. Bubacz, J. Choina, D. Dolat, and A. W. Morawski, "Methylene Blue and Phenol Photocatalytic Degradation on nanoparticles of anatase TiO_2," *Polish J. Environ. Stud.*, vol. 19, no. 4, pp. 685–691, 2010.

[5] M. Habib, M. Muslim, M. Shahadat, M. Islam, I. M. Ismail, T. S. Islam, and A. Mahmood, "Photocatalytic decolorization of crystal violet in aqueous nano-ZnO suspension under visible light irradiation," *J. Nanostructure Chem.*, vol. 3, no. 1, p. 70, 2013.

[6] M. M. Rahman, F. A. Choudhury, D. Hossain, and N. Islam, "A Comparative Study on the Photocatalytic Degradation of Industrial Dyes using Modified Commercial and Synthesized TiO_2 Photocatalysts," vol. C, no. 2, 2012.

[7] W. Rezig and M. Hadjel, "Photocatalytic Degradation of Vat Green 03 Textile dye , Using the Ferrihydrite-Modified Diatomite with TiO_2 / UV Process," 2014.

[8] I. Nuramdhani, "Towards Environmentally Benign Wastewater Treatment – Photocatalytic Study of Degradation of Industrial Dyes by," 2011.

[9] I. M. Alfa, C. a Okuofu, D. B. Adie, S. O. Dahunsi, U. S. Oranusi, and S. A. Idowu, "International Journal of Green Chemistry and Bioprocess," vol. 2, no. 4, pp. 34–38, 2012.

[10] N. Riaz, F. K. Chong, B. K. Dutta, Z. B. Man, M. S. Khan, and E. Nurlaela, "Photodegradation of Orange II under visible light using Cu–Ni/TiO_2: Effect of calcination temperature," *Chem. Eng. J.*, vol. 185–186, pp. 108–119, 2012.

[11] "Photocatalytic Degradation of Alizarin Red S and Bismarck Brown R Using TiO_2 Photocatalyst," vol. 1, no. 1, pp. 1–7, 2014.

[12] U. G. Akpan and B. H. Hameed, "Parameters affecting the photocatalytic degradation of dyes using TiO2-based photocatalysts: A review," *J. Hazard. Mater.*, vol. 170, no. 2–3, pp. 520–529, 2009.

[13] R. C. Meena, "MBIR DOWEX-11 Assisted Photocatalytic Degradation of Azo Dyes : A Review," *Sci. Revs. Chem. Commun.*, vol. 3, no. 4, pp. 181–189, 2013.

[14] P. G. Nair, S. Vijayakumar, and T. Lisluke, "Degradation of Dyestuff Pollutant Sudan I Using Advanced Oxidation Process," *J. Water Resour. Prot.*, no. October, pp. 1276–1283, 2014.

[15] Z. Meng, L. Zhu, J. Choi, C. Y. Park, and W. Oh, "Ultrasonics Sonochemistry Sonocatalytic degradation of Rhodamine B in the presence of C 60 and CdS coupled TiO_2 particles," *Ultrason. - Sonochemistry*, vol. 19, no. 1, pp. 143–150, 2012.

[16] K. Mondal and A. Sharma, "Photocatalytic Oxidation of Pollutant Dyes in Wastewater by TiO_2 and ZnO nano-materials – A Mini-review," pp. 36–72.

[17] L. Wang, J. Zheng, Z. Zhang, T. Wang, and B. Che, "Determination of Eight Sudan Dyes in Chili Powder by UPLC-MS / MS," *Sci. Res.*, vol. 2013, no. October, pp. 154–157,

2013.

[18] "Sudan IV dye in our palm oil_ Many more tears for Ghanaian consumer - Graphic Online." pp. accessed on 3rd May, 2016, http://www.graphic.com., 2015.

[19] V. B. Patil, "A Comparative Study on Photo Degradation of Methylene Blue Dye Effluent by Advanced Oxidation Process by Using TiO_2 / Zno Photo Catalyst .," vol. 4, no. 4, pp. 814–819, 2011.

[20] S. Fassi, K. Djebbar, and T. Sehili, "Photocatalytic Degegradation of Bromocresol green by TiO_2 / UV in aqueous medium," vol. 5, no. 4, pp. 1093–1098, 2014.

[21] L. M. Soto-vázquez, T. Rodríguez, and F. Márquez, "Catalytic Photodegradation of p-aminobenzoic Acid on TiO_2 Nanowires with High Surface Area," *Ambientis*, pp. 20–27, 2014.

[22] R. Ali, and B. Siew, "Photodegradation of New Methylene Blue in Aqueous Solution Using Zinc Oxide And Titanium Dioxide As Catalyst " vol. 45, pp. 31–41, 2007.

[23] Y. Su, Y. Yang, H. Zhang, Y. Xie, Z. Wu, Y. Jiang, N. Fukata, Y. Bando, and Z. L. Wang, "Enhanced photodegradation of methyl orange with TiO_2 nanoparticles using a triboelectric nanogenerator.," *Nanotechnology*, vol. 24, no. 29, p. 295401, 2013.

[24] H. Faghihian and R. Sadeghinia, "Photo Degradation-Adsorption Process as a Novel Desulfurization Method," vol. 3, no. 3, 2014.

[25] M. Zhang, J. Wu, D. Lu, and J. Yang, "Enhanced Visible Light Photocatalytic Activity for TiO_2 Nanotube Array Films by Codoping with Tungsten and Nitrogen," vol. 2013, 2013.

[26] A Selvaraj, R. Parimiladevi, and K. B. Rajesh, "Synthesis of Nitrogen Doped Titanium Dioxide (TiO_2) and its Photocatalytic Performance for the Degradation of Indigo Carmine

Dye," *J. Environ. Nanotechnol.*, vol. 2, no. 1, pp. 28–31, 2013.

[27] J. Choi, "Development of Visible-Light-Active Photocatalyst for Hydrogen Production and Environmental Application," vol. 2010, p. 229, 2010.

[28] M. Cerna, C. Guillard, E. Puzenat, M. Vesely, and P. Dzik, "Hydrothermal synthesis of TiO_2 : influence of process conditions on photocatalytic activity," *Int. J. Chem. Environ. Eng.*, vol. 2, no. 4, 2011.

[29] T. S. Natarajan, M. Thomas, K. Natarajan, H. C. Bajaj, and R. J. Tayade, "Study on UV-LED/TiO_2 process for degradation of Rhodamine B dye," *Chem. Eng. J.*, vol. 169, no. 1–3, pp. 126–134, 2011.

[30] K. Thamaphat, P. Limsuwan, and B. Ngotawornchai, "Phase Characterization of TiO_2 Powder by XRD and TEM," *Kasetsart J. (Nat. Sci.) 42*, vol. 361, pp. 357–361, 2008.

[31] T. Theivasanthi and M. Alagar, "Titanium dioxide (TiO_2) Nanoparticles - XRD Analyses – An Insight," *Cent. Res. Post Grad. Dep. Physics, Ayya Nadar Janaki Ammal Coll. Sivakasi*, 2013.

[32] E. M. Mahdi, M. Hamdi, M. Y. M. S, and P. Wilfred, "XRD and EDXRF Analysis of Anatase Nano-TiO_2 Synthesized from Mineral Precursors," *Adv. Mater. Res.*, vol. 620, pp. 179–185, 2013.

[33] C. Sung, J. Ho, D. Kim, S. Cho, and W. Oh, "Processing Research Reaction morphology and the effect of pH on the preparation of TiO_2 nanoparti- cles by a sol-gel method," *Ceram. Process. Res.*, vol. 11, no. 6, pp. 736–741, 2010.

[34] "Crystal structure of TiO_2: (a) rutile (b) anatase and (c) brookite, accesed on 12th June, 2016," *http://ruby.colorado.edu/~smyth/min/tio2.html*.

[35] A. S. Edelstein and R. C. Cammarata, *Nanomaterials: Synthesis, Properties and Applications*. 1996.

[36] S. Pavasupree, S. Ngamsinlapasathian, Y. Suzuki, and S. Yoshikawa, "Application of High Surface Area TiO_2 Nanosheet in Dye-sensitized Solar Cells," *2nd Jt. Int. Conf. "Sustainable Energy Environ.*, vol. 008, no. November, pp. 21–26, 2006.

[37] K. Allan, K. Herodes, and I. Leito, "' Fast peaks ' in chromatograms of Sudan dyes," *J. Chromatogr.*, vol. 1160, pp. 227–231, 2007.

[38] M. F. Al-kadhemy, I. F. Alsharuee, and A. A. D. Al-zuky, "Analysis of the Effect of the Concentration of Rhodamine B in Ethanol on the Fluorescence Spectrum Using the Gauss Mod Function," *J. Phys. Sci.*, vol. 22, no. 2, pp. 77–86, 2011.

[39] J. Wu and T. Zhang, "Photodegradation of rhodamine B in water assisted by titania films prepared through a novel procedure," *J. Photochem. Photobiol.*, vol. 162, pp. 171–177, 2004.

[40] M. M. Ba-abbad, A. A. H. Kadhum, A. B. Mohamad, and M. S. Takriff, "Synthesis and Catalytic Activity of TiO_2 Nanoparticles for Photochemical Oxidation of Concentrated Chlorophenols under Direct Solar Radiation," *Int. J. Electrochem. Sci*, vol. 7, pp. 4871–4888, 2012.

[41] R. Rathore, R. Ameta, and S. C. Ameta, "Role of Nickel Vanadate in Photocatalytic Degradation of Azure A," *J. Curr. Chem. Pharm. Sc.*, vol. 4, no. 4, pp. 157–163, 2014.

[42] M. Nan, Z. Yang, P. Eong, B. Jin, and R. Aryal, "Synthesis, Characterisation and Application of TiO_2–Zeolite Nanocomposites for the Advanced Treatment of Industrial Dye Wastewater," *J. Taiwan Inst. Chem. Eng.*, vol. 000, no. 2014, pp. 1–9, 2015.

[43] D. R. Black, D. Windover, D. G. Albert Henins, J. Filliben, and P. C. James, "Standard Reference Material 640d FOR X-Ray Metrology," *Natl. Inst. Stand. Technol. Gaithersburg, MD, 20899*.

[44] G. Caglioti, A. Paoletti, and F. P. Ricci, "Choice of collimators for a crystal spectrometer for neutron diffraction," *Nucl. Instr. Meth*, vol. 3, no. 223, 1958.

[45] P. Scardi and M. Leoni, "Whole Powder Pattern Modelling," *Acta Cryst.*, vol. A58, no. 190, pp. 1–18, 2002.

[46] M. Leoni, T. Confente, and P. Scardi, "PM2K: a flexible program implementing Whole Powder Pattern Modelling," *Z. Krist. Suppl.*, vol. 23, no. 249, 2006.

[47] M. Y. Gamarnik, "Size Changes of Lattice Parameters in Small Particles of Hexagonal Crystals," *Phys. status solidi*, vol. 170, no. 1, pp. 27–38, 1992.

[48] R. S. Devi, D. R. Venckatesh, and D. R. Sivaraj, "Synthesis of Titanium Dioxide Nanoparticles by Sol-Gel Technique," *Int. J. Innov. Res. Sci. Eng. Technol.*, vol. 03, no. 08, pp. 15206–15211, 2014.

[49] G. Cheng, M. S. Akhtar, O. Yang, and F. J. Stadler, "Electrochimica Acta Structure modification of anatase TiO_2 nanomaterials-based photoanodes for efficient dye-sensitized solar cells," *Electrochim. Acta*, vol. 113, pp. 527–535, 2013.

[50] E.-Y. Kim, D. S. Kim, and B.-T. Ahn, "Synthesis of Mesoporous TiO_2 and Its Application to Photocatalytic Activation of Methylene Blue and E . coli a b c d," *Bull. Korean Chem. Soc.*, vol. 30, no. 1, 2009.

[51] "Photocatalyst Mosquito Fly Trap Killer Principle @ Supesolar, http://www.google.com/supsolar." p. accessed on 30th June, 2016.